

Lawrence Berkeley National Laboratory

Recent Work

Title

SURFACE CHEMISTRY

Permalink

<https://escholarship.org/uc/item/4t34w39x>

Authors

Bare, S.R.
Somorjai, G.A.

Publication Date

1986

c.2



Lawrence Berkeley Laboratory

UNIVERSITY OF CALIFORNIA

Materials & Molecular Research Division

RECEIVED
LAWRENCE
BERKELEY LABORATORY

JAN 1986

LIBRARY AND
DOCUMENTS SECTION

To be published as a chapter in Encyclopedia of Physical Science and Technology, M. Yelles, Ed., Academic Press Inc., Orlando, FL, 1986

SURFACE CHEMISTRY

S.R. Bare and G.A. Somorjai

January 1986

TWO-WEEK LOAN COPY
*This is a Library Circulating Copy
which may be borrowed for two weeks.*



LBL-20904
c.2

DISCLAIMER

This document was prepared as an account of work sponsored by the United States Government. While this document is believed to contain correct information, neither the United States Government nor any agency thereof, nor the Regents of the University of California, nor any of their employees, makes any warranty, express or implied, or assumes any legal responsibility for the accuracy, completeness, or usefulness of any information, apparatus, product, or process disclosed, or represents that its use would not infringe privately owned rights. Reference herein to any specific commercial product, process, or service by its trade name, trademark, manufacturer, or otherwise, does not necessarily constitute or imply its endorsement, recommendation, or favoring by the United States Government or any agency thereof, or the Regents of the University of California. The views and opinions of authors expressed herein do not necessarily state or reflect those of the United States Government or any agency thereof or the Regents of the University of California.

LBL-20904

SURFACE CHEMISTRY

Simon R. Bare and G. A. Somorjai

**Materials and Molecular Research Division, Lawrence Berkeley Laboratory
and Department of Chemistry, University of California
Berkeley, CA 94720**

**This work was supported by the Assistant Secretary for Energy Research,
Office of Basic Energy Sciences, Materials Sciences Division of the
U. S. Department of Energy under Contract No. DE-AC03-76SF00098.**

SURFACE CHEMISTRY

Simon R. Bare and G. A. Somorjai

Materials and Molecular Research Division, Lawrence Berkeley Laboratory
and Department of Chemistry, University of California
Berkeley, CA 94720 USA

- I. Surface Structure of Clean Surfaces
 - (i) Techniques sensitive to surface structure
 - (ii) Surface relaxation
 - (iii) Surface reconstruction
 - (iv) Stepped and kinked surfaces
- II. Surface Structure of Adsorbates on Solid Surfaces
 - (i) The ordering of adsorbed monolayers
 - (ii) Ordered adsorbate structures
 - (iii) Vibrational spectroscopies
- III. Thermodynamics of Surfaces
 - (i) Surface tension
 - (ii) Adhesion, equilibrium shape, nucleation
 - (iii) Physical and chemical adsorption
 - (iv) Adsorption isotherms
 - (v) Heat of adsorption
- IV. Electrical Properties of Surfaces
 - (i) Surface dipole and surface space charge
 - (ii) Work function
 - (iii) Surface states
 - (iv) Electron emission from surfaces

V. Surface Dynamics

- (i) Atomic vibrations
- (ii) Surface diffusion
- (iii) Stoichiometric surface reactions
- (iv) Catalytic surface reactions
- (v) Photochemical surface reactions

GLOSSARY

Physisorption	The binding of molecules to surfaces by weak chemical forces
Chemisorption	The binding of molecules to surfaces by strong chemical forces
Adsorption	The process by which molecules are taken up on the surface by chemical or physical action
Desorption	The process by which molecules are removed from the surface
Adsorbate	An adsorbed atom or molecule
Heat of adsorption	The binding energy of the adsorbed species
Sticking probability	The ratio of the rate of adsorption to the rate of collision of the gaseous molecule with the surface
Surface free energy	The energy necessary to create a unit area of surface
Surface relaxation	The equilibration of surface atoms to new positions that changes the interlayer distance between the first and second layers of atoms

Surface reconstruction	The equilibration of surface atoms to new positions that changes the bond angles and rotational symmetry of the surface atoms
Work function	Minimum energy required to remove an electron from the surface into the vacuum outside the solid
Surface state	An electronic state localized at the surface
Surface unit cell	The two-dimensional repeating unit which fully describes the surface structure

Surfaces constitute the boundaries of condensed matter, solids and liquids. Surface chemistry explores the structure and composition of surfaces and the bonding and reactions of atoms and molecules on them. There are many macroscopic physical phenomena that occur on surfaces, or are controlled by the electronic and physical properties of surfaces. These include heterogeneous catalysis, corrosion, crystal growth, evaporation, lubrication, adhesion and integrated circuitry. Surface chemistry examines the science of these phenomena as well.

SURFACE STRUCTURE OF CLEAN SURFACES

Introduction

To the naked eye the surface of a single crystal of a metal looks perfectly planar, with no imperfections. If this crystal is now examined with an optical microscope features of the surfaces down to the wavelength of visible light ($\sim 5000 \text{ \AA}$) can be resolved. The surface will look granular, with distinct regions of crystallinity separated from each other by boundaries or dislocations. These dislocations indicate areas on the surface where there is a mismatch of the crystalline lattice, and they can take several forms, for example edge dislocations or screw dislocations. The presence of these dislocations or defects can dominate certain physical properties of the material. Dislocation densities of the order $10^6 - 10^8 \text{ cm}^{-2}$ are commonly found on metal single crystals, whereas the number is lower, $10^4 - 10^6 \text{ cm}^{-2}$, on semiconductor surfaces due to the different nature of the bonding. These defect densities must be compared with the total concentration of surface atoms, about 10^{15} cm^{-2} . On further magnification, for example using a scanning electron microscope, features can be resolved down to about 1000 \AA , and our view of the surface will change further. The surface will look pitted, with distinct planar areas (terraces) bounded by walls many atomic layers in height. Thus, on the microscopic and submicroscopic scale the surface morphology appears to be very heterogeneous, with many different surface sites which differ by the number of neighboring atoms surrounding them. What about the nature of the surface on an atomic scale?

In order to be able to discuss and understand the structure of surfaces it is necessary to understand the techniques which are capable of viewing the surface on an atomic scale. We will briefly describe such techniques, illustrating their capabilities with pertinent examples. The techniques more commonly used are field-ion microscopy (FIM), low energy electron diffraction (LEED), helium atom diffraction, and high energy ion scattering. In addition, the relatively new technique of scanning tunneling microscopy (STM) is proving to be a very promising tool. Only brief descriptions are given here and the reader is referred to some of the excellent books on the subject given in the bibliography.

Techniques Sensitive to Surface Structure

Field Ion Microscopy

Field ion microscopy is one of the oldest techniques used for surface structure determination, being invented by Müller in 1936. The basic microscope can be very simple. In an ultra-high vacuum cell, a potential of about 10,000 V is applied between a hemispherical tip of refractory metal of radius $\sim 10^{-4}$ cm and a fluorescent screen. The tip is charged positively, and a gas (usually helium) is allowed to impinge on the surface. Under the influence of the very strong electric field helium atoms that are incident on the tip are ionized. The positive ions thus created are repelled radially from the surface and accelerated onto the fluorescent screen, where a greatly magnified image of the crystal tip is displayed. The ionization probability depends strongly on the local field variations induced by the atomic

structure of the surface--protruding atoms generate stronger ionization than atoms embedded in close-packed planes, thereby producing individual bright spots on the screen. The small radius of the tip is needed to produce the large fields necessary for ionization, but also permits the immense magnification of the microscope. The tip surface is directly imaged with magnification of about 10^7 . Figure 1 depicts the image of a tungsten field ion tip. Well defined atomic planes of the crystal tip can be readily identified, indicating that there is order on the atomic scale, i.e., most of the surface atoms in any crystal face are situated in ordered rows separated by well-defined interatomic distances. The technique is limited to the refractory metals (W, Ta, Ir, Re) which can withstand the strong electric field at the tip without desorption or evaporation from the surface. However, its great advantage is that individual atoms can be imaged on the screen, which also allow studies of surface diffusion.

Low Energy Electron Diffraction

Another method which has demonstrated that crystal surfaces are ordered on an atomic scale is low energy electron diffraction (LEED). This method is the most frequently used technique, such that nowadays virtually all modern surface science laboratories rely upon it for surface structural information.

In order to obtain diffraction from surfaces, the incident wave has to satisfy the condition $\lambda \leq d$ where λ is the wavelength of the incident beam and d is the interatomic distance in the surface. In addition, the incident beam should not penetrate much below the

surface plane but should back-diffract predominantly from the surface so that the scattered beam reflects the properties of the surface atoms and not those of the bulk. The de Broglie wavelength of electrons, λ , is given by λ (in Å) = $\sqrt{150/E}$ where E is in eV. Thus in the energy range 10 to 500 eV, the wavelength varies from 3.9 to 0.64 Å, smaller, or equal to, most interatomic distances, and the escape depth of the backscattered electrons in this energy range is 5-10 Å, thereby providing surface sensitivity. These elastically scattered low energy electrons yield surface structural information. The technique of LEED is depicted schematically in Fig. 2, while a schematic of the LEED apparatus is shown in Fig. 3. A collimated primary beam of electrons with a diameter of 0.1-1 mm, at energies 15-350 eV, is impinged on a surface and the elastically backscattered electrons, after travelling through a field-free region, are spatially analyzed. This is achieved most commonly (see Fig. 3) by passing the scattered electrons through four hemispherical grids. The first grid is at the crystal potential while the second and third are at a retarding voltage to eliminate inelastic electrons, and the fourth is at ground. After passing through these grids the diffracted beams are accelerated onto a hemispherical phosphor screen.

If the crystal surface is well-ordered, a diffraction pattern consisting of bright, well-defined spots will be displayed on the screen. The sharpness and overall intensity of the spots are related to the degree of order of the surface. When the surface is less ordered, the diffraction beams broaden and become less intense, while

some diffuse intensity appears between the beams. A typical set of diffraction patterns from a well ordered surface is shown in Fig. 4. The presence of the sharp diffraction spots clearly indicates that the surface is ordered on an atomic scale. Similar LEED patterns have been obtained from solid single crystal surfaces of many types: metals, semiconductors, alloys, oxides and intermetallics.

Due to the importance of LEED in surface chemistry we shall briefly discuss other aspects of the technique which make it one of the most powerful surface sensitive tools. It is convenient to subdivide the technique into "two-dimensional" LEED and "three-dimensional" LEED. In two-dimensional LEED one observes only the symmetry of the diffraction pattern on the fluorescent screen. The bright spots which correspond to the two-dimensional reciprocal lattice belonging to the repetitive crystalline surface structure, yield immediate information about the size and orientation of the surface unit cell i.e. the geometry of the surface layer. This is important information since reconstruction-induced and adsorbate-induced new periodicities are immediately visible. The diffuse background intensity also contains information about the nature of any disorder present on the surface. In three-dimensional LEED the information gained from the two-dimensional pattern is supplemented by the intensities of the diffraction spots which are measured as a function of incident electron energy. By comparing these intensity versus voltage curves ($I(V)$ curves) with those simulated numerically with the help of a suitable theory, the precise location of atoms or molecules in the

surface with respect to their neighbors is determined. Thus the bond length and bond angles in the surface layer are calculated. It should be mentioned, however, that the analysis of the LEED beam intensities requires a theory of the diffraction process which is a non-trivial point due to multiple scattering of LEED electrons by the surface, and this is not simple to represent in a theory.

Atomic Beam Diffraction

Another technique which utilizes the principle of diffraction is atomic or molecular beam diffraction. The de Broglie wavelength, λ , associated with helium atoms is given by:

$$\lambda(\text{\AA}) = \frac{h}{(2ME)^{1/2}} = \frac{0.14}{E(\text{eV})^{1/2}} \quad (1)$$

where h is Planck's constant, and M and E are the mass and energy of the helium atom respectively. Atoms with a thermal energy of ~ 20 meV have $\lambda = 1$ \AA and can readily diffract from surfaces. The information obtained from atomic beam diffraction is similar to that from LEED, but there are differences between the two techniques. In LEED the relatively high energy (20-200 eV) electrons used penetrate the crystal, multiple scattering events are important, and the LEED electrons are scattered primarily from the ion cores of the crystal lattice. In atom diffraction, there is virtually no penetration of the low energy (10-200 meV) atomic beam, making it much more surface sensitive than the electron beam, and the atomic beam is primarily scattered from the valence electrons of the surface atoms. In fact, their scattering is usually simulated by a "hard wall" around the

atoms in the top layer of the surface so that diffraction is from a "corrugated hard-wall" with the periodicity of the surface mesh. As in LEED the location of the diffracted beams indicates the surface periodicity. Their intensities are related to the structure of the scattering potential within a unit mesh, in this case to the relative amplitude and positions of corrugations around the surface atoms.

The essential elements of the apparatus necessary to perform atomic beam diffraction are an atomic beam of gas and a detector. The atomic beam is usually generated from a nozzle source incorporating several skimmers. The energy (wavelength) of the beam is varied by either heating or cooling the nozzle. The detector usually employed is a mass spectrometer, mounted on a rotatable device to enable it to be movable over a large range of scattering angles. The atomic beam is chopped with a variable-frequency chopper before it impinges on the surface. In this way, an alternating intensity of the beam is generated at the mass spectrometer detector that is readily separated from the "noise" due to helium atoms in the background.

To illustrate the type of data that is obtained, Fig. 5 shows the He diffraction traces from a Au(110)-(1x2) surface at two different wavelengths.

He diffraction is an especially sensitive technique to surface order on an atomic scale. On scattering from a well-ordered single crystal surface nearly 15% of the scattered helium atoms appear in the specular helium beam whereas this fraction can drop to 1% when the surface is disordered. Measurements of the fraction of specularly

scattered helium can therefore provide information on the degree of atomic disorder in the solid surface.

Scanning Tunneling Microscopy

The relatively new technique of scanning tunneling microscopy also clearly demonstrates order on an atomic scale on single crystal surfaces. It images surface topographies in real space with a lateral resolution of $\sim 2 \text{ \AA}$ and vertical resolution of $\sim 0.05 \text{ \AA}$. The technique utilizes the tunnel effect. Due to the wave nature of electrons, they are not strictly confined to the interior bounded by the surface atoms. Therefore, the electron density does not drop to zero at the surface, but decays exponentially on the outside, with a decay length of a few Angstroms. If two metals are approached to within a few \AA , the overlap of their surrounding electron clouds becomes substantial, and a measurable current can be induced by applying a small voltage between them. This tunnel current is a measure of the wave-function overlap, and depends very strongly on the distance between the two metals. This is the physical basis of the scanning tunneling microscope. Experimentally one of the electrodes is sharpened to a pointed tip which is scanned over the surface to be investigated (the other electrode) at constant tunnel current. The tip thus traces contours of constant wave-function overlap, and in the case of constant decay length, the trace is an almost true image of the surface atomic positions, i.e. the surface topography. An example is shown in Fig. 6.

Ion Scattering

Ion scattering from surfaces is usually subdivided into two scattering regions: low energy ion scattering (LEIS), energies typically ~ 1 keV, and high energy scattering (HEIS), energies 0.1-1 MeV. HEIS is a probe which tests the local position of surface atoms relative to their bulk-like sites. In HEIS the velocity of the ion is such that it is moving fast compared to the thermal motions of the atoms in the solid, thus the beam senses a frozen lattice. If the target is amorphous each atom would sense a uniform distribution of impact parameters of the ions and diffuse scattering results. However, the scattering spectrum from a single crystal aligned with a major symmetry axis parallel to the beam is drastically modified from that of the amorphous target. The impact parameter distribution is also uniform at the first monolayer, but the first atom shadows the second from the beam and small angle scattering events determine the impact parameter distribution at the second atom. This results in a unique (non-uniform) flux distribution at the second atom. Figure 7 illustrates the effect of small angle scattering in a two-atom model. Ions incident at the smallest impact parameter undergo large angle scattering, those at large impact parameter suffer small deflections which determine the flux distribution of ions near the second atom. The closest approach of the ion to the second atom, R , can be approximated assuming Coulomb scattering

$$R = 2(Z_1 Z_2 e^2 d/E)^{1/2} \quad (2)$$

where Z_1 , Z_2 are the masses of the incident and target atoms,

respectively, d is the atomic spacing and E is the incident ion energy. This gives rise to a shadow cone beneath the surface atom as illustrated in Fig. 7. The flux distribution at the second atom, within the Coulomb approximation, can be written analytically which leads to an estimate of the two atom surface peak intensity, I , as:

$$I = 1 + \left(1 + \frac{R^2}{2\rho^2}\right) \exp\left(\frac{-R}{2\rho}\right) \quad (3)$$

where ρ is the two-dimensional root mean square thermal vibrational amplitude. The first term represents the unit contribution from the first atom in the string, the second represents the variable contribution from the second atom. While the two atom Coulomb approximation is not adequate enough to compare to experiment, it illustrates that the surface peak intensity is a function of one parameter, ρ/R .

The intensity of the surface peak is thus sensitive to the atomic arrangement on the surface, i.e. the positions of the surface atoms with respect to their bulk-like positions. The effect on the surface peak of different surface structures is depicted in Fig. 8. The nature of reconstructed, relaxed and adsorbate covered surfaces will be discussed in the following sections.

HEIS is also a sensitive tool for answering other important questions in surface chemistry, namely what type of atoms are present on the surface, and how many are present.

All of the techniques discussed so far indicate that the solid surface is ordered on an atomic scale. Most of the surface atoms

occupy equilibrium atomic positions that are located in well-defined rows separated by equal interatomic positions. This atomic order is predominant despite the fact that there are large numbers of atomic positions on the surface where atoms have different numbers of neighbors. A pictorial representation of the topology of a monatomic crystal on an atomic scale is shown in Fig. 9. The surface may have atoms in any of the positions shown in the figure. There are atoms in the surface at kink positions and in ledge positions, and there are adatoms adsorbed on the surface at various sites. Atomic movement from one position to another proceeds by surface diffusion. To the first approximation, the binding energy of the surface atoms is proportional to the number of nearest and next-nearest neighbors. Therefore, for example, atoms at a ledge are bound more strongly than are adatoms. In equilibrium there is a certain concentration of all these surface species, with those species predominating whose binding energies are greatest. Thus the adatom concentration on clean well-equilibrated surfaces should be very small indeed. However, while these surfaces are ordered on an atomic scale their structure is not always one of simple termination of the bulk unit cell, relaxation or reconstruction being common.

Surface Relaxation

Generally, the surface unit cells of clean metal surfaces have been found to be those expected from the projection of the bulk x-ray unit cell onto the surface, referred to as a (1x1) structure (in Miller Indices notation), and the uppermost layer z-spacing (spacing in the

direction normal to the surface plane) is equal to the bulk value within about 5%. Such surfaces include the (111) crystal faces of face centered cubic aluminium, platinum, nickel, and rhodium, and the (0001) crystal faces of hexagonal close packed cadmium and beryllium. This information has almost exclusively been determined by a detailed intensity analysis of the diffraction beams in LEED as a function of incident electron energy, and the interatomic positions in the surface layer are calculated to within 0.1 Å. The Al (110) surface shows a 5 to 15% contraction, the Mo (100) surface a 11 to 12% contraction and the W (100) surface a 6% contraction of the top-layer z-spacing with respect to the bulk, while retaining the (1x1) surface unit cell. Generally, crystal planes whose atoms are less densely packed (for example bcc (100) and fcc (110) planes) will be more likely to show relaxation than the more densely packed planes. In forming a surface of the less densely packed planes it is necessary to remove a larger number of nearest neighbor atoms. Thus, to minimize the surface free energy a relocation of the surface atoms from their bulk positions is quite likely. There are several explanations as to why surface relaxation is prevalent on the more open surfaces. First, it can be imagined that the electron cloud attempts to smooth its surface, thereby producing electrostatic forces that draw the surface atoms towards the substrate, the effect being stronger the less closely packed the surface. Second, with fewer neighbors the two body repulsion energy is smaller, allowing greater atomic overlap and therefore more favorable bonding at shorter bond lengths. Third,

for surface atoms the bonding electrons are partly redistributed from the broken bonds to the remaining unbroken bonds, thereby the charge content of the latter is increased, reducing the bond length.

Surface Reconstruction

Surface atoms in any crystal are in an anisotropic environment which is very different from that around bulk atoms. The crystal symmetry that is experienced by each surface atom is markedly lower than when the atom is in the bulk. This symmetry change, and lack of neighbors in the direction perpendicular to the surface allows displacement of surface atoms in ways which are not allowed in the bulk. Surface relaxation is one consequence of this, the other major consequence being surface reconstruction. Here the two-dimensional surface unit cell is different from that given by the termination of the bulk structure on the plane of interest. Surface reconstruction can give rise to a multitude of different structures depending upon the electronic structure of a given substance. The phenomenon is more frequent on semiconductor surfaces than on metal surfaces. While the geometry is readily observed in the LEED pattern, the actual elucidation of the real space reconstructed surface structure is often extremely difficult, and in some cases even after years of study and many proposals of the structure, the true structure is still not known. Such a system is the Si (111) surface. Upon cleaving in UHV at room temperature, the surface exhibits a (2x1) surface structure. On heating to about 700 K the surface structure changes to one with (7x7) periodicity. This (7x7) structure is then the stable structure

of the (111) face. While this surface has been studied by a multitude of techniques, including LEED, STM and He atom diffraction there is still no generally accepted structure of either the (2x1) or (7x7) reconstructions.

One of the best known examples of reconstruction of metallic surfaces is that for the (100) faces of three 5d transition metals that are neighbors on the periodic table: gold, platinum and iridium. The ideal unreconstructed surfaces have a square net of atoms. Surface reconstruction produces a superlattice that is basically five times larger in one direction than for the ideal surface. For Ir (100) the superlattice is denoted (5x1), for Pt (100) by the matrix notation $\begin{pmatrix} 5 & 1 \\ -1 & 14 \end{pmatrix}$, and for Au (100) by the superlattice (5x20). From LEED $I(V)$ analyses, evidence indicates that the nature of the reconstruction is similar on all three metals and consists of a close-packed hexagonal top layer that is positioned in slightly different ways on the square net substrate. These reconstructions are consistent with the knowledge that the (111) face of fcc metals is energetically the most favorable. It is worth noting here that the adsorption of gases such as oxygen, carbon monoxide or hydrogen, or the presence of impurities can inhibit these surface reconstructions. On the other hand, the presence of such adsorbates can also induce different surface reconstructions.

The nature and cause of these surface phase-transformations are not well established at present. The case of structural change from metastable to stable upon adsorption or removal of adsorbates indicates the likelihood of electronic transitions that accompany re-

construction. At the surface there are fewer nearest neighbors as compared to atoms in the bulk. The electronic structure that is the most stable in this reduced-symmetry environment may be substantially different from that of the bulk metal. Since the surface atoms are surrounded by atoms only on one side, and there is vacuum on the other, they may change their coordination number by slight relocation with simultaneous changes in the electronic structure. It is indeed surprising that more surfaces do not show reconstruction.

Stepped and Kinked Surfaces

The close-packed faces of solids (low-Miller-index faces) have the lowest surface free energy, and therefore they are the most stable with respect to rearrangement on disordering up to or near the melting point. However, stepped and/or kinked surfaces (high-Miller-index faces), although of higher surface free energy, are very important. They are known to play important roles during evaporation, condensation and melting. Steps and kinks are sites where atoms break away as an initial process leading to desorption, or where atoms migrate during condensation to be incorporated into the crystal lattice. Theories of crystal growth, evaporation and the kinetics of melting have identified the significance of these lower-coordination number sites in controlling the rate processes associated with phase changes. In addition, studies of chemisorption and catalysis using single-crystal surfaces have revealed different binding energies and enhanced chemical activity at steps and kinks on high-Miller-index transition metal surfaces as compared to low-Miller-index surfaces. Adsorption of dia-

tomic or polyatomic molecules frequently leads to dissociation with greater probability of steps and kinks than on flat atomic terraces.

The presence of steps on a single crystal surface are readily discernible by LEED. The LEED patterns differ from those expected from crystals with low-index faces in that the diffraction beams are split into doublets. This splitting (see Fig. 10) is a function of ordered steps on the surface. The distance between the split beams is inversely related to the distance between the steps, i.e., the terrace width. From the variation of the intensity maximum of the doublet spots with electron energy the step height can be determined.

Many stepped surfaces exhibit high thermal stability. In particular the one-atom-height step periodic terrace configuration appears to be the stable surface structure of many high-Miller-index surfaces. While most of the stepped surfaces are stable when clean in their one-atom-height step ordered terrace configuration, in the presence of a monolayer of carbon or oxygen many stepped surfaces undergo structural rearrangement. The step height and terrace width may double, or faceting may occur. Faceting is when the step orientation becomes as prominent as that of the terrace, and new diffraction features become recognizable in LEED. Upon removing the impurities from the surface, the original one-atom-height step ordered terrace surface structure is usually regenerated.

SURFACE STRUCTURE OF ADSORBATES ON SOLID SURFACESIntroduction

While the knowledge of the structure of clean solid surfaces is important in its own right for determining various properties of those surfaces, many phenomena are associated with the presence of adsorbates on the surfaces. In fact, in the natural environment of our planet, surfaces are never truly free of adsorbates. On approaching a surface each atom or molecule encounters a net attractive potential. This results in a finite probability that it will be trapped on the surface. This trapping, adsorption, is always an exothermic process. At the low pressure of 1×10^{-6} Torr, approximately 1×10^{15} gas molecules collide with each cm^2 of surface per second. Since the surface concentration of atoms is about 10^{15} cm^{-2} , at this pressure the surface may be covered with a monolayer of gas within seconds - this is the major reason why surface studies are performed under ultra-high vacuum conditions ($P < 1 \times 10^{-8}$ Torr). The very low pressure is needed to maintain clean surface conditions for a time long enough to perform experimental measurements. At atmospheric pressure the surface will be covered within a fraction of a second. The constant presence of the adsorbate layer influences the chemical, mechanical and surface electronic properties. Adhesion, lubrication, resistance to mechanical or chemical attack or photoconductivity are just a few of the many macroscopic surface processes that are controlled by various properties of monolayers.

Two macroscopic experimentally determinable parameters characterize the adsorbed monolayer: the coverage and the heat of adsorption. The coverage, θ , is defined as the ratio of the number of adsorbed atoms or molecules to the total number of adsorption sites, (usually taken as the number of atoms in the surface plane). The heat of adsorption ΔH_{ads} , is implicitly linked to the strength of the adsorbate-substrate bond. A knowledge of both parameters often reveals the nature of bonding in the adsorbed layer.

Atoms or molecules that impinge on the solid surface from the gas phase will have a residence time, τ , on the surface. If the impinging molecules achieve thermal equilibrium with the surface atoms $\tau = \tau_0 \exp \Delta H_{\text{ads}}/RT$, where τ_0 is related to the average vibrational frequency associated with the adsorbate. The heat of adsorption, is always positive and is defined as the binding energy of the adsorbed species. A larger ΔH_{ads} and lower temperature increase the residence time. For a given incident flux, larger ΔH_{ads} and lower temperature yield higher coverages.

It is conventional to divide adsorption into two categories: physisorption and chemisorption. Physisorption (or physical adsorption) systems are characterized by weak interactions ($\Delta H_{\text{ads}} < 15 \text{ kcal mol}^{-1}$, accompanied by short residence times) and require adsorption studies to be performed at low temperature and relatively high pressure (high flux). Adsorbates that are characterized by stronger chemical interactions ($\Delta H_{\text{ads}} \geq 15 \text{ kcal mol}^{-1}$), where near-monolayer adsorption commences even at room temperature and at low pressures ($\leq 10^{-6}$ Torr)

are called chemisorption systems. While the two names imply two distinct types of adsorption, there is a gradual change from the physisorption to the chemisorption regime.

One of the most fascinating facts about the structure of these physisorbed and chemisorbed overlayers in the sub-monolayer to few monolayer regime is the preponderance of the formation of long-range ordered structures. Well over one thousand two-dimensional unit cells have been documented in the literature. While only the shape, size and orientation of the cells are known for most of them, the adsorption site and bond lengths have been determined for about 500 of them.

The Ordering of Adsorbed Monolayers

The ordering process in the adlayer is due to an interplay of the bonding with the substrate and the bonding between the adatoms or ad-molecules. Once a molecule adsorbs it may diffuse on the surface or remain bound at a specific site during most of its residence time. Thermal equilibration among the adsorbate and between the adsorbate and substrate atoms (i.e. adsorption) is assured if ΔH_{ads} and $\Delta E_{\text{D}}^*(\text{bulk})$, the activation energy for bulk diffusion, are high enough as compared to kT ($\geq 10 kT$). However, ordering primarily depends on the depth of the potential energy barrier that keeps an atom or molecule from hopping to a neighboring site along the surface. The activation energy for surface diffusion, $\Delta E_{\text{D}}^*(\text{surface})$ is an experimental parameter that is of the magnitude of this potential energy barrier. ΔE_{D}^* can be experimentally determined on well-characterized surfaces by field ion microscopy for example, and for Ar, W

adatoms and 0 atoms on tungsten surfaces has the value 2 kcal mol^{-1} , 15 kcal mol^{-1} and 10 kcal mol^{-1} respectively. For small values of $\Delta E_{D(\text{surface})}^*$ ordering is restricted to low temperatures, since as the temperature is increased the adsorbate becomes very mobile. As the value of $\Delta E_{D(\text{surface})}^*$ increases, ordering cannot commence at low temperature since the adsorbate atoms need to have a considerable mean free path along the surface to find their equilibrium position once they land on the surface at a different location. Naturally, if the temperature is too high, the adsorbate will desorb or vaporize.

The binding forces of adsorbates on substrates have components perpendicular and parallel to the surface. The perpendicular component is primarily responsible for the binding energy (ΔH_{ads}), while the parallel component often determines the binding site on the surface. The binding site may also be affected by adsorbate-adsorbate interactions, which produce ordering within an overlayer. These interactions may be subdivided into direct adsorbate-adsorbate interactions (not involving the substrate at all) and substrate mediated interactions. The latter are complicated many-atom interactions, for example dipole-dipole interactions.

The adsorbate-adsorbate interactions may be repulsive; they always are repulsive at sufficiently small adsorbate-adsorbate separations. At larger separations they may be attractive, giving rise to the possibility of island formation. They may also be oscillatory, moving back and forth between attractive and repulsive as a function of adsorbate-adsorbate separation, with a period of several angstroms giving rise, for example, to non-close-packed islands.

Except for the strong repulsion at close separations, the adsorbate-adsorbate interactions are usually weak compared to the adsorbate-substrate interactions, even when one considers only the components of the forces parallel to the surface. In the case of chemisorption, where the adsorbate-substrate interaction dominates, the adsorbates usually choose an adsorption site that is independent of the coverage and of the overlayer arrangement (the positions the other adsorbates choose). This adsorption site is usually that location which provides the largest number of nearest substrate neighbors, which is independent of the position of other adsorbates. Adsorbates with these properties normally do not accept close packing; the substrate controls the overlayer geometry and imposes a unique adsorption site. Close packing of an adsorbate layer is also observed. In this case the overlayer chooses its own lattice (normally a hexagonal close-packed arrangement) with its own lattice constant independent of the substrate lattice and results in the formation of incommensurate lattices. In this case no unique adsorption site exists; each adsorbate is differently situated with respect to the substrate. This situation is especially common in the physisorption of rare gases. Their relatively weak adsorbate-substrate interactions allow the adsorbate-adsorbate interactions to play the dominant role in determining the overlayer geometry.

The chemisorption case is exemplified by oxygen and sulfur on metals; the physisorption case by krypton and xenon on metals and graphite. Intermediate cases exist. Although undissociated CO on

metals is not physisorbed but chemisorbed, it sometimes produces incommensurate close-packed hexagonal overlayers.

The Effect of Temperature on Ordering

Temperature has a major effect on the ordering of adsorbed monolayers: all of the important ordering parameters (the rates of desorption, and surface and bulk diffusion) are exponential functions of the temperature.

The influence of temperature on the ordering of C_3 - C_8 saturated hydrocarbons on the Pt(111) crystal face is shown in Fig. 11. At the highest temperatures, adsorption may not take place, since under the exposure conditions the rate of desorption is greater than the rate of condensation of the vapor molecules. As the temperature is decreased, the surface coverage increases and ordering becomes possible. First, one-dimensional lines of molecules form, then at lower temperatures ordered two-dimensional surface structures form. Not surprisingly, the temperatures at which these ordering transitions occur depend on the molecular weights of the hydrocarbons, which also control their vapor pressure, heats of adsorption, and activation energies for surface diffusion. As the temperature is further decreased, multilayer adsorption may occur and epitaxial growth of crystalline thin films of hydrocarbon commences.

Figure 11 clearly demonstrates the controlling effect of temperature on the ordering and the nature of ordering of the adsorbed monolayer. Although changing the pressure at a given temperature may be used to vary the coverage by small amounts and thereby change the

surface structures in some cases, the variation of temperature has a much more drastic effect on ordering.

Temperature also markedly influences chemical bonding to surfaces. There are adsorption states that can only be populated if the molecule overcomes a small potential-energy barrier. The various bond-breaking processes are similarly activated. The adsorption of most reactive molecules on chemically active solid surfaces takes place without bond breaking at sufficiently low temperatures. As the temperature is increased, bond breaking occurs sequentially until the molecule is atomized. Thus the chemical nature of the molecular fragments will be different at various temperatures. There is almost always a temperature range for the ordering of intact molecules in chemically reactive adsorbate-substrate systems. It appears that for these systems ordering is restricted to low temperatures below 150 K, and consideration of surface mobility becomes, perhaps, secondary.

The Effect of Surface Irregularities on Ordering

A solid surface exhibits a large degree of roughness on a macroscopic scale. Therefore it is to be expected that if nucleation is an important part of the ordering process, surface roughness is likely to play an important role in preparing ordered surface structures. The transformation temperature or pressure at which one adsorbate surface structure converts into another can also be affected by the presence of uncontrolled surface irregularities (surface defects). Other causes that could influence ordering are the presence of small amounts of surface impurities that block nucleation sites or interfere with

the kinetics of ordering, or impurities below the surface that are pulled to the surface during adsorption and ordering.

The effect of surface irregularities on ordering can be investigated in a more controlled way using stepped crystal surfaces. In general, the smaller the ordered terrace between the steps, the stronger the effect of steps on ordering. For instance, the ordering of small molecular adsorbates on a high Miller index Rh(S)-[6(111) x (100)] is largely unaffected by the presence of steps whereas on the Rh(S)[3(111) x (111)] the ordering is influenced by the higher step density. Steps can also affect the nucleation of ordered domains. It is frequently observed on W and Pt stepped surfaces that when two or three equivalent ordered domains may form in the absence of steps, only one of the ordered domains grows in the presence of steps.

The Effect of Coadsorbates on Ordering

Recently it has been found that although certain molecules may not order when present on their own on a surface they can be induced to order by coadsorption of either carbon monoxide or nitric oxide. For example Table 1 summarizes the ordered structures that have been observed by the coadsorption of alkylidynes, acetylene, aromatics and alkalis with CO on Rh(111).

At low temperature both Na and ethynylidyne form (2 x 2) overlayers on Rh(111), but with increasing temperature begin to disorder. If CO is coadsorbed then the adsorbates can be re-ordered into a c(4 x 2) unit cell.

It is thought that the nature of this type of ordering process is due to adsorbate-adsorbate interactions: a molecule which might not otherwise order due to weak adsorbate-adsorbate interactions is ordered by coadsorbing a molecule such as CO which has interactions strong enough to induce ordering in the overlayer. Similar phenomena have been observed on Pt(111) and it is thought that this coadsorbate-induced ordering may prove to be a very general phenomenon.

Ordered Adsorbate Structures

As mentioned in the introduction to this section well over one thousand ordered adsorbate structures have been observed with LEED. A full listing and discussion of these structures is outside the scope of this article, but they can be found for instance in the book by Somorjai. Instead, one example of each of the three following categories of adsorption will be presented to give an illustrative indication of the types of structures found: (i) an ordered monolayer of atoms (ii) ordered organic monolayer and (iii) ordered molecular monolayer. First, a few generalities of the ordered adsorbate structures are discussed, based on the large number of LEED observations: the so-called "rules of ordering."

(a) The rule of close-packing. Adsorbed atoms or molecules tend to form surface structures characterized by the smallest unit cell permitted by the molecular dimensions and adsorbate-adsorbate and adsorbate-substrate interactions. They prefer close-packing arrangements. Large reciprocal unit meshes are uncommon and the most frequently observed meshes are the same size as the substrate mesh i.e.

(1 x 1), or are approximately twice as large e.g. (2 x 2), c(2 x 2), (2 x 1), ($\sqrt{3} \times \sqrt{3}$).

(b) The rule of rotational symmetry. Adsorbed atoms or molecules form ordered structures that have the same rotational symmetry as the substrate surface. If the surface unit mesh has a lower symmetry than the substrate, then domains of the various possible mesh orientations are to be expected on different areas of the surface with a resulting increase in symmetry.

(c) The rule of similar unit cell vectors. Adsorbed atoms as molecules in monolayer thickness tend to form ordered surface structures characterized by unit cell vectors closely related to the substrate unit cell vectors. The surface structure bears a closer resemblance to the substrate structure than to the structure of the bulk condensate.

These are not hard-and-fast rules but rather are generalizations of a great many systems.

(i) Ordered atomic monolayers.

Some important conclusions can be drawn from the known structures of atomic adsorbates on single crystal surfaces. First, the adsorbed atoms tend to occupy sites where they are surrounded by the largest number of substrate atoms (largest coordination number). This site is usually the one that the bulk atoms would occupy in order to continue the bulk lattice into the overlayer. The tendency toward occupying the site with the largest coordination number during adsorption on metals holds independently of the crystallographic face of a given

metal, the metal for a given crystallographic face, and the adsorbate for a given substrate. Second, the adsorbed atom-substrate atom bond lengths are similar to the bond lengths in organometallic compounds that contain the atom pairs under consideration.

The most common adsorption geometries are displayed in Fig. 12. The threefold hollow sites on the fcc(111) and hcp(0001) and bcc(110) are shown both in top and side views. Similarly, the fourfold hollow sites on the fcc(100) and bcc(100) crystal faces are shown. Finally, the center, long-bridge, and short-bridge sites on the fcc(100) crystal face and the location of atoms in an underlayer in the hcp(0001) crystal face are also displayed.

In addition to the situations discussed, there exist some unique atomic adsorbate geometries. For example small atoms such as nitrogen and hydrogen often prefer to sit below the surface, as in the case of titanium single crystal surfaces. Also in the presence of strong chemical interactions there may be a rearrangement of the substrate layer (an adsorbate induced reconstruction). One example is oxygen on the Fe(100) crystal face.

As an example of ordered atomic adsorption Fig. 13 portrays the two structures of sulfur on Ni(100). At a coverage of one quarter of a monolayer of S, a p(2 x 2) overlayer is formed, and at one-half of a monolayer a c(2 x 2) structure is observed. In both cases the S sits in the 4-fold hollow site (highest coordination). A LEED intensity analysis has been performed for both structures, and within experimental error the bond lengths are the same for both structures.

(ii) Ordered molecular monolayers

Molecules adsorbed on surfaces may retain their basic molecular identity, bonding as a whole to the substrate. They may dissociate into their constituent atoms, which bond individually to the substrate. Alternatively, molecules may break up into smaller fragments which become largely independent or recombine into other configurations. There are also cases of intermediate character where relatively strong bonding distorts the molecule.

One example of ordered molecular monolayers is CO on Pd(111). The (111) surface of fcc metals is the close-packed plane and shows similar ordering for adsorbed CO for a variety of transition metals. That is the $(\sqrt{3} \times \sqrt{3})\text{-R}30^\circ$ structure, formed at a coverage of one-third of a monolayer on the (111) faces of Pd, Ni, Fe, Ir, Cu and Rh. This similarity in ordering is probably due to their surfaces being rather smooth with respect to variations in the CO adsorption energy. Smaller diffusion barriers between different adsorption sites are to be expected, and for large coverages repulsive interactions will be mainly responsible for the arrangement of the adlayer. Figure 14 shows a schematic representation of this $(\sqrt{3} \times \sqrt{3})\text{-R}30^\circ$ CO structure on Pd(111) and the corresponding observed LEED pattern. A LEED structural analysis has not been performed for this structure, but supporting evidence using infrared spectroscopy indicates that the CO molecules sit in the 3-fold hollow sites. As the coverage, θ , is increased to one-half of a monolayer the LEED pattern transforms to a $c(4 \times 2)$. In this structure the CO molecules all sit in twofold bridge sites. If the adsorp-

tion takes place at low temperature (90 K), increasing the CO coverage beyond $\theta = 0.5$ leads to the appearance of a series of LEED patterns arising from hexagonal superstructures, which by a continuous compression and rotation of the $c(4 \times 2)$ unit cell lead to a (2×2) coincidence pattern at a coverage of $\theta = 0.75$. These transformations are also shown schematically in Fig. 14.

(iii) Ordered Organic Monolayers

The adsorption characteristics of organic molecules on solid surfaces are important in several areas of surface science. The nature of the chemical bonds between the substrate and the adsorbate, and the ordering and orientation of the adsorbed organic molecules, play important roles in adhesive, lubrication, and hydrocarbon catalysis.

There are many examples in the literature of ordered structures observed by LEED, but only a few of these structures have been calculated from the diffraction beam intensities. However, the ordering characteristics and size and orientation of the unit cells have been determined from the geometry of the LEED patterns. By studying the systematic variation of their shape and bonding characteristics correlations can be made between these properties and their interactions with the metal surfaces.

Examples of ordered organic monolayers are normal paraffins on platinum and silver (111) surfaces. If straight-chain saturated hydrocarbon molecules from propane (C_3H_8) to octane (C_8H_{18}) are deposited from the vapor phase onto Pt or Ag (111) between 100 to 200 K ordered monolayers are produced. As the temperature is decreased a

thick crystalline film can condense. The paraffins adsorb with their chain axis parallel to the platinum substrate, and their surface unit cell increases smoothly with increasing chain length as shown in Fig. 15.

Multilayers condensed on top of the ordered monolayers maintain the same orientation and packing found in the monolayers. The monolayer structure determines the growth orientation and the surface structure of the growing organic crystal. This phenomenon is called pseudomorphism and, as a result, the surface structures of the growing organic crystals do not correspond to planes in their reported bulk crystal structures.

Vibrational Spectroscopy

Vibrational frequencies have been used for many years by chemists to identify bonding arrangements in molecules. Each bond has its own frequency, so the vibrational spectrum yields information on the molecular structure. This same information can now be obtained when molecules are adsorbed on single-crystal surfaces and, when combined with another surface-structure sensitive technique e.g. LEED, gives a very powerful combination of surface-structure determination. Vibrational spectroscopy also provides significant information on the identity of the surface species, its geometric orientation, the adsorption site, the adsorption symmetry, the nature of the bonding involved, and in some cases, bond lengths, bond angles, and bond energies. For example, if CO is adsorbed and one observes the C-O stretching mode the adsorption is molecular, whereas if the individual modes of metal-C

and metal-O are observed then dissociation has taken place. In addition, each of these vibrational modes (C, O, CO) has a different frequency for each bonding site. The intensities also relate to the concentration of each species on the surface.

The most common type of vibrational spectroscopy which is used for studying surface-adsorbate complexes on single-crystal surfaces is high resolution electron energy loss spectroscopy (EELS).

Electrons scattering off surfaces can lose energy in various ways. One of these involves excitation of the vibrational modes of atoms and molecules on the surface. The technique to detect vibrational excitation from surfaces by incident electrons is called high-resolution electron energy loss spectroscopy (EELS).

Experimentally, a highly monoenergetic beam of electrons is directed towards the surface, and the energy spectrum and angular distribution of electrons backscattered from the surface is measured. In a typical experiment the kinetic energy of the incident electron beam is in the range 1-10 eV. Under these conditions the electrons penetrate only the outermost few layers of the crystal, and the backscattered electrons contain only surface information. The incident electrons, monochromatized typically between 3 and 10 meV ($\sim 25-80 \text{ cm}^{-1}$, $1 \text{ meV} = 8.065 \text{ cm}^{-1}$) and with energy E_i , can lose energy $\hbar\omega$ upon exciting a quantized vibrational mode. These backscattered electrons of energy $E_i - \hbar\omega$ produce the vibrational spectrum. There are several designs of electron monochromator and electron energy analyzers for performing EELS, and one of the most common designs, that of a single-pass 127°

cylindrical electrostatic deflector, is shown in Fig. 16. A typical EELS spectrum, that of CO on Rh(111) is shown in Fig. 17.

The sensitivity of EELS in detecting submonolayer quantities of adsorbates on the sample depends on the particular parameters of the spectrometer, the sample, and the adsorbate. However, typical sensitivity is quite high due in part to the high inelastic electron cross section. A detection limit of $\sim 10^{-4}$ monolayers can be achieved for a strong dipole scatterer such as CO. In addition, unlike many other surface spectroscopies, EELS is also capable of detecting adsorbed hydrogen, although at a lower sensitivity (typically 10^{-1} - 10^{-2} monolayers). It is a non-destructive technique, and can be used to explore the vibrational modes of weakly adsorbed species and those susceptible to beam damage, such as hydrocarbon overlayers.

The spectral range accessible with HREELS is quite large. Typical experiments examine between 200 and 4000 cm^{-1} , but much larger regions can be analyzed. Vibrational modes as far out as 16,000 cm^{-1} have been examined. Besides fundamentals, energy losses due to overtones, combination bands, and multiple losses are distinguishable.

A distinct advantage of EELS is that electrons can excite the vibrational modes of the surface by three different mechanisms: dipole scattering, impact scattering, and resonance scattering. By analyzing the angular dependence of the inelastically scattered electrons a complete symmetry assignment of the surface-adsorbate complex can be made.

The restrictions on the adsorption system are minimal: ordered or disordered overlayers can be examined, as can either well-structured single crystal samples or optically rough surfaces. Hence, chemisorption on evaporated films can be studied, as can the nature of metal overlayer-semiconductor interactions. In addition, coadsorbed atoms and molecules can be studied without difficulty.

The major disadvantage of EELS, especially compared to optical techniques, is the relatively poor instrumental resolution, which usually varies between 3-10 meV (25-80 cm^{-1}). The spectral resolution hinders assignment of vibrations due to individual modes, although peak assignments can be made to within 10 cm^{-1} . The high-sensitivity of EELS coupled with the advantages discussed above has encouraged rapid development and use of this technique, despite resolution limitations, such that it has now been used to study hundreds of adsorptions systems.

As an example of the type of surface chemistry that can be followed using EELS, Fig. 18 shows a series of EELS spectra of the adsorption and thermal decomposition of ethylene on Rh(111).

THERMODYNAMICS OF SURFACES

Introduction

The environment of atoms in a surface is substantially different to that of atoms in the bulk of the solid. Surface atoms are surrounded by fewer nearest neighbors than bulk atoms, and these neighbors are not distributed evenly around the surface atoms. An atom in

the interior experiences no net forces, but these forces become unbalanced at the surface. Consequently the thermodynamic parameters used to describe surfaces are defined separately from those that characterize the bulk phase. The specific surface energy, E^S , the energy per surface area, is related to the total energy E , by

$$E = NE^0 + AE^S \quad (4)$$

where A is the surface area of a solid comprised of N atoms, and E^0 is the energy of the bulk phase per atom. E^S is therefore the excess of total energy that the solid has over E^0 , which is the energy that the system would have if the surface were in the same thermodynamic state as the interior.

The other surface thermodynamic functions are defined similarly, for example the specific surface free energy, G^S is given by

$$G^S = H^S - TS^S \quad (5)$$

where H^S and S^S are the specific surface enthalpy and entropy respectively.

Surface Tension in a One-Component System

Creating a surface involves breaking chemical bonds and removing neighboring atoms, and this requires work. Under conditions of constant temperature and pressure at equilibrium, the surface work δW^S is given by

$$\delta W_{T,P}^S = d(G^S A) \quad (6)$$

where ΔA is the increase in the surface area. If G^S is independent of the surface area, surface work is

$$\delta W_{T,P}^S = G^S dA \quad (7)$$

In a one-component system the specific surface free energy, G^S is frequently called the surface tension or surface pressure, and is denoted by γ . γ may be viewed as a pressure along the surface opposing the creation of new surface. It has dimensions of force per unit length (dyn/cm, ergs/cm² or N/m). The surface tension γ , for an unstrained phase, is also equal to the increase of the total free energy of the system per unit increase of the surface area

$$\gamma = G^S = \left(\frac{\partial G}{\partial A} \right)_{T,P} \quad (8)$$

The free energy of formation of a surface is always positive, since work is required in creating a new surface which increases the total free energy of the system. In order to minimize their free energy solids or liquids assume shapes in equilibrium with the minimum exposed surface area as possible. For example, liquids tend to form a spherical shape and crystal faces which exhibit the closest packing of atoms tend to be the surfaces of lowest free energy of formation and thus the most stable. Surface tension is one of the most important thermodynamic parameters characterizing the condensed phase. Table 2 lists selected experimentally determined values of surface tensions of liquids and solids that were measured in equilibrium with their vapor.

Comparing the surface tension values of metals and oxides in Table 2 it can be seen that oxides have in general a low surface tension. Therefore, a reduction in the total free energy of the system can be achieved by oxidation of the surface and a uniform oxide layer covering the surface is expected under conditions near thermodynamic equilibrium. Similarly, deposition and growth of a metal film on a metallic substrate of higher surface tension should yield a uniform layer that is evenly spread to completely cover the substrate surface. Likewise, a very poor spreading of the film is expected upon deposition of a metal of high surface tension on a low surface tension substrate. This latter condition results in "island growth" and the deposited high surface tension metal will grow as whiskers to expose as much of the low surface tension substrate during the growth as possible. These, of course, are surface thermodynamic predictions, and may be overridden by the presence of impurities at the surface or difficulties of nucleation.

Since atomic bonds have to be broken to create surfaces, it is expected that the specific surface free energy will be related to the heat of vaporization, which is related to the energy input necessary to break all the bonds of atoms in the condensed phase. In fact it has been found experimentally that the molar surface free energy of a liquid metal can be estimated by:

$$\gamma_{lm} = 0.15 \Delta H_{vap} \quad (9)$$

where ΔH_{vap} is the heat of vaporization of the liquid, and the molar surface free energy of a solid metal by:

$$\gamma_{\text{sm}} = 0.16 \Delta H_{\text{sub}} \quad (10)$$

where ΔH_{sub} is the heat of sublimation of the solid.

For other materials, oxides, or organic molecules, such a simple relationship does not work due to the complexity of bonding and the rearrangement or relaxation of surface atoms at the freshly created surfaces.

Surface Tension of Multicomponent Systems

In many important surface phenomena, such as heterogeneous catalysis or passivation of the surface by suitable protective coatings, the chemical composition of the top-most layer controls the surface properties, and not the composition in the bulk. Thus, investigations of the physical-chemical parameters that control the surface composition are of great importance. One of the major driving forces for the surface segregation of impurities from the bulk and for the change of composition of alloys and other multicomponent systems is the need to minimize the surface free energy of the condensed phase system.

The change of the total free energy of a multicomponent system can be expressed with the inclusion of the surface term as

$$dG = SdT + VdP + \gamma dA + \sum_i \mu_i dn_i \quad (11)$$

where μ_i is the chemical potential of the i^{th} component and dn_i is the change in the number of moles of the i^{th} component. At con-

stant temperature and pressure, equation (11) can be rewritten as

$$dG_{T,p} = \gamma dA - \sum_i \mu_i dn_i \quad (12)$$

where the minus sign indicates the decrease of the bulk concentration of the i^{th} component. Comparing this equation with Eq. (8), the surface tension γ is no longer equal to the specific surface free energy per unit area for a multicomponent system. Using simple arguments in which number of moles of the condensed phase are transferred to the freshly created surface, the Gibbs equation can be derived

$$d\gamma = -S^S dT - \sum \Gamma_i d\mu_i \quad (13)$$

where Γ_i is the excess number of moles of compound i at the surface. Just like the free energy relations for bulk phases, the Gibbs equation predicts changes in surface tension as a function of experimental variables such as temperature and surface concentration of various components. As a result of the Gibbs equation, the surface composition in equilibrium with the bulk for a multicomponent system can be very different from the bulk composition.

As an example we will discuss the surface composition of an ideal binary solution. For such a solution at a constant temperature the Gibbs equation can be expressed as

$$d\gamma_T = -\Gamma_1 d\mu_1 - \Gamma_2 d\mu_2 \quad (14)$$

and it has been shown that the surface tension of component 1 in an

idea dilute solution is given by

$$\gamma = \gamma_1 + (RT/a) \ln (X_1^S/X_1^b) \quad (15)$$

where γ_1 is the surface tension of the pure component and a is the surface area occupied by one mole of component 1. Perfect behavior is assumed, i.e. the surface areas occupied by the molecules in the two different components are the same ($a_1 = a_2 = a$). X_1^S and X_1^b are the atom fractions of component 1 in the surface and in the bulk, respectively. It is also assumed that the surface consists of only the topmost atomic layer. For a two component system, Eq. (15) can be rewritten in the form

$$\frac{X_1^S}{X_2^S} = \frac{X_1^b}{X_2^b} \exp \left[\frac{(\gamma_2 - \gamma_1)a}{RT} \right] \quad (16)$$

where X_1^S , X_2^S , X_1^b , X_2^b have their meaning defined above, γ_1 and γ_2 are the surface tensions of the pure components, and the other symbols have their usual meaning. From Eq. (16), it can be seen that the component that has the smaller surface tension will accumulate on the surface.

Equation (16) also predicts that the surface composition of ideal solutions should be an exponential function of temperature. While the bulk composition of a multicomponent system is little affected by temperature, the surface concentration of the constituents may change markedly.

The surface segregation of one of the constituents becomes more pronounced the larger the difference in surface tensions between the components that make up the solution. Surface segregation is expected to be prevalent for metal solutions, since metals have the highest surface tensions.

In reality, however, metallic alloys are not ideal solutions since they have some finite heat of mixing. In such a case the surface composition can be approximated in the regular solution monolayer approximation

$$\frac{x_2^S}{x_1^S} = \frac{x_2^b}{x_1^b} \exp\left[\frac{(\gamma_1 - \gamma_2)a}{RT}\right] \exp\left\{\frac{\Omega(1+m)}{RT} \left[(x_1^b)^2 - (x_2^b)^2\right] + \frac{\Omega l}{RT} \left[(x_2^S)^2 - (x_1^S)^2\right]\right\} \quad (17)$$

where Ω is the regular solution parameter and is directly related to the heat of mixing ΔH_m by

$$\Omega = \frac{\Delta H_m}{x_1^b(1 - x_1^b)}$$

l is the fraction of nearest neighbors to a atom in the plane and m is the fraction of nearest neighbors below the plane containing the atom. In this approximation the surface composition becomes a fairly strong function of the heat of mixing, its sign, and its magnitude in addition to the surface tension difference and temperature.

Auger electron spectroscopy (AES) and ion scattering spectroscopy (ISS) are two experimental techniques which are most frequently used for quantitative determination of the surface composition. Figure 19 shows the surface atom fraction of gold, determined by AES and ISS, plotted as a function of the bulk atom fraction for the Ag-Au system. The solid line gives the calculated surface composition using the regular solution model and the dashed line indicates the curve that would be obtained in the absence of surface enrichment. The regular solution model appears to overestimate somewhat the surface segregation in this case, although the surface is clearly enriched in silver.

Table 3 lists several binary alloy systems that have been investigated experimentally by AES or ISS and the segregating components that were experimentally observed and also predicted by the regular solution model. The agreement is certainly satisfactory. It appears that for binary-metal-alloy systems that exhibit regular solution behavior there are reliable methods to predict surface composition.

So far we have discussed the surface composition of multicomponent systems that are in equilibrium with their vapor or in which clean surface-bulk equilibrium is obtained in ultrahigh vacuum. In most circumstances, however, the surface is covered with a monolayer of adsorbates that frequently form strong chemical bonds with the surface atoms. This solid-gas interaction can markedly change the surface composition in some cases. For example, carbon monoxide, when adsorbed on the surface of a Ag-Pd alloy, forms much stronger bonds with Pd. While the clean surface is enriched with Ag, in the presence of

CO, Pd is attracted to the surface to form strong carbonyl bonds. When the adsorbed CO is removed, the composition returns to its original Ag-enriched state. Nonvolatile adsorbates, such as carbon or sulfur, may have a similar influence on the surface composition as long as their bonding to the various constituents of the multicomponent system is different.

Adsorbates should therefore be viewed as an additional component of the multicomponent system. A strongly interacting adsorbate converts a binary system to a ternary system. As a result, the surface composition may markedly change with changing ambient conditions.

The mechanical properties of solids, embrittlement, and crack propagation, among others, depend markedly on the surface composition. These studies indicate that the surface composition, and the mechanical properties of structural steels, may change drastically when the ambient conditions are changed from reducing to oxidizing environments.

Equilibrium Shape of a Crystal or a Liquid Droplet

In equilibrium the crystal will take up a shape that corresponds to a minimum value of the total surface free energy. In order to have the equilibrium shape, the integral $\int \gamma dA$ over all surfaces of the crystal must be a minimum. Crystal faces that have high atomic density have the lowest surface free energy and are therefore most stable. The plot of the surface free energy as a function of crystal orientation is called the γ -plot.

Solids and liquids will always tend to minimize their surface area in order to decrease the excess surface free energy. For liquids, therefore, the equilibrium surface becomes curved where the radius of curvature will depend on the pressure difference on the two sides of the interface and on the surface tension. In equilibrium

$$(P_{in} - P_{ext}) = \frac{2\gamma}{r} \quad (18)$$

where P_{in} and P_{ext} are the internal and external pressures respectively and r is the radius of curvature. In equilibrium a pressure difference can be maintained across a curved surface. The pressure inside the liquid drop or gas bubble is higher than the external pressure, because of the surface tension. The smaller the droplet or larger the surface tension, the larger the pressure difference that can be maintained. For a flat surface $r = \infty$, and the pressure difference normal to the interface vanishes.

Let us now consider how the vapor pressure of a droplet depends on its radius of curvature, r . We obtain

$$\ln\left(\frac{p}{p_0}\right) = \frac{2\gamma V_{in}}{RT r} \quad (19)$$

where V_{in} is the internal volume. This is the well-known Kelvin equation for describing the dependence of the vapor pressure of any spherical particle on its size. Small particles have higher vapor pressures than larger ones. Similarly, very small particles of solids

have greater solubility than large particles. If we have a distribution of particles of different sizes, we will find that the larger particles will grow at the expense of the smaller ones. Nature's way to avoid the sintering of small particles that would occur according to the Kelvin equation is to produce system with particles of equal size. This is the world of colloids where particles are of equal size and therefore stabilized and are usually charged either all negative or all positive or to repel each other by long range electrostatic forces. Milk, our blood are only two examples of systems that contain colloids.

Adhesion and the Contact Angle

Let us turn our attention to the interfacial tension, that is, the surface tension that exists at the interface of two condensed phases. Let us place a liquid droplet on a solid surface. The droplet either retains its shape and forms a curved surface or it is spread evenly over the solid. These two conditions indicate the lack of wetting or wetting of the solid by the liquid phase, respectively. The contact angle between the solid and the liquid, to a large extent, permits us to determine the interfacial tension between the solid and the liquid. The contact angle is defined by Fig. 20. If the contact angle is large (θ approaching 90°), the liquid does not readily wet the solid surface. If θ approaches zero, complete wetting of the solid surface takes place. For θ larger than 90° the liquid tends to form spherical droplets on the solid surface that may easily run off; i.e., the liquid does not wet the solid surface at all. Remembering that the surface tension

always exerts a pressure tangentially along a surface, the surface free energy balance between the surface forces acting in opposite directions at the point where the three phases solid, liquid, and gas meet is given by

$$\cos\theta = (\gamma_{sg} - \gamma_{sl})/\gamma_{lg} \quad (20)$$

Here γ_{lg} is the interfacial tension at the liquid-gas interface, and γ_{sg} and γ_{sl} are the interfacial tensions between the solid-gas and the solid-liquid interfaces, respectively. Knowing γ_{lg} and the contact angle in equilibrium at the solid-liquid-gas interface, we can determine the difference $\gamma_{sg} - \gamma_{sl}$, but not their absolute values. Since the wetting ability of the liquid at the solid interface is so important in practical problems of adhesion or lubrication, there is a great deal of work being carried out to determine the interfacial tensions for different combinations of interfaces.

The usefulness of a lubricant is determined by the extent to which it wets the solid surface and maintains complete coverage of the surface under various conditions of use. The strength of an adhesive is determined by the extent to which it lowers the surface free energy by adsorption on the surface. The work of adhesion is defined as

$$W_A^S = \gamma_{l,0} + \gamma_{s,0} - \gamma_{sl} \quad (21)$$

where $\gamma_{l,0}$ and $\gamma_{s,0}$ are the surface tensions in vacuum of the liquid and solid, respectively. In general, solids and liquids that have large surface tension form strong adhesive bonds, i.e., have

large work of adhesion. The work of adhesion is in the range of 40-150 ergs/cm² for solid-liquid pairs of various types. Organic polymers often make excellent adhesives because of the large surface area covered by each organic molecule. The adhesive energy per mole is much larger than that for adhesion between two metal surfaces or between a liquid and a solid metal, because of the many chemical bonds that may be formed between the substrate and the adsorbed organic molecule.

Nucleation

Another important phenomenon that owes its existence to positive surface free energy is nucleation. In the absence of a condensed phase, it is very difficult to nucleate one from vapor atoms because the small particles that would form have a very high surface area and dispersion and, as a result, a very large surface free energy. The total energy of a small spherical particle has two major components: its positive surface free energy, which is proportional to $4\pi r^2\gamma$, where r is the radius of the particle, and its negative free energy of formation of the particle with volume V . The volumetric energy term is proportional to $-r^3 \ln(P/P_{eq})$, where P is the pressure over the system and P_{eq} is the equilibrium vapor pressure

$$\Delta G(\text{total}) = -\left(\frac{4\pi r^3}{3V_m}\right) RT \ln\left(\frac{P}{P_{eq}}\right) + 4\pi r^2\gamma \quad (22)$$

where V_m is the molar volume of the forming particle. Initially, the atomic aggregate is very small and the surface-free-energy term is

the larger of the two terms. In this circumstance a condensate particle cannot form from the vapor even at relatively high saturation: $P > P_{eq}$. Similarly, a liquid may be cooled below its freezing point without solidification occurring.

Above a critical size of the spherical particles the volumetric term becomes larger and dominates since it decreases as $\sim r^3$, while the surface-free-energy term increases only as $\sim r^2$. Therefore, a particle that is larger than this critical size grows spontaneously at $P > P_{eq}$. This is shown in Fig. 21. Because of the difficulty of obtaining this critical size, which involves as many as 30 to 100 atoms or molecules, homogeneous nucleation is very difficult indeed. To avoid this problem one adds to the system particles of larger than critical size that "seed" the condensation or solidification. The use of small particles to precipitate water vapor in clouds to start rain and the use of small crystallites as seeds in crystal growth are two examples of the application of heterogeneous nucleation.

Physical and Chemical Adsorption

The concepts of physical adsorption (physisorption) and chemical adsorption (chemisorption) were introduced earlier. The nature of the two classifications is linked to the heat of adsorption, ΔH_{ads} , which is defined as the binding energy of the adsorbed species. Physical adsorption is caused by secondary attractive forces (Van der Waals) such as dipole-dipole interaction and induced dipoles and is similar in character to the condensation of vapor molecules onto a liquid of the same composition.

The interaction can be described by the one-dimensional potential energy diagram shown in Fig. 22. An incoming molecule with kinetic energy E_k has to lose at least this amount of energy in order to stay on the surface. It loses energy by exciting lattice phonons in the substrate for example, and the molecule comes to equilibrium in a state of oscillation in the potential well of depth equal to the binding energy or adsorption energy, $E_a = \Delta H_{ads}$. In order to leave the surface (desorb) the molecule must acquire enough energy to surmount the potential-energy barrier E_a . The desorption energy is equal to the adsorption energy. The binding energies of physisorbed molecules are typically ≤ 15 kcal/mol.

Chemisorption involves chemical bonding, it is similar to a chemical reaction, and involves transfer of electronic charge between adsorbent and adsorbate. The most extreme form of chemisorption occurs when integral numbers of electrons are transferred, forming a pure ionic bond. More usually there is an admixture of the wavefunctions of the valence electrons of the molecule with the valence electrons of the substrate into a new wavefunction. The electrons responsible for the bonding can then be thought of as moving in orbitals between substrate and adatoms and a covalent bond has been formed. Two examples of the potential energy diagrams for chemisorption are shown in Fig. 23. Some of the impinging molecules are accommodated by the surface and become weakly bound in a physisorbed state (also called a precursor state) with binding energy E_p . During their stay time in this state, electronic or vibrational processes can occur which allow

them to surmount the energy barrier and electron exchange occurs between the adsorbate and substrate. The molecule, or atoms in the case of dissociative chemisorption, now finds itself in a much deeper well; it is chemisorbed. Figure 23(a) shows the case where the energy barrier for chemisorption is less than E_p , so there is no overall activation energy to chemisorption. Figure 23(b) illustrates the case where there is an overall activation energy, ΔE^* , to chemisorption. In the former case the activation energy for desorption, E_d , is equal to the heat of adsorption, while in the latter case the heat of adsorption is given by the difference between the heat of desorption and the activation energy. The occurrence of an activation energy to chemisorption is by far the exception rather than the rule.

From the above considerations it is expected that to a first approximation physisorption will be non-specific, any gas will adsorb on any solid under suitable circumstances. However, chemisorption will show a high degree of specificity. Not only will there be variations from metal surface to metal surface, as would be expected from the differences in chemistries between the metals, but also different surface planes of the same metal may show considerable differences in reactivity towards a particular gas.

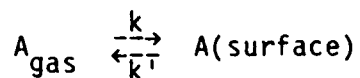
Adsorption Isotherms

An adsorption isotherm is the relationship at constant temperature between the partial pressure of the adsorbate and the amount adsorbed at equilibrium. Similarly an adsorption isobar expresses the functional relationship between the amount adsorbed and the temperature at

constant pressure, and an adsorption isostere relates the equilibrium pressure of the gaseous adsorbate to the temperature of the system for a constant amount of adsorbed phase. Usually it is easiest from an experimental viewpoint to determine isotherms. The coordinates of pressure at the different temperatures for a fixed amount adsorbed can then be interpolated to construct a set of isosteres, and similarly to obtain an isobaric series.

Adsorption isotherms can be used to determine thermodynamic parameters that characterize the adsorbed layer (heats of adsorption and the entropy and heat capacity changes associated with the adsorption process), and in the case of adsorption isotherms for physical adsorption, to determine the surface area of the adsorbing solid.

Consider a uniform surface with a number, n_0 , of equivalent adsorption sites. The ratio of the number of adsorbed atoms or molecules, n , to n_0 is defined as the coverage, $\theta = n/n_0$. Atoms or molecules impinge on the surface from the gas phase, where they establish a surface concentration $[n_a]_s$ (molecules/cm²). Assuming that only one type of species of concentration $[n_a]_g$ (molecules/cm³) exists in the gas phase the adsorption process can be written



and the net rate of adsorption as

$$F(\text{molecules/cm}^2\text{s}) = k[n_a]_g - k'[n_a]_s \quad (23)$$

where k and k' are the rate constants for adsorption and desorption

respectively. Starting with a nearly clean surface far from equilibrium, the rate of desorption may be taken as zero and Eq. (23) becomes

$$F(\text{molecules/cm}^2/\text{s}) = k[n_a]_g \quad (24)$$

where k , derived from the kinetic theory of gases, equals $\alpha \left(\frac{RT}{2\pi M} \right)^{1/2}$ cm/s. α is the adsorption coefficient and M the molecular weight of the impinging molecules. The surface concentration $[n_a]_s$ under these conditions is the product of the incident flux, F , and the surface residence time, τ .

$$[n_a]_s = F\tau \quad (25)$$

τ is the surface residence time, given by

$$\tau = \tau_0 \exp(\Delta H_{\text{ads}}/RT) \quad (26)$$

Replacing $[n_a]_g$ by the pressure using the ideal gas law, Eq. (25) can be rewritten as

$$[n_a]_s = \frac{\alpha P N_A}{(2\pi MRT)^{1/2}} \tau_0 \exp\left(\frac{\Delta H_{\text{ads}}}{RT}\right) \quad (27)$$

The simplest adsorption isotherm is obtained from Eq. (27) which can be rewritten as

$$\theta = k''P \quad (28)$$

where $k'' = \frac{1}{n_0} \frac{\alpha N_A}{(2\pi MRT)^{1/2}} \tau_0 \exp\left(\frac{\Delta H_{\text{ads}}}{RT}\right)$ (29)

The coverage is proportional to the first power of the pressure at a given temperature provided that there are an unlimited number of adsorption sites available and ΔH_{ads} does not change with coverage.

The isotherm of Eq. (28) is unlikely to be suitable to describe the overall adsorption process, but the Langmuir isotherm is a simple modification which represents a more real situation. The Langmuir isotherm assumes that adsorption is terminated upon completion of one molecular adsorbed gas layer (monolayer) by asserting that any gas molecule that strikes an adsorbed atom must reflect from the surface. All the other assumptions used to derive Eq. (28) are maintained (i.e. homogeneous surface, non-interacting adsorbed species). If $[n_0]$ is the surface concentration of a completely covered surface, the number of surface sites available for adsorption, after adsorbing $[n_a]_s$ molecules is $[n_0] - [n_a]_s$. Of the total flux incident on the surface, a fraction $([n_a]_s/[n_0])F$ will strike molecules already adsorbed and therefore be reflected. Thus a fraction $(1 - [n_a]_s/[n_0])F$ of the total incident flux will be available for adsorption. Equation (25) should then be modified as

$$[n_a]_s = \left(1 - \frac{[n_a]_s}{[n_0]}\right)F\tau \quad (30)$$

which can be rearranged to give

$$[n_a]_s = \frac{[n_0] F\tau}{[n_0] + F\tau} = \frac{[n_0] kP}{[n_0] + kP} \quad (31)$$

from which

$$\theta = \frac{k'P}{1 + k'P} \quad (32)$$

where $k' = k/[n_0]$.

Equation (32) is the Langmuir Isotherm. The adsorption of CO on Pd(111) obeys the Langmuir isotherm, and typical isotherms from this system are shown in Fig. 24. It can readily be shown that in the case of dissociative adsorption the Langmuir isotherm becomes

$$P = \frac{1}{k'P} \left(\frac{\theta}{1 - \theta} \right)^2$$

or

$$\theta = \frac{(k'P)^{1/2}}{1 + (k'P)^{1/2}} \quad (33)$$

A clear weakness of the Langmuir model is the assumption that the heat of adsorption is independent of coverage. Several other isotherms have been developed which are all modifications of the Langmuir model. For example the Temkin isotherm can be derived if a linearly declining heat of adsorption is assumed, i.e. $\Delta H = \Delta H_0(1 - \beta\theta)$, where ΔH_0 is the initial enthalpy of adsorption. The isotherm is

$$\theta = \frac{RT}{\beta\Delta H_0} \ln AP \quad (34)$$

where A is a constant related to the enthalpy of adsorption.

The possibility of multi-layer adsorption is envisaged in the Brunauer-Emmett-Teller (BET) isotherm. The assumption is made that the first layer is adsorbed with a heat of adsorption H_1 and the second and subsequent layers are all characterized by heats of adsorption equal to the latent heat of evaporation, H_L . By considering the dynamic equilibrium between each layer and the gas phase the BET isotherm is obtained,

$$\frac{p}{V(p_0 - p)} = \frac{1}{V_m c} + \frac{c - 1}{V_m c} \frac{p}{p_0} \quad (35)$$

In this equation V is the volume of gas adsorbed, p is the pressure of gas, p_0 is the saturated vapour pressure of the liquid at the temperature of the experiment and V_m is the volume equivalent to an adsorbed monolayer. The BET constant c is given by

$$c = \exp(H_1 - H_L)/RT \quad (36)$$

The BET equation owes its importance to its wide use in measuring surface areas, especially of films and powders. The method followed is to record the uptake of an inert gas (Kr) or nitrogen at liquid nitrogen temperature (-195.8°C). A plot of $P/V(p_0 - p)$ vs. p/p_0 , usually for P/p_0 up to about 0.3, yields V_m , the monolayer uptake. This value is expressed as an area by assuming that the area per molecule for nitrogen is 16.2 Å and 25.6 Å for krypton.

In general the BET isotherm is most useful for describing physisorption for which H_1 and H_L are of the same order of magnitude while the preceding isotherms are more useful for chemisorption. It is worth noting that the BET isotherm reduces to the Langmuir isotherm when $H_1 \gg H_L$.

Heat of Adsorption

An important physical-chemical property that characterizes the interaction of solid surfaces with gases is the bond energy of the adsorbed species. The determination of bond energy is usually made indirectly by measuring the heat of adsorption (or heat of desorption)

of the gas. The heat of adsorption can readily be determined in equilibrium by measuring several adsorption isotherms. The Clausius-Clapeyron equation

$$\left(\frac{\partial(L_n P)}{\partial T}\right)_\theta = \frac{\Delta H_{\text{ads}}}{RT^2} \quad (37)$$

can be integrated to give

$$\ln\left(\frac{P_1}{P_2}\right)_\theta = \frac{-\Delta H_{\text{ads}}}{R} \left(\frac{1}{T_1} - \frac{1}{T_2}\right)$$

Measuring the adsorption isotherm at two different temperatures, provided that proper equilibrium is established between the adsorbed and gas phase, yields the heat of adsorption.

The heat of adsorption can also be obtained by direct calorimetry. The method most commonly used consists of measuring the temperature rise caused by the addition of a known amount of gas to a film of the metal prepared by evaporation in vacuo. This measurement will yield the differential heat of adsorption q_d at the particular value of θ . The differential heat of adsorption is related to the isosteric heat of adsorption by

$$q = q_d + RT \quad (38)$$

the difference is only RT which is within experimental error.

The last, and most common, method of determining the heat of adsorption is a kinetic method called temperature programmed desorption (TPD). The method is as follows. The sample is cleaned in ultrahigh vacuum and a gas is allowed to adsorb on the surface at known pressures while the surface is kept at a fixed temperature. Then the sample is heated at a controlled rate, and the pressure changes during the desorption of the molecules are recorded as a function of time and temperature. The pressure-temperature profile is usually referred to as the "desorption spectrum." The desorption rate $F(t)$ is commonly expressed as

$$F(t) = \nu f(\sigma) \exp\left(-\frac{E_{\text{des}}}{RT}\right) \quad (39)$$

where ν is the preexponential factor, $f(\sigma)$ is an adsorbate concentration-dependent function. The various procedures for determining these parameters are well described in the literature.

Assuming that ν and E_{des} are independent of the adsorbate concentration σ and t , E_{des} can be obtained for zero-, first-, and second-order desorption, respectively, as

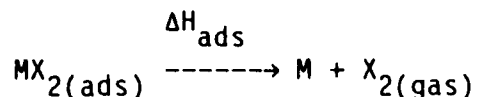
$$E_0/R = \frac{\nu_0}{\sigma a} \exp\left(-\frac{E}{RT_p}\right) \quad (40)$$

$$E_1/RT_p^2 = (\nu_1/\alpha) \exp\left(-\frac{E_1}{RT_p}\right) \quad (41)$$

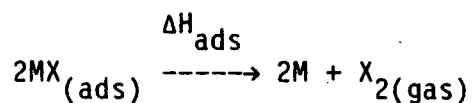
$$E_2/RT_p^2 = (\nu_2\sigma/\alpha) \exp\left(-\frac{E_2}{RT_p}\right) \quad (42)$$

where T_p is the temperature at which a desorption peak is at a maximum and σ is the initial adsorbate concentration. Suffix 0, 1, or 2 denotes the zeroth-, first-, or second-order desorption processes, α is a constant of proportionality for the temperature rise with time, usually $T = T_0 + \alpha t$, that is, the temperature of the sample is raised linearly with time. As seen from the equations, T_p is independent of σ for the first-order desorption process. Alternatively, T_p is increased or is decreased with σ_0 for the zeroth- or second-order process, respectively. Equations (40), (41), and (42) allow one to determine the activation energy and the preexponential factor and also to distinguish between zeroth-, first-, and second-order desorption processes from the measurements of the dependence of the peak temperatures upon initial adsorbate concentrations and heating rate, α . A typical TPD spectrum is shown in Fig. 25.

The bond energy, ΔH_{bond} , is readily extracted from the heat of adsorption. In the case of the chemisorption of a diatomic molecule X_2 onto a site on a uniform solid surface M the molecule may adsorb without dissociation to form MX_2 . In this case, the heat of adsorption, ΔH_{ads} is defined as the energy needed to break the $M-X_2$ bond



If the molecule adsorbs dissociatively, the heat of adsorption is defined as



The energy of the surface chemical bond is then given by

$$\Delta H_{bond}(MX_2) = \Delta H_{ads} \quad \text{for associative adsorption}$$

or

$$\Delta H_{bond}(MX) = \left(\frac{\Delta H_{ads} + D_{X_2}}{2} \right) \quad \text{for dissociative adsorption.}$$

Where D_{X_2} is the dissociation energy of the X_2 gas molecule.

The heat of adsorption is not a constant quantity for a particular adsorbate-substrate system; there are several factors which affect the value of ΔH_{ads} . First, the heat of adsorption can change markedly with the coverage, θ , of the adsorbed phase. An example of this is shown in Fig. 26 for CO on a Pd(111) surface. Decreasing values of ΔH_{ads} with increasing adsorbate coverage are commonly observed due to repulsive adsorbate-adsorbate interactions.

Second, the surface is heterogeneous by nature. There are many sites where the adsorbed species have different binding energies. Perhaps the most striking effect is that for adsorption on stepped and kinked platinum and nickel single crystal surfaces where molecules dissociate in the presence of these surface irregularities while they remain intact on the smooth low-Miller index surfaces. If a polycrystalline surface is utilized for chemisorption studies instead of a structurally well-characterized single-crystal surface the measured ΔH_{ads} will be an average of adsorption at the various binding sites.

In fact, even on the same crystal surface molecules may occupy several different adsorption sites with different coordination numbers and rotational symmetries, and each site may exhibit a different binding energy and therefore a different heat of chemisorption. For example on the (111) face of fcc metals the adsorbates may occupy a threefold site, a twofold bridge site, or an on-top site. Figure 27 shows the measured heats of adsorption of CO on single-crystal surfaces for many different transition metals while Fig. 28 shows the heats of adsorption of CO on polycrystalline transition metal surfaces. The heats of chemisorption on single-crystal planes indicate the presence of binding sites on a given surface which differ by ~ 20 kcal/mol. It is not possible to identify one value of the heat of chemisorption of an adsorbate on a given transition metal unless the binding state is specified or it is certain that only one binding state exists. A polycrystalline surface however exhibits all the adsorption sites of the faces from which it is composed. Since these sites are present simultaneously heats of chemisorption for these surfaces represent an average of the binding energies of the different surface sites. As a result the measured heats of adsorption of Fig. 28 do not show the large structural variations that can be seen in Fig. 27.

The adsorbate may also change bonding as a function of temperature as well as the adsorbate concentration. For example, oxygen may be molecularly adsorbed at low temperatures while it dissociates at higher temperatures.

ELECTRICAL PROPERTIES OF SURFACES

Introduction

Many of the physical and chemical properties of solid surfaces are directly influenced by the concentration of mobile charge carriers (electrons and diffusing ions). The concentration of these free charge carrier varies widely for materials of different types. Metals, which are good conductors of electricity with resistivities in the $10^{-4}\Omega\text{ m}$ range, have large free electron concentrations; almost every atom contributes one electron to the lattice as a whole. For insulators, with a resistivity of $10^9\Omega\text{ m}$, and semiconductors with intermediate values, often less than 1 out of every 10^6 atoms may contribute a free electron. The temperature dependence of the carrier concentration and the conductivity may be different for different materials depending on the mechanism of excitation by which the mobile charge carriers are created.

Under incident radiation or bombardment by an electron beam surfaces emit photons, electrons or both. The emission properties of solid surfaces differ widely, just as their mechanisms of relaxation after excitation by high-energy radiation differ. Many surface sensitive experimental techniques providing information related to the electronic properties of surfaces are based upon these processes, for example Auger electron spectroscopy (AES), x-ray photoelectron spectroscopy (XPS) and ultra-violet photoelectron spectroscopy (UPS). These will be discussed briefly later in this section.

The underlying reason for the differences of the conductivity mechanisms and emission properties on the surfaces of the different materials lies in the differences in their electronic band structure. The band structure model of solids has been successful in explaining many solid state properties and one may apply it with confidence in studies of solid surfaces. There are many excellent textbooks on the subject of solid state physics giving detailed descriptions of the band theory of solids, and a description will not be presented here. In the following section a basic understanding of electron bands is assumed.

The Energy Level Diagram

For many purposes, in analyzing the electrical properties of metals or semiconductors, we are not concerned with the detailed shape of the electronic bands. One may conveniently represent schematically the electronic bands by straight lines where the potential energy of the electron near the top of the valence band and at the bottom of the conduction band is plotted against distance x through the crystal starting from the surface ($x = 0$). The energy gap represents the minimum potential energy difference between the two bands. In this type of diagram the electron energy increases upward and the energy of the positive hole increases downward, as indicated in Fig. 29. For a homogeneous crystal the bands may be horizontal, as shown in this figure. At the surface the bands may vary in energy with respect to their value in the bulk of the solid since the free carrier concentrations at the surface may be different from those in the bulk of the crystal.

Surface Dipole and Surface Space Charge

The anisotropic environment of surface atoms not only gives rise to such processes as surface relaxation and surface reconstruction but also to a redistribution of charge density. For a metal this redistribution can be explained as follows. In the bulk of a metal each electron lowers its energy by "pushing" the other electrons aside to form an "exchange correlation hole." This attractive interaction, V_{exch} , is lost when the electron leaves the solid, so there is a sharp potential barrier V_s at the surface. In a quantum mechanical description, the electrons are not totally trapped at the surface and there is a finite probability for them to spread out into the vacuum. This is depicted in Fig. 30. This charge redistribution induces a surface dipole, V_{dip} , that modifies the barrier potential. The work function, ϕ (which will be discussed in detail below) is the minimum energy necessary to remove an electron at the Fermi energy, E_F , from the metal into the vacuum. The magnitude of this induced surface dipole is different at various sites on the heterogeneous metal surface. For example a step site on a tungsten surface has a dipole of 0.37 Debye (D) per edge atom as measured by work function studies. At a tungsten adatom on the surface there is a dipole moment of 10.

At semiconductor and insulator surfaces the separation of negative and positive charges leads to the formation of a space-charge region. This space-charge region near the surface is formed by the accumulation or depletion of charge carriers in the surface with respect to the bulk carrier concentration. Such a space charge may also be

induced by the application of an external electric field or by the presence of a charged layer on the surface such as adsorbed ions or electronic surface states which act as a source or sink of electrons. The height of the surface potential barrier, V_s , and its distance of penetration into the bulk, d , depends on the concentration of mobile charge carriers in the surface region.

It can be shown that

$$d \approx \left(\frac{2\epsilon\epsilon_0 V_s}{e n_e(\text{bulk})} \right)^{1/2} \quad (43)$$

where ϵ is the dielectric constant in the solid, ϵ_0 is the permittivity of free space, and $n_e(\text{bulk})$ is the bulk carrier concentration. The higher the free carrier concentration in the material, the smaller the penetration depth of the applied field into the medium. Using a typical value of $\epsilon = 16$, for electron concentrations of 10^{17} cm^{-3} or larger, the space charge is restricted to distances on the order of one atomic layer or less. This is due to the large free carrier density screening the solid from the penetration of the electrostatic field caused by the charge imbalance. In most metals almost every atom contributes one free valence electron and since the typical atomic density is of the order of 10^{22} cm^{-3} the free carrier concentration in metals is in the range $10^{20} - 10^{22} \text{ cm}^{-3}$. V_s and d are so small that they can usually be neglected. For semiconductors, or insulators on the other hand, typical free carrier concentrations at room temperature are in the range $10^{10} - 10^{16} \text{ cm}^{-3}$. Therefore, at the surfaces of these materials, there is a space-charge barrier of appreciable height (sev-

eral eV) and penetration depth that could extend over thousands of atomic layers ($\approx 10^4$ Å) into the bulk. This is the reason for the sensitivity of semiconductor devices to ambient changes that affect the space-charge barrier height. There is an induced electric field at the surface under most experimental conditions due to the adsorption of gases or because of the presence of electronic surface states. The electronic and many other physicochemical properties of semiconductor and insulator surfaces depend very strongly on the properties of the space charge. For example, the conduction of free carriers across the solid or along its surface could become space charge limited. The rate of charge transfer from the solid to the adsorbed gas, which results in chemisorption or chemical reaction, can become limited by the transfer rate of electrons over the space-charge barrier.

When the energy level diagram was introduced, it was assumed that the electron energy levels remained unchanged right to the surface ($x = 0$). However, the presence of the space charge (and also surface states) leads to a bending of the bands. If the surface region becomes depleted of electrons it would require more energy to transfer an electron to the conduction band from, for example, the reference state E_F , due to the space charge potential barrier. This is depicted schematically in Fig. 31. Conversely, it is now easier to transfer a hole to the surface since the difference between E_F and E_V becomes smaller.

It is very likely that there is accumulation or depletion of charges at semiconductor or insulator surfaces under all ambient conditions. For surfaces under atmospheric conditions, adsorbed gases or liquid

layers at the interface provide trapping of charges or become the source of free carriers. For clean surfaces in ultrahigh vacuum, there are electronic surface states that act as traps or sources of electrons and produce a space-charge layer of appreciable height. Thus the mobile carriers from the surface layer are swept into the interior or are trapped at the surface as the space-charge layer consists dominantly of static charges, is the one most frequently encountered in experimental situations.

We have so far considered the space-charge-layer properties only in the insulating solid, assuming that the surface layer that acts as a donor or electron trap is of monolayer thickness. However, considering the properties of solid-liquid interfaces or semiconductor-insulator contacts, it should be recognized that the space-charge layer may extend to effective Debye lengths on both sides of the interface. This is a most important consideration when one investigates the surface properties of colloid systems or of semiconductor-electrolyte interfaces.

Work Function and Contact Potential

The work function of a solid is a fundamental physical property of the solid which is related to its electronic structure. It is defined as the potential that an electron at the Fermi level must overcome to reach the level of zero kinetic energy in the vacuum. In semiconductors and insulators it can be regarded as the difference in energy between an electron at rest in the vacuum just outside the solid (i.e., at the level of zero kinetic energy) and the most loosely bound elec-

trons in the solid. Thus the work function is evidently an important parameter in situations where electrons are removed from the solid.

A schematic energy level diagram assuming the free-electron model of a metal showing the work function is depicted in Fig. 32.

From the figure it can be seen that the value of ϕ depends upon W , the depth of the potential well bonding the conduction electrons into the solid. W is a bulk property determined by the attraction for its electrons of the lattice of positive ions as a whole, it has an energy of the order of a few electron volts.

The origin of the work function itself can be considered as being due to the image potential of the escaping electron. Electrostatic theory shows that a charge $-e$ outside a conductor is attracted by an image charge $+e$ placed at the position of the optical image of $-e$ in the conducting plane. If $-e$ is a distance x from the plane the image force is $e^2/16\pi\epsilon_0 x^2$. This force is experienced by the electron escaping into the vacuum and is negligible beyond 10^{-6} - 10^{-5} cm away from the surface.

The image potential is a specific surface contribution to W , and a second surface contribution is the existence of a surface double layer or dipole layer. Surface atoms are in an unbalanced environment, they have other atoms on one side of them but not on the other, thus the electron distribution around them will be unsymmetrical with respect to the positive ion cores. This leads to the formation of a double layer. Two important effects emanate from this; the work function is

sensitive to both the crystallographic plane exposed and to the presence of adsorbates.

The orientation of the exposed crystal face affects ϕ because the strength of the electric double layer depends upon the density of positive ion cores which in turn will vary from one face to another. The work function of various crystal planes of tungsten and molybdenum are listed in Table 4. It can be seen that there is more than 0.3 eV difference in work function values. This variation of work function from one crystal face to another can clearly be demonstrated using a field emission microscope (FEM). This microscope is identical in construction to the FIM described earlier. However, instead of having helium or other imaging gas in the vacuum, no gas is admitted. The potential on the sample tip is reversed so that electrons are accelerated out of it by a very high local electric field ($\sim 4 \times 10^7 \text{ V cm}^{-1}$). The current emitted from the tip surface where the work function is ϕ is approximately proportional to $\exp(-A\phi^{3/2})$ and is a very fast function of ϕ . The brightness observed on the fluorescent screen is a function of the value of ϕ at that place on the tip, and the FEM image will consist of darker and brighter areas, the brightness depending upon the work function of each crystal face exposed. An image is shown in Fig. 33 which is the FEM image of a tungsten tip. The changes in ϕ produced by adsorbed atoms or molecules can be followed in the FEM.

As mentioned the work function of a solid is also sensitive to the presence of adsorbates. In fact, in virtually all cases of adsorption the work function of the substrate either increases or decreases; the

change being due to a modification of the surface dipole layer. The formation of a chemisorption bond is associated with a partial electron transfer between substrate and adsorbate and the work function will change. Two extreme cases are: (i) the adsorbate may only be polarized by the attractive interaction with the surface giving rise to the build up of a dipole layer, as in the physisorption of rare gases on metal surfaces and (ii) the adsorbate may be ionized by the substrate, as in the case of alkali metal adsorption on transition metal surfaces. If the adsorbate is polarized with the negative pole towards the vacuum the consequent electric fields will cause an increase in work function. Conversely, if the positive pole is towards the vacuum then the work function of the substrate will decrease.

The work function is a rather complicated (and not fully understood) function of the surface composition and geometry. Nevertheless, general systematic observations of $\Delta\phi$ are quite helpful. For example, the sign of $\Delta\phi$ for atomic adsorption is mostly that implied by the magnitude of the ionization potential, electron affinity, or dipole moment of the adsorbates as one would expect. The most common usage of work function changes in surface chemistry is in the monitoring of the various stages of adsorption as a function of coverage. Often the work function change will go through a maximum or minimum at particular coverages corresponding to the completion of an ordered atomic arrangement.

Experimentally, the most accurate way of measuring changes in work function is by the Kelvin method, which uses a vibrating probe as a variable capacitor. A contact potential difference is set up between two conductors connected externally and the sample and a reference electrode form a parallel plate condenser. The distance between the two is periodically varied, thus generating an alternating current in the connecting wire. If a voltage source is placed in the connecting circuit just balancing out the contact potential difference, no current will flow. Once this situation has been achieved for the clean surface, a change in work function due to adsorption is simply the additional voltage which needs to be applied to compensate the change and keep the current zero. Accuracies of $\Delta\phi$ to within ± 1 meV are obtainable.

Intimately linked to the concept of work function is the process of thermionic emission. Thermionic emission is, as the name suggests, the phenomenon whereby electrons are ejected from a metal when it is heated in vacuum. The electrons that require the least amount of thermal energy to overcome their binding energy in the solid and escape are those in the high energy tail of their equilibrium distribution in the metal. Thermionic emission is the most frequently used method to produce electron beams, for instance in oscilloscope tubes and electron microscopes. Refractory metals (e.g., W) have traditionally been used as filaments in electron guns, mainly due to the fact that they can be heated to high temperatures and thus produce a relatively intense thermionic current. Since, the work function of W is relatively high W

filaments are often coated with a metal for lower work function, for example Th ($\phi = 2.7$ eV) to enable them to be operated at lower temperature for the same current thereby extending their lifetime.

Surface States

In a bulk solid the infinite array of ion cores in crystallographic sites leads to a potential that varies in a three-dimensionally periodic manner. The solutions to Schrödinger's equation for such a potential lead to allowed energy bands, which are occupied by the electrons in the solid, and to particular values of the wave vector k of the electron where no travelling-wave solutions exist. The absence of eigenstates for these values of k leads to the band gaps in the electronic structure of the solid. The solid, however, is not infinite, but is bounded by surfaces. In turn, surface atoms have fewer nearest neighbors and are in an asymmetric environment. The introduction of such a discontinuity as the surface perturbs the periodic potential and gives rise to solutions of the wave equation that would not have existed for the infinite crystal. These are derived by using appropriate boundary conditions to terminate the crystal and are called surface-state wave functions. These special solutions are waves which can travel parallel to the surface but not into the solid. They are localized at the surface and can have energies within the band gap of the bulk band structure. These states can trap electrons or release them into the conduction band. The concentration of electronic surface states in clean surfaces can be equal to

the concentration of surface atoms ($\sim 10^{15} \text{ cm}^{-2}$). Impurities or adsorbed gases can reduce the surface state density.

One important consequence of the presence of electronic surface states is that the electron bands are modified at the surface even in the absence of a space charge or electron acceptor or donor species (such as adsorbed gases). The shape of the conduction band at the surface of an intrinsic semiconductor in the presence of electron-donor and electron-acceptor surface states is shown in the energy-level diagrams in Fig. 34(a) and (b).

Surface states can be associated not only with the termination of a three dimensional potential at a perfect clean bulk exposed plane but also with changes in the potential due to relaxation, reconstruction, structural imperfections or adsorbed impurities. If the charge associated with any of these surface states is different from the bulk charge distribution then band-bending will occur.

Surface states can be observed for example using ultraviolet photoelectron spectroscopy, which is discussed below.

Electron Emission from Surfaces

The most important methods of analyzing the surface electronic and chemical composition involve energy analysis of electrons emitted from a surface during its bombardment with electrons, ultraviolet photons or x-ray photons. For example, part of the experimental verification of the band theory of metals comes from the measured intensity and energy distribution of electrons emitted under excitation by photons. It should be remembered that we have already mentioned two ways in

which electrons can be emitted from surfaces; (i) by applying a very high electric field ($\sim 10^7$ V cm⁻¹) which pulls electrons from the surface, as used in FEM, and (ii) by heating the solid as in thermionic emissions.

Before discussing the two major electron emission techniques from surfaces, photoelectron spectroscopy and Auger Electron Spectroscopy (AES) it is pertinent to briefly discuss the surface sensitivity of the interaction of electrons with solids. Figure 35 shows the mean free path of electrons in metallic solids as a function of the electron energy. This curve is often called the "universal curve", and shows a broad minimum in the energy range between 10 and 500 eV with the corresponding mean free path on the order of 4 to 20 Å. Electron emission from solids with energy in this range must originate from the top few atomic layers. Therefore, all experimental techniques involving the incidence and/or convergence from surfaces of electrons having energy between 10 and 500 eV are surface sensitive. For incident electrons of higher energy (1-5 kV) the surface sensitivity can be enhanced by having the electron beam impinging on the surface at grazing incidence. Photons have a much larger penetration depth into the solid due to the much smaller scattering cross-section. However, electrons created by excitation below a few atomic layers from the surface cannot escape due to inelastic scattering within the solid. If a monoenergetic beam of electrons of energy E_p strikes a metal surface then a typical plot of the number of scattered electrons $N(E)$ as a function of their kinetic energy, E , is shown in Fig. 36. The curve

is dominated by a strong peak at low energies due to secondary electrons created as a result of inelastic collisions between the incident electrons and electrons bound to the solid. Other features in the spectrum include (i) the elastic peak at E_p that is utilized in LEED (ii) inelastic peaks at loss energies of 10-500 meV which provide information about the vibrational structure of the surface-adsorbate complex utilized in EELS (iii) inelastic peaks at greater loss energies (plasmon losses) which provide information about the electronic structure of surface atoms and (iv) small peaks on the large secondary electron peak due to Auger electrons which provide information on the chemical composition of the surface.

Auger Electron Spectroscopy (AES)

Auger electron spectroscopy is the most common technique for determining the composition of solid and liquid surfaces. Its sensitivity is about 1 percent of a monolayer, and it is a relatively simple technique to perform experimentally. Auger electron emission occurs in the following manner. When an energetic beam of electrons or x-rays (1000 to 5000 eV) strikes the atoms of a material, electrons, which have binding energies less than the incident beam energy, may be ejected from the inner atomic level. By this process a singly ionized, excited atom is created. The electron vacancy formed is filled by de-excitation of electrons from other electron energy states. The energy released in the resulting electronic transition can, by electrostatic interaction, be transferred to still another electron in the same atom or in a different atom. If this electron has a binding energy that is

less than the energy transferred to it from the deexcitation of the previous process that involves the filling of the deep-lying electron vacancy, it will be ejected into vacuum, leaving behind a doubly ionized atom. The electron that is ejected as a result of the deexcitation process is called an Auger electron and its energy is primarily a function of the energy-level separations in the atom. These processes are schematically displayed in Fig. 37. To a first approximation the energy of the Auger electron depicted in Fig. 37 is given by

$$E_{\text{Auger}} = E_K - E_{\text{LI}} - E_{\text{LIII}} \quad (44)$$

and is independent of the energy of the incident beam. This is an important difference between AES and photoelectron spectroscopy, and means that it is not necessary to monochromatize the electron beam which adds to the experimental convenience.

There are two major experimental designs for AES. One is using the retarding grid analyzer which uses the same electron optics of LEED, thus LEED and AES can be performed using the same apparatus. The second is the cylindrical mirror analyzer (CMA) which has an inherently better signal-to-noise ratio. Scanning Auger microprobes are now in widespread use in the microelectronics industry for spatial chemical analysis of surfaces. With the exception of hydrogen and helium, all other elements are detectable by Auger electron spectroscopy.

The Auger spectrum is usually presented as the second derivative of intensity, d^2I/dV^2 , as a function of electron energy, eV. This way the Auger peaks are readily separated from the background, due to

other electron loss processes that occur simultaneously. A typical Auger spectrum of molybdenum is shown in Fig. 38.

By suitable analysis of the experimental data, as well as by the use of suitable reference surfaces, the Auger electron spectroscopy study can provide quantitative chemical analysis in addition to elemental compositional analysis of the surface. It is possible to separate the surface composition from the composition of layers below the surface by appropriate analysis of the Auger spectral intensities. In this way the surface composition as well as the composition in the near-surface region can be obtained.

When chemical analysis is desired in the near-surface region, AES may be combined with ion sputtering to obtain a depth-profile analysis of the composition. Using high-energy ions, the surface is sputtered away layer by layer while, simultaneously, AES analysis detects the composition in depth. Sputtering rates of 100 Å/min are usually possible and the depth resolution of the composition is about 10 Å, which is mainly determined by the statistical nature of the sputtering process.

A different aspect of AES concerns shifts in the observed peak energies that are due to chemical shifts of atomic core levels (in a way analogous to x-ray photoelectron spectroscopy). For example, studies of different oxidation states of oxygen at metal surfaces have shown chemical shifts that grow with the formation of higher oxidation states.

Photoelectron Spectroscopy

Photoelectron spectroscopy is a technique whereby electrons directly ejected from the surface region of a solid by incident photons are energy analyzed and the spectrum is then related to the electron energy levels of the system. The field is usually arbitrarily divided into two classes: ultraviolet photoelectron spectroscopy (UPS) and x-ray photoelectron spectroscopy (XPS). The names derive from the energies of the photons used in the particular spectroscopy. UPS studies the properties of valence electrons that are in the outermost shell of the atom and utilizes photons in the vacuum ultraviolet region of the electromagnetic spectrum (He I (21.22 eV), He II (40.8 eV) and Ne I (16.85 eV) resonance lamps are the most commonly used photon sources). XPS investigates the properties in the inside shells of atoms and uses photons in the x-ray region (Mg K_{α} (1253.6 eV) and Al K_{α} (1486.6 eV) being the most common). With the advent of synchrotron radiation, a polarized, tunable light source covering the entire useful energy range, the division is now somewhat redundant.

In both types of spectroscopy, if the incident photon has enough energy, $h\nu$, it is able to ionize an electronic shell and an electron which was bound to the solid with energy E_B is ejected into vacuum with kinetic energy E_k . By conservation of energy:

$$E_k = h\nu - E_B. \quad (39)$$

If the incident radiation is monochromatic and of known energy, and if E_k can be measured using a high resolution energy analyzer

(such as either a concentric hemispherical or cylindrical mirror analyzer), then the binding energy E_B can be deduced.

Equation (39) gives a highly simplified relationship between the kinetic energy, E_k of the emitted photoelectrons and their binding energy. E_k is modified by the work function of the energy analyzer and by several atomic parameters that are associated with the electron emission process. The ejection of one electron leaves behind an excited molecular ion. The electrons in the outermost and in other orbitals experience a change in the effective nuclear charge due to an alteration of screening by other electrons. This gives rise to satellite peaks near the main photoelectron peaks. Several other effects, including spin-orbit splitting, Jahn-Teller effect, and resonant absorption of the incident photon by the atom, influence the detected photoelectron spectra.

One of the most important applications of XPS is the determination of the oxidation state of elements at the surface. The electronic binding energies for inner-shell electrons shift as a result of changes in the chemical environment. An example of these shifts can be seen in nitrogen, indicating the photoelectron energy for various chemical environments (Fig. 39). These energy shifts are closely related to charge transfer in the outer electronic level. The charge redistribution of valence electrons induces changes in the binding energy of the core electrons, so that information on the valence state of the element is readily obtainable. A loss of negative charge (oxidation) is in general accompanied by an increase in the binding energy, E_B , of the core electrons.

Relative surface coverages can also be obtained with XPS by monitoring the intensities of the core level peaks. Absolute coverages can be obtained from the core level intensities but it is usual to calibrate against another technique.

As mentioned previously UPS probes the valence electrons of the solid. It is these electrons which form a chemisorption bond and a knowledge of electronic density of states at a surface is of vital importance in attempts to understand the formation of chemical bonds between solid surfaces and adsorbed atoms or molecules. UPS can provide even more information about the system if the emitted electrons are both energy and spatially analyzed. This is known as angle-resolved UPS (ARUPS). Using ARUPS the band structures of clean and adsorbate-covered surfaces have been determined, mapping out the dispersion of electronic states. ARUPS also reveals directional effects due to the spatial distribution of electronic orbitals of atoms and molecules at the surface. By changing the angle of incidence and the angle of detection, the electronic orbitals from which the photoelectrons are ejected can be identified. ARUPS provides detailed information about the surface chemical bond that includes the direction of the bonding orbitals and the orientation of the molecular orbitals of adsorbed species on the surface.

SURFACE DYNAMICSAtomic Vibrations

Up until now it has been convenient to discuss both the properties and methods in terms of rigid lattices of atoms or molecules. In reality, the atoms are in motion and this motion should be included in a complete treatment of any properties it may affect.

In x-ray diffraction experiments it is well known that the intensity of the scattered rays decrease as the temperature is increased. Simultaneously, the intensity of the diffuse background of the diffraction pattern increases. The simplest explanation for this observation is that the atoms are not rigid, but are vibrating about their equilibrium positions, and as a result, the exact Bragg condition is not met. Scattered waves from the rigid lattice that were adding up in phase now have a phase difference fluctuating with time due to the atomic motion. The effect of this motion upon the intensity of the elastically diffracted beams is described in most good solid state physics texts. Briefly, if I_0 is the intensity elastically diffracted by a rigid lattice then the intensity I due to scattering by the vibrating lattice in the direction determined by Bragg scattering due to a reciprocal-lattice vector \bar{g} is given by

$$I = I_0 \exp(-\alpha \langle u^2 \rangle |g|) \quad (40)$$

assuming that the atoms are in simple harmonic motion. $\langle u^2 \rangle$ is the mean-square amplitude of vibration in the direction \bar{g} and α is a constant related to the number of dimensions in which the atoms are allowed to vibrate. In one-dimension $\alpha = 1$, in three dimensions

$\alpha = 1/3$. The exponential factor in equation 40 is called the Debye-Waller factor and is often denoted as $\exp(-2M)$.

The same kind of effect is observed in LEED only because LEED intensities arise from the just few atomic layer of a crystal the value of $\langle u^2 \rangle$ is that for the surface atoms. Because of the absence of nearest neighbors on the vacuum side it is to be expected that $\langle u^2 \rangle$ at the surface will be greater than in the bulk.

By using the Debye model of the solid it is possible to relate the observed intensity of the elastically scattered electrons in LEED to measurable quantities. One obtains:

$$I_{00}(T) = I_{00}(0) \exp \left\{ \left| - \frac{12h^2}{mk} \left(\frac{\cos \theta}{\lambda} \right)^2 \frac{T}{\theta_D^2} \right| \right\} \quad (41)$$

where $I_{00}(T)$ is the temperature-dependent intensity of the (0,0) beam resulting from a beam of electrons of wavelength λ incident upon the surface at an angle θ relative to the surface normal. $I_{00}(0)$ is the specularly reflected intensity from a rigid lattice, h is Plank's constant, m is the atomic mass, k is Boltzman's constant, T is the temperature and θ_D is the Debye temperature. (The Debye temperature is associated with the energy of the highest frequency, ω_{\max} , phonon mode possible in the Debye model of vibrations in the solid:

$$h\omega_{\max} = k\theta_D).$$

Equation 41 implies that a plot of the logarithm of the intensity at a given energy (wavelength) as a function of temperature is a straight line, the slope of which yields θ_D , a measure of the surface vibrational amplitude perpendicular to the surface.

In reality, the electron beam penetration varies as a function of energy, so that Eq. 41 provides, at any given energy, an effective Debye temperature, which is some average of the surface and bulk layers. In empirical fashion, however, one may arrive at a surface Debye temperature from the low-energy limit of this effective Debye temperature.

Adsorbates should have a marked influence on surface-atom vibrations, since they change the bonding environment with respect to that on the clean surface. The adsorption of oxygen on tungsten increases the surface Debye temperature with respect to the bulk value due to the stronger W-O bond as compared to the W-W bond. Studies of surface-atom vibrations in the presence of adsorbates provide information on the nature of the surface bond.

Surface Diffusion

As discussed above, at any finite temperature the atoms at the surface of a crystal are vibrating at some frequency ν_0 . Thus ν_0 times every second each atom strikes the potential-energy barrier separating it from its nearest neighbors (see Fig. 40). The thermal energy causing the atoms to oscillate with increasing amplitude as the temperature is increased is not sufficient to dislodge most of them from their equilibrium positions. The thermal energy ($3RT \approx 1.8$ kcal/mol at 300 K) tied up in lattice vibrations is only a small fraction of the total energy necessary to break an atom from its neighbors and to move along the surface. This bond breaking energy is of the order 15-50 kcal/mol for many metal surfaces. As the

temperature of the surface is increased, more and more surface atoms may acquire enough activation energy to break bonds with their neighbors and move along the surface. Such surface diffusion plays an important role in many surface phenomena involving atomic transport e.g., crystal growth, vaporization and adsorption. The migration of atoms or molecules along the surface is one of the most important steps in surface reactions and has proven to be the rate-limiting step for many reactions that have been studied at low pressures.

A surface contains many defects on an atomic scale. Atoms in different surface sites have different binding energies. Surface diffusion can be considered as a multistep process whereby atoms break away from their lattice position (e.g., a kink site at a ledge) and migrate along the surface until they find a new equilibrium site.

The frequency, f , with which an atom will escape from a site will depend upon the height, ΔE_D^* of the potential energy barrier it has to climb in order to escape

$$f = z\nu_0 \exp\left(-\frac{\Delta E_D^*}{k_B T}\right) \quad (42)$$

where z is the number of equivalent neighboring sites. For a (111) face of an f.c.c. metal, $z = 6$, the vibration frequency is of the order of 10^{12} s^{-1} . Assuming that ΔE_D^* is 20 kcal/mol^{-1} , at 300 K the atom makes one jump in every 50s. While at 1000 K one in 10^{-8} s . Thus, the rate of surface diffusion varies rapidly with temperature. This is the case for a single jump to a neighboring equilibrium surface site. What is of great importance is the long distance motion of a surface

atom. The result is derived from considering a mathematical treatment of an atom executing a random walk for a time t over a mean square distance $\langle X^2 \rangle$.

For a six-fold symmetrical surface, one obtains:

$$\langle X^2 \rangle = \frac{f t d^2}{3} \quad (43)$$

The value of $f d^2$ is a property of the material that characterizes its atomic transport. Its value provides information about the mechanism of atomic transport, and it is customary to define the diffusion coefficient, D , as

$$D = \frac{f d^2}{2b} \quad (44)$$

where b is the number of coordinate directions in which diffusion jumps may occur with equal probability.

Equation 44 can therefore be rewritten as

$$D = D_0 \exp \left(- \frac{\Delta E_D^*}{k_B T} \right) \quad (45)$$

where $D_0 = \frac{v_0 d^2}{6}$, $\frac{v_0 d^2}{4}$ for 6-fold or 4-fold symmetry respectively. D is usually given in units of square centimeters per second. If D is determined experimentally as a function of temperature, then a plot of $\ln D$ vs. $1/T$ will yield us the activation energy of the diffusion process, provided that the diffusion occurs by a single mechanism.

The rms distance $\langle X^2 \rangle^{1/2}$ can be expressed in terms of the diffusion coefficient by substitution of Eq. 44 into 43 to give for $b = 6$

$$\langle x^2 \rangle^{1/2} = (4Dt)^{1/2} \quad (46)$$

From measurements of the mean travel distance of diffusing atoms the diffusion coefficient can be evaluated. Conversely, knowledge of the diffusion coefficient allows one to estimate the rms distance or the time necessary to carry out the diffusion. For example, the diffusion coefficients of silver ions on the surface of silver bromide can be estimated to be 10^{-9} and 10^{-13} cm^2/sec at 300 and 100 K, respectively. Assuming that a rms distance of 10^{-4} cm is required for silver particle aggregation (print-out) to commence, of what duration are the light-exposure times required? Using Eq. 46 we have $t = 5$ sec and $t = 5 \times 10^4$ sec at 300 and 100 K, respectively. The exponential temperature dependence of D is, of course, the reason that silver bromide photography cannot be carried out at low temperatures (much below 300 K) but is easily utilized at about room temperature. We can also see that at slightly elevated temperature (~ 450 K) the thermal diffusion of silver particles should be rapid enough ($D \approx 3 \times 10^{-7}$ cm^2/sec) so that their aggregation will take place rapidly even in the dark ($t \approx 10^{-2}$ sec) in the absence of any photo-reaction.

Surface diffusion has so far been discussed in terms of a single surface atom. However, on a real surface many atoms diffuse simultaneously and in most diffusion experiments the measured diffusion distance after a given diffusion time is an average of the diffusion lengths of a large, statistical number of surface atoms. A thermodynamic treatment in terms of macroscopic parameters can be followed to yield

$$D = D_0 \exp \left(- \frac{Q}{RT} \right) \quad (47)$$

where Q is the total activation energy for the overall diffusion process, and only one diffusion mechanism is involved.

Experimentally, the diffusion coefficient, D , is obtained by using a relationship between the diffusion rate and coverage gradient, namely Fick's Second Law of diffusion in one dimension

$$\frac{\partial c}{\partial t} = D \frac{\partial^2 c}{\partial x^2} \quad (48)$$

where c is the concentration of adatoms, t the time and x the distance along the surface. In most surface diffusion studies the surface concentration of diffusing atoms, c , is measured as a function of distance x along the surface and Eq. 48 is solved by the use of boundary conditions that approximate the experimental geometry. These experiments are by no means trivial, and many novel experimental techniques have been applied to study surface diffusion on single crystals.

A technique which has been used to measure surface diffusion rates is scanning Auger electron spectroscopy, which can follow adsorbate diffusion. A particular Auger transition of the adsorbate under investigation is used as a monitor of relative concentration versus distance scanned across the surface. Profiles are recorded after heating periods to observe the change in concentration profile as a function of time and temperature.

While this technique monitors mass transport, and values of D and Q are averaged values, ion microscopy can be used to follow the diffusion of individual atoms across a surface. To study diffusion, the

metal is vapor deposited onto the tip. The tip is then heated to remove evaporated adatoms until only one or two remain on the surface plane of interest. The diffusion is then examined by photographically recording the position of the adatom at low temperatures, removing the applied field and heating to the desired temperature for a given time. The tip is then cooled, the field re-applied and the field ion image examined to see if the atom has moved to a neighboring site. This process is then repeated many times to obtain useful values of diffusion rates, and by examining the diffusion over a temperature range, the activation barrier to surface diffusion can be determined. Figure 41 shows a series of field ion images of a Rh atom on the W(112) plane at 327°K. The field ion images are taken at one minute intervals and the Rh atom can clearly be seen to have diffused across the surface. Unfortunately because of the high field strengths employed, adsorbates such as O or N tend to be stripped from the surface as ions, so their microscopic diffusion cannot be studied by this method. An interesting result from FIM studies of metal adatoms on metals is the recognition of clusters as important contributions to material transport. It has been found that rhenium dimers diffuse more rapidly than single Rh atoms on the W(112) plane, and Rh trimers diffuse at roughly the same rate as dimers. This is not a general trend, however, as iridium dimers move much more slowly than singles.

While the single adatom diffusion technique gives us detailed microscopic information, the mass transport techniques are of use as they help to give understanding of the technologically important processes such as sintering and creep.

Surface Reactions

Heterogeneous catalysis, corrosion, photosynthesis and adhesion are examples of chemical processes that are partially or fully controlled by reactions at surfaces. For the case of gas-solid reactions the surface reactions can be divided into two major categories: 1) Stoichiometric surface reactions where the solid surface participates directly in the reaction by compound formation. 2) Catalytic surface reactions where the reaction occurs at the solid surface, but the surface does not undergo any net chemical change. In both cases gaseous molecules impinge on the surface, adsorb, react, form various intermediates of varying stability and then the products desorb into the gas phase if they are volatile.

All surface reactions involve a sequence of elementary steps that begins with the collision of the incident atoms or molecules with the surface. As the gas species approaches the surface it experiences an attractive potential whose range depends upon the electronic and atomic structures of the gas and surface atoms. A certain fraction of the incident gas molecules is trapped in this attractive potential well with a sticking probability given by:

$$S(\theta, T) = S_0(1-\theta) \exp(-E_a/RT) \quad (49)$$

where S_0 is the initial (zero coverage) sticking coefficient, θ is the surface coverage ($0 < \theta < 1$), and E_a is the activation energy for adsorption. If this force attraction is due to a Van der Waals interaction, the trapping is due to physical adsorption. If the attraction is much stronger, having the character of chemical bonding

and we have chemisorption and the process is known as sticking. The boundary between the two types of bonding is usually set at a binding energy of 15 kcal/mol. Sticking by chemisorption is often preceded by trapping into a physisorbed state, in which case the physisorbed state is known as a "precursor state" for chemisorption. The presence of a precursor state is indicated by a sticking coefficient which remains almost constant as surface coverage increases until a saturation coverage is reached, when it rapidly falls to zero. This behavior arises because molecules in the relatively mobile precursor state diffuse to parts of the surface which are not covered by chemisorbed molecules. In direct chemisorption the sticking coefficient varies strongly with coverage and with ordering of the chemisorbed layer.

The adsorbed species may also desorb from the surface if its energy overcomes the attractive surface forces. When a surface reaction occurs a certain proportion of the adsorbed species either decomposes (unimolecular reaction) or reacts with a second adsorbed species (bimolecular reaction) before the product desorbs.

During the initial interaction of the gas molecule with the surface as the incoming molecule falls into a potential well the kinetic energy normal to the surface increases. Unless this energy is transferred to some other degree of freedom the molecule will simply bounce off; there will be no trapping or sticking. In the case of physisorption energy transfer via phonons is usually most important while for chemisorption electronic excitation via electron-hole pairs is thought to be important.

The exchange of translational energy, T , with the phonons, V_s , is called $T-V_s$ energy exchange. The gas molecule may also exchange internal energy, rotation, R , or vibration, V , with the vibrating surface atoms. In this case there are also $R-V_s$ and $V-V_s$ energy transfer processes.

In order to understand the dynamics of gas-surface interaction, it is necessary to determine how much energy is exchanged between the gas and surface atoms through the various energy-transfer channels. In addition the kinetic parameters (rate constants, activation energies, preexponential factors) for each elementary surface step of adsorption, diffusion, and desorption are required in order to obtain a complete description of the gas-surface energy transfer process.

Most surface reactions take place at high pressures (1 - 100 atmospheres) either because of the chemical environment of our planet or to establish optimum reaction rates in chemical processing. Under these conditions, surfaces are usually covered by at least one monolayer of adsorbed species. Since activation energies for adsorption and surface diffusion are generally small (a few kT), equilibrium among the different surface species, reactants, reaction intermediates, and products, is readily established. In the simplest (but not general and important) case of localized, associative adsorption into a single state, the surface coverage by adsorbed species is given in terms of the gas pressure, P , by the Langmuir isotherms:

$$\theta = KP/(1 + KP). \quad (50)$$

where K is an equilibrium constant. Catalyzed surface reactions

usually take place between two or more coadsorbed species which compete for adsorption sites on the surface. When j gases adsorb competitively and associatively, the surface coverage by species i is given by

$$\theta = K_i P_i / (1 + \sum_j K_j P_j). \quad (51)$$

Many catalyzed surface reactions can be treated as a two-step process with an adsorption equilibrium followed by one rate-determining step (diffusion, surface reaction, or desorption). The surface reaction kinetics are usually discussed in terms of two limiting mechanisms, the Langmuir-Hinshelwood (LH) and Eley-Rideal (ER) mechanisms. In the LH mechanism, reaction takes place directly between species which are chemically bonded (chemisorbed) on the surface. For a bimolecular LH surface reaction, $A_{ads} + B_{ads} \rightarrow$ products, with competitive chemisorption of the reactants, the rate of reaction is given by the expression

$$\text{Rate} = k_R \theta_A \theta_B = k_R K_A K_B P_A P_B / (1 + K_A P_A + K_B P_B)^2 \quad (52)$$

The reaction rate is proportional to the surface coverages θ_A and θ_B and to the reaction rate constant k_R . For non-competitive adsorption, the rate expression becomes

$$\text{Rate} = k_R \theta_A \theta_B = k_R K_A K_B P_A P_B / (1 + K_A P_A)(1 + K_B P_B) \quad (53)$$

General rate expressions of the form given in equations and have been experimentally verified for many types of LH reactions. Similar but more complicated rate expressions are easily derived assuming different (non-Langmuir) isotherms, higher order reaction steps, or dissociative chemisorption of the reactants. In the ER mechanism, surface reaction takes place between a chemisorbed species and a non-chemisorbed

species, e.g. $A_{\text{ads}} + B_{\text{g}} \rightarrow \text{products}$. The non-chemisorbed species may be physisorbed or weakly held in a molecular precursor state. In this case, the rate expression for the surface reaction becomes

$$\text{Rate} = k_R \theta_A P_B = k_R K_A P_A P_B / (1 + K_A P_A). \quad (54)$$

Presently no proven examples exist in which surface reaction occurs by the ER mechanism.

Surface reaction kinetics determined experimentally are often expressed in the form of a power rate law,

$$\text{Rate} = k_R \prod_i P_i^{\alpha_i} \quad (55)$$

where k_R is the apparent rate constant and α_i is the experimental order of the reaction (positive, negative, integer, or fraction) with respect to the reactants and products. The apparent rate constant in equation 55 is not that of an elementary reaction step (it contains adsorption equilibrium constants), but it can usually be represented by an Arrhenius equation,

$$k_R = A \exp(-E_R/RT) \quad (56)$$

where A is an apparent pre-exponential factor and E_R is the apparent activation energy for the surface reaction. The magnitude of A and E_R can provide important information about the rate determining step of a surface reaction, and very frequently, k_R and A display a compensation effect. A related quantity is the reaction probability, $\gamma_i = (2 \pi mKT)^{1/2} v_R / P_i = \text{rate}/\text{flux}$, that is, the probability that an incident reactant molecule will undergo reaction.

The simplified isotherms and rate expressions developed in this section are extremely useful despite the implicit assumption that a single state exists for the adsorbed species. Real surfaces are heterogeneous on an atomic scale with a variety of distinguishable adsorption sites. Gas molecules adsorbed at each type of site may display a wide distribution of excited rotational, vibrational, and electronic states. Experimentally, one can measure meaningful rate and adsorption equilibrium constants provided that adsorption and desorption are fast compared with surface reactions so that an adsorption equilibrium exists. In this circumstance the kinetic parameters are an ensemble average over all surface sites and states of the system.

Molecular Beam Scattering

The most powerful experimental technique for investigating the dynamics of the gas-solid interaction is molecular beam surface scattering (MBS). The experimental arrangement is similar to that already described for helium atom diffraction. Instead of using an atomic beam of a light molecular weight gas and observing diffraction effects, a well-collimated beam of molecules strikes the oriented, preferably single crystal, surface, and the species that are scattered at a specific solid angle are detected by a mass spectrometer. The angular distribution of the scattered molecules can be obtained by rotation of the mass spectrometer about the sample. The velocity distribution of the molecules after scattering is deduced by chopping the scattered molecules and thereby measuring their time-of-flight to the detector. The

surface residence times of the molecules, together with their angular and velocity distributions provide detailed information about the $T-V_s$ energy transfer processes that occur during the gas-surface interaction. A complete dynamical description for this interaction ($T-V_s$ plus $R-V_s$ and $V-V_s$) can be determined if the distribution of internal energy states for the product molecules is determined simultaneously with their velocity distributions. This type of detection is known as state selective detection.

The angular distribution of scattered molecules is usually displayed by plotting the intensity of detected molecules per unit solid angle versus the angle of scattering, θ_r , that is measured with respect to the surface normal. Angular distributions in the two limiting cases of gas-surface interaction, cosine and specular scattering, are shown in Fig. 42. The scattered intensity for the cosine distribution decreases as $\cos\theta$ with respect to the surface normal. Cosine scattering is expected when the adsorbed species have long residence times, or strongly coupled to the vibrational states of the surface atoms. It is a necessary criterion for complete thermal accommodation, a situation in which the molecules desorb with a kinetic temperature or velocity distribution that is the same as the temperature of the solid surface. Specular scattering occurs when the scattered intensity is sharply peaked at the angle of incidence (specular angle). In this case the interaction is elastic or quasi-elastic and little or no energy transfer takes place between the incident gas molecules and the surface. Sharply peaked angular distributions for surface reaction

products ($I(\theta) \sim \cos^m \theta$, $m > 1$) indicate that a repulsive barrier exists in the exit channel. Measurements of velocity distributions provide more direct information on inelastic scattering than angular distributions alone. Although considerable information can be gained from such studies it has been impossible to get state specific information and indeed it is often unclear whether internal states present more efficient energy transfer channels than phonons or vice-versa. The difficulties in studying internal energy transfer in molecular collisions with surfaces can be resolved by the application of state specific detection techniques. Laser induced fluorescence, multiphonon ionization, IR excitation with bolometric detection and IR emission techniques have all been used to obtain state resolved measurements of the internal energy distributions of molecules scattering from surfaces. It has also been possible to separate experimentally direct inelastic and trapping-desorption scattering. In the direct inelastic scattering of diatomics, coupling to rotational energy has been found to be very important and to exhibit several interesting phenomena: rotational rainbows and the production of rotationally aligned molecules in scattering.

Molecular Beam Reactive Scattering

While molecular beam scattering has made great advances in our understanding of the energy exchange processes during the gas-surface collision, molecular beam techniques have also made important contributions to the understanding of the mechanisms of chemical reactions occurring at surfaces, in the form of molecular beam reactive

scattering (MBRS). The use of time-of-flight techniques permits measurement of product velocity distributions and the detailed time resolution of fast transient reactions. Also of great value is the use of state specific detection methods to determine product vibrational and rotational states. Although MBRS can only be utilized at low pressures ($\leq 10^{-4}$ Torr) its pressure range permits wide variations of surface coverages. The reaction probabilities upon a single scattering can be determined together with the surface residence times of adsorbates. The surface kinetic information is obtained by measurements of the intensity and the phase shift of the product molecules with respect to the reactant flux. Residence times in the range 10^{-6} to 1 s can be monitored with relative ease, and activation energy is determined from the temperature dependences of the intensities and the phase shifts. The phase shift of the product molecules is usually measured at different chopping frequencies of the incident beam. At a given chopping frequency, only those product molecules are detected that are formed in the surface process and desorbed in less time than the chopping period.

As an example of an investigation of the dynamics of a catalyzed surface reaction studied by MBRS we will consider the isotope exchange reaction, H_2-D_2 . Exchange of hydrogen and deuterium to form HD is one of the simplest reactions that can be catalyzed on clean metal surfaces at temperatures as low as 100 K. The same reaction is immeasurably slow in the gas phase due to the very high dissociation energies of the reacting molecules (103 kcal/mol). The H_2-D_2 exchange reaction

has been studied over flat (111) and stepped (332) single crystal surfaces of platinum. The Pt(332) surface contains high concentrations of periodic surface irregularities (steps) that are one atom in height. Reaction probabilities averaged over the cosine HD angular distributions were 0.07 on the (111) surface and 0.35 on the (332) surface under identical experimental conditions ($T_s = 1100$ K, $T_g = 300$ K). The reaction probability on the stepped surface varied markedly with the angle of incidence of the mixed H_2-D_2 molecular beam. This is shown in Fig. 43. The reaction probability was highest when the beam was incident upon the open edge of the step and lowest when the bottom of the step was shadowed (curve a). When the H_2-D_2 beam was incident parallel to the steps, the rate of HD production was independent of the angle of incident at all angles of crystal rotation (curve b). These results indicate that the atomic step sites are about seven times more active than the (111) terrace sites for the dissociative chemisorption of hydrogen and deuterium molecules. Detailed analysis of the scattering data revealed a barrier height of 4-8 kJ/mole for dissociative H_2 chemisorption on the (111) surface. On the other hand, this barrier did not exist ($E_a = 0$) on the stepped surface. This difference in activation energy alone accounts for the different reaction probabilities of the step and terrace sites. While the dissociation probability of hydrogen molecules was higher on the stepped surface than on Pt(111), the kinetics and mechanism of HD recombination appear to be identical over both surfaces once dissociation takes place. On both surfaces, HD formation follows a

parallel LH mechanism with one of the reaction branches operative over the entire temperature range of 300–1075 K. This branch has an activation energy and pseudo-first-order pre-exponential factor of $E_a = 54$ kJ/mole and $A_1 = 8 \times 10^4 \text{ sec}^{-1}$ for the stepped surface, and $E_a = 65$ kJ/mole and $A_1 = 3 \times 10^5 \text{ sec}^{-1}$ for the Pt(111) surface. A second branch is observed for temperatures above 575 K, but the kinetic parameters for this pathway could not be accurately determined.

Stoichiometric Surface Reactions

Stoichiometric surface reactions are those where the surface participates directly in the reaction by compound formation. Oxidation and corrosion are the two most important classes of such reactions.

Surface oxidation of metals encompasses a series of at least three reaction steps that include (1) dissociative chemisorption of oxygen on the metal surface, (2) rearrangement of the surface atoms with dissolution of oxygen into the near surface region, and (3) nucleation of oxide islands which grow laterally and eventually condense to produce continuous oxide films. The oxide islands appear to precipitate suddenly once a critical oxygen concentration is reached in the near surface region. Nucleation takes place most readily at surface irregularities such as atomic steps, dislocations, and stacking faults. At room temperature, noble metals such as Rh, Ir, Pd, and Pt display little tendency for oxygen incorporation or surface rearrangement. Initial heats of oxygen chemisorption on these metals are much greater than the heats of formation of the corresponding bulk oxides. Other

metals such as Cr, Nb, Ta, Mo, W, Re, Ru, Co and Ni, dissolve surface oxygen by a place exchange mechanism where oxygen atoms interchange positions with underlying metal atoms. These metals display heats of adsorption for oxygen that are comparable to the heats of formation of the stable metal oxides. Metals such as Ti, Zr, Mn, Al, Cu, and Fe dissolve oxygen more readily and form stable oxide films even at room temperature. At low oxygen pressures these films often assume a crystalline structure, whereas at higher pressures ($>10^{-3}$ atm) the films tend to be amorphous. At higher temperatures (400-1000 K), oxide formation occurs readily on the surfaces of nearly all metals.

Growth of surface oxide films takes place only if cations, anions, and electrons can diffuse through the oxide layer. The growth kinetics of very thin films ($\sim 10-50$ Å) often follows the Mott or Cabrera-Mott mechanisms in which electrons tunnel through the film and associate with oxygen atoms to produce oxide ions at the surface. A large local electric field ($10^6 - 10^7$ V/cm) results at the surface which facilitates cation diffusion from the metal-oxide interface to an interstitial site of the oxide. The film thickness, Z , at time, t , is given by a logarithmic,

$$Z = \alpha_1 \ln(\alpha_2 t + 1) \quad (57)$$

or inverse logarithmic

$$1/Z = \alpha_3 - \alpha_4 \ln t \quad (58)$$

law of growth depending upon whether electron tunneling or cation diffusion is rate limiting. The constants $\alpha_1 - \alpha_4$ are determined by the material, its structure, and the reaction conditions. The electron

field strength and rate of growth decrease exponentially as the film thickens, resulting in an effective limiting thickness for the surface oxide layer.

In addition to surface oxides, a vast array of surface compounds can be produced from the reactions of halogens, chalcogenides, and carbon-containing molecules with metal surfaces. Chemisorption of chlorine near 300 K on Cu, Ti, W, Mo, Ta, Ni, Pd, and Au, for example, results in the formation of stable surface compound which often evaporate as molecular chlorides upon heating at elevated temperatures. Chemisorption of chlorine at 300 K on Ag(100) and Ag(111) produces chemisorbed chlorine overlayers which react irreversibly at about 425 K to produce AgCl with an activation energy of 56 kJ/mole. Upon heating, AgCl desorbs at about 830 K with a desorption activation energy of 192 kJ/mole.

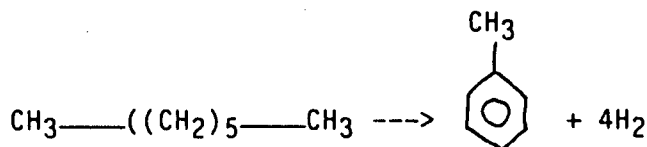
MBRS has been used to investigate the dynamics of several surface corrosion reactions at low reactant pressures. Systems studied include the oxidation Si, Ge, Mo, and graphite, and the halogenation of Si, Ge, Ta, and Ni. With the exception of silicon and germanium oxidation, where dissociative chemisorption of oxygen is apparently rate-limiting, the kinetics of these surface reactions generally appear to be controlled by surface or bulk diffusion of the reacting species.

Catalytic Surface Reactions

A major goal of basic surface chemistry is in trying to understand heterogeneous catalysis on an atomic scale. Virtually all chemical technologies and many technologies in other fields use catalysis as an

essential part of the process. The most important catalytic processes are summarized in Table 5. These processes are listed together with the pertinent chemical reactions, widely used catalysts, and typical reaction conditions. There are several definitions of a catalyst; one general definition being that it is a substance that accelerates a chemical reaction without visibly undergoing chemical change. Indeed, a major role of a catalyst is in accelerating the rate of approach to chemical equilibrium. However, a catalyst cannot change the ultimate equilibrium determined by thermodynamics.

Another major function of a catalyst is to provide reaction selectivity. Under the conditions in which the reaction is to be carried out, there may be many reaction channels, each thermodynamically feasible, that lead to the formation of different products. The selective catalyst will accelerate the rate of only one of these reactions so that only the desired product molecules form with near-theoretical or 100 percent efficiency. One example is the dehydrocyclization of n-heptane to toluene,



This is a highly desirable reaction that converts aliphatic molecules to aromatic compounds. The larger concentration aromatic component in gasoline, for example, greatly improves its octane number. However, n-heptane may participate in several competing simpler reactions. These include hydrogenolysis, which involves C - C bond scission to

form smaller-molecular-weight fragments (methane, ethane, propane); partial dehydrogenation, which produces various olefins; and isomerization, which yields branched chains. All of these reactions are thermodynamically feasible, and since they appear to be less complex than dehydrocyclization, they compete effectively. A properly prepared platinum catalyst surface catalyzes the selective conversion of n-heptane to toluene without permitting the formation of other products. The catalyst selectivity is equally important for the reactions of small molecules (such as the hydrogenation of CO to produce a desired hydrocarbon) or very large molecules of biological importance, where enzyme catalysts provide the desired selectivity.

Catalysis is a kinetic phenomenon; we would like to carry out the same reaction at an optimum rate over and over again using the same catalyst. In most cases such a steady-state operation is desirable and aimed for. In the sequence of elementary reactions that include adsorption, surface migration, chemical rearrangements, and reactions in the adsorbed state, and desorption of the products, the rate of each step must be of steady state. The rate of the overall catalytic reaction per unit area catalyst surface can be expressed as (moles of product/catalyst area x time). Another expression for catalytic rate is the turnover number or turnover frequency. This is the (number of molecules of product/number of catalyst sites x time). For most heterogeneous catalyzed small molecule reactions the turnover number varies between 10^{-2} and 10^2 s^{-1} . The calculation of the turnover number is limited by the difficulty of determining the true number of active sites.

The reaction probability reveals the overall efficiency of a catalyst. It is defined as

$$\text{reaction probability} = \frac{\text{rate of formation of product molecules}}{\text{rate of incidence of reactant molecules}}$$

The determination of the rates of the net catalytic reactions and how the rates change with temperature and pressure is of great practical importance. Although there are many excellent catalysts that permit the achievement of chemical equilibria (for example, Pt for oxidation of CO and hydrocarbons to CO₂ and H₂O), most catalyzed reactions are still controlled by the kinetics of one of the surface processes. From the knowledge of the activation energy and the pressure dependencies of the overall reaction, the catalytic process can be modeled and the optimum reaction conditions can be calculated. Such kinetic analysis, based on the macroscopic rate parameters, is vital for developing chemical technologies based on catalytic reactions.

The rates of reactions are extremely sensitive to small changes of chemical bonding of the surface species that participate in the surface reaction. Since the energy necessary to form or break the surface bonds appears in the exponent of the Arrhenius expression for the rate constant for the overall reaction, it can increase or decrease the rate exponentially. For example, a change of 3 kcal in the activation energy alters the reaction rate by over an order of magnitude at 500 K. Small variations of chemical bonding at different surface irregularities, steps, and kinks, as compared to atomic terraces, can give rise to a very strong structure sensitivity of the reaction

rates and the product distribution. Rate measurements exponentially magnify the energetic alterations that occur on the surface and could provide a very sensitive probe of structural and electronic changes at the surface and changes of surface bonding on the molecular scale.

One of the most important considerations in catalysis is the need to provide a large contact area between the reactants and the surface. The total rate (moles of product/time) is proportional to the surface area. As a consequence, a lot of effort is expended to prepare large surface area catalysts and to accurately measure the surface area. One example of high surface area catalysts is the group of catalysts known as zeolites, which are aluminosilicates used for the cracking of hydrocarbons, and have crystal structures full of pores 8-20Å in size. The structure of one of the many zeolites used for catalysis, faujasite, is shown in Fig. 44. Since the catalytic reactions occur inside the pores, an enormous inner surface area, of several hundred square meters per gram of catalyst, is available in these catalyst systems. Transition-metal catalysts are generally employed in a small, 10 to 100-Å-diameter particle form dispersed on large-surface-area "supports." The support can be a specially prepared alumina or silica framework (or a zeolite) that can be produced with surface areas in the $10^2\text{-m}^2/\text{g}$ range. These "supported" metal catalysts are often available with near-unity dispersion (dispersion is defined as the number of surface atoms per total number of atoms in the particle) of the metal particles and are usually very stable in this configuration during the catalytic reaction. The metal is frequently

deposited from solution as a salt, and then reduced under controlled conditions. Alloy catalysts and other multicomponent catalyst systems can also be prepared in such a way that small alloy clusters are formed on the large-surface-area oxide supports.

Most catalytic reactions take place via the formation of intermediate compounds between the reactants or products and the surface. The surface atoms of the catalyst form strong chemical bonds with the incident molecules, and it is this strong chemical surface-adsorbate interaction which provides the driving force for breaking high binding energy chemical bonds (C-C, C-H, H-H, N-N and C=O bonds), which are often an important part of the catalytic reaction.

A good catalyst will also permit rapid bond breaking between the adsorbed intermediates and the surface, and the speedy release or desorption of the products. If the surface bonds are too strong, the reaction intermediates block the adsorption of new reactant molecules and the reaction stops. For too weak adsorbate-catalyst bonds, the necessary bond-scission processes may be absent. Hence the catalytic reaction will not occur. A good catalyst is thought to be able to form chemical bonds of intermediate strength. These bonds should be strong enough to induce bond scission in the reactant molecules. However, the bond should not be too strong to assure only short residence times for the surface intermediates and rapid desorption of the product molecules, so that the reaction can proceed with a large turnover number.

Of course, activity is only one of many parameters that are important in catalysis. The selectivity of the catalyst, its thermal and chemical stability and dispersion, are among the other factors that govern our choices. While macroscopic chemical-bonding arguments can explain catalytic activity in some cases, atomic-scale scrutiny of the surface intermediates, catalyst structure, and composition, and an understanding of the elementary rate processes, are necessary to develop the optimum selective catalyst for any chemical reaction.

One of the important directions of research in catalysis is the identification of the reaction intermediates. The surface residence times of many of these species are longer than 10^{-5} sec under most catalytic reaction conditions (as inferred from the turnover frequency). They may be detected by suitable spectroscopic techniques either during the steady-state reaction or when isolated by interrupting the catalytic process.

The concept of active sites is an important one in catalysis. A surface generally possesses active sites in numbers that are smaller than the total number of surface atoms. The presence of unique atomic sites of low coordination and different valency that are very active in chemical reactions have been clearly demonstrated by atomic scale studies of metal and oxide surfaces. A catalytic reaction is defined to be structure sensitive if the rate changes markedly as the particle size of the catalyst is changed. Conversely, the reaction is structure-insensitive on a given catalyst if its rate is not influenced appreciably by changing the dispersion of the particles under the

usual experimental conditions. In Table 6 we list several reactions that belong to these two classes. Clearly, variations of particle size give rise to changes of atomic surface structure. The relative concentrations of atoms in steps, kinks, and terraces are altered. Nevertheless, no clear correlation has been made to date between variations of macroscopic particle size and the atomic surface structure.

Most surface reactions and the formation of surface intermediates involve charge transfer, either an electron transfer or a proton transfer. These processes are often viewed as modified acid-base reactions. It is common to refer to an oxide catalyst as acidic or basic according to its ability to donate or accept electrons or protons.

The electron transfer capability of a catalyst is expressed according to the Lewis definition. A Lewis acid is a surface site capable of receiving a pair of electrons from the adsorbate. A Lewis base is a site having a free pair of electrons that can be transferred to the adsorbate. The proton-transfer capability of a catalyst is expressed according to the Bronsted definition. A Bronsted acid is a surface site capable of losing a proton to the adsorbate while a Bronsted base is a site that can accept a proton from the adsorbed species.

Perhaps the most widely used catalysts, the zeolites, best represent the group of oxides that exhibit acid-base catalysis. Zeolites are alumina silicates, some of which are among the more common minerals in nature. Modern synthesis techniques permit the preparation of families of zeolite compounds with different Si/Al ratios. Since the Al^{3+} ions lack one positive charge in the tetrahedrally coordinated

silica, Si^{4+} , framework, they are sites of proton or alkali-metal affinity. Variation of the Si/Al ratio gives rise to a series of substances of controlled but different acidity. By using various organic molecules during the preparation of these compounds that build into the structure, subsequent decomposition leaves an open pore structure, where the pore size is controlled by the skeletal structure of the organic deposit. Very high internal surface area catalysts ($10^2 \text{m}^2/\text{g}$) can be obtained this way with controlled pore sizes of 8 to 20 Å and controlled acidity [(Si/Al) ratio]. These catalysts are utilized in the cracking and isomerization of hydrocarbons that occur in a shape-selective manner as a result of the uniform pore structure and are the largest volume catalysts in petroleum refining. They are also the first of the "high-technology" catalysts where the chemical activity is tailored by atomic-scale study and control of the internal surface structure and composition.

A catalyst used in industry is very rarely a pure element or compound. Most catalysts contain a complex mixture of chemical additives or modifiers that are essential ingredients for high activity and selectivity. Promoters are beneficial additives that increase activity, selectivity or useful catalyst lifetime (stability). Structural promoters inhibit sintering of the active catalyst phase or prevent compound formation between the active component and the support. The most frequently used chemical promoters are electron donors such as the alkali metals or electron acceptors such as oxygen and chlorine. For example, in the petroleum industry, chlorine and oxygen are often

added to commercial platinum catalysts used for re-forming reactions by which aliphatic straight-chain hydrocarbons are converted to aromatic molecules (dehydrocyclization) and to branched isomers (isomerization).

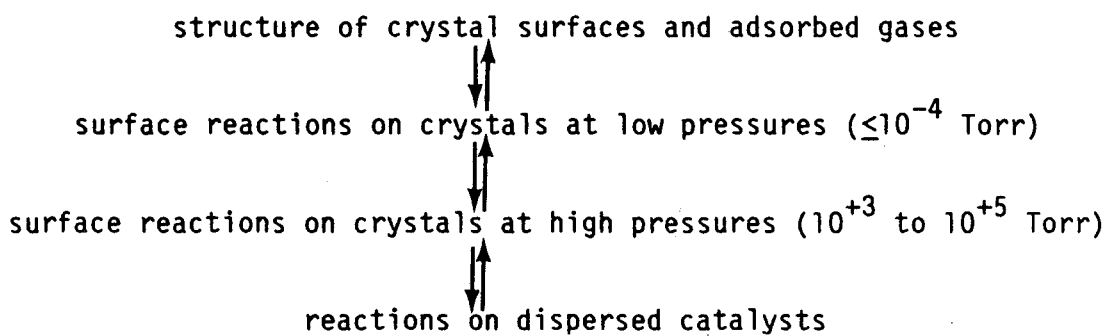
These additives accomplish several tasks during the reaction. By changing the chemical bonding of some of the surface intermediates, the steady-state concentration of these intermediates may be altered, and thus a somewhat higher concentration of the catalytically active species is obtained. In this way the rate of the reaction is increased and the selectivity may be improved.

Often multicomponent catalyst systems are utilized to carry out reactions consisting of two or more active metal components or both oxide and metal constituents. For example, a Pt-Rh catalyst facilitates the removal of pollutants from car exhausts. Platinum is very effective for oxidizing unburned hydrocarbons and CO to H₂O and CO₂, and rhodium is very efficient in reducing NO to N₂, even in the same oxidizing environment. Dual functional or multifunctional catalysts are frequently used to carry out complex chemical reactions. In this circumstance the various catalyst components should not be thought of as additives, since they are independently responsible for different catalytic activity. Often there are synergistic effects, however, whereby the various components beneficially influence each other's catalytic activity to provide a combined additive and multifunctional catalytic effects.

It should be clear from the discussion above that the working, active, and selective catalyst is a complex, multicomponent chemical system. This system is finely tuned and buffered to carry out desirable chemical reactions with high turnover frequency and to block the reaction paths for other thermodynamically equally feasible but unwanted reactions. Thus an iron catalyst or a platinum catalyst is composed not only of iron or platinum but of several other constituents as well to assure the necessary surface structure and oxidation state of surface atoms for optimum catalytic behavior. Additives are often used to block sites, prevent side reactions, and alter the reaction paths in a variety of ways.

While industrial catalytic systems are complex, and are not readily suited to basic science studies to understand how they work on an atomic scale, one approach to their understanding is the "synthetic approach". In this approach one begins with a very simple system then synthesizes complexity from this. The catalyst particle is viewed as composed of single crystal surfaces, as shown in Fig. 45. Each surface has different reactivity and the product distribution reflects the chemistry of the different surface sites. One may start with the simplest single crystal surface [for example, the (111) crystal face of platinum] and examine its reactivity. It is expected that much of the chemistry of the dispersed catalyst system would be absent on such a homogeneous crystal surface. Then high-Miller-index crystal faces are prepared to expose surface irregularities, steps and kinks of known structure and concentration, and their catalytic behavior is tested

and compared with the activity of the dispersed supported catalyst under identical experimental conditions. If there are still differences, the surface composition is changed systematically or other variables are introduced until the chemistries of the model system and the working catalyst become identical. This approach is described by the sequence:



Investigations in the first step define the surface structure and composition on the atomic scale and the chemical bonding of adsorbates. Studies in the second step, which are carried out at low pressures, reveal many of the elementary surface reaction steps and the dynamics of surface reactions. Studies in the third and fourth steps establish the similarities and differences between the model system and the dispersed catalyst under practical reaction conditions.

The advantage of using small-area catalyst samples is that their surface structure and composition can be prepared with uniformity and can be characterized by the many available surface diagnostic techniques.

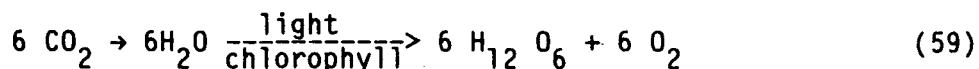
In this approach to catalytic reaction studies the surface composition and structure are determined in the same chamber where the

reactions are performed, without exposing the crystal surface to the ambient atmosphere. This necessitates the combined use of an ultrahigh vacuum enclosure, where the surface characterization is carried out, and a high pressure isolation cell, where the catalytic studies are performed. Such an apparatus is shown in Fig. 46. The small-surface-area (approximately 1 cm^2) catalyst is placed in the middle of the chamber, which can be evacuated to 10^{-9} Torr. The surface is characterized by LEED and AES and by other surface diagnostic techniques. Then the lower part of the high-pressure isolation cell is lifted to enclose the sample in a 30-cm^3 volume. The isolation chamber can be pressurized to 100 atm if desired and is connected to a gas chromatograph that detects the product distribution as a function of time and surface temperature. The sample may be heated resistively, both at high pressure or in ultrahigh vacuum. After the reaction study the isolation chamber is evacuated, opened, and the catalytic surface is again analyzed by the various surface-diagnostic techniques. Ion-bombardment cleaning of the surface or means to introduce controlled amounts of surface additives by vaporization are also available. The reaction at high pressures may be studied in the batch or the flow mode.

Typical catalytic reactions that have been investigated, in some detail, using this approach are include: hydrocarbon conversion on platinum and modified platinum surfaces (isomerization, hydrogenolysis, hydrogenation, dehydrogenation and cyclization), dehydrosulfurization on molybdenum, ammonia synthesis on iron and carbon monoxide hydrogenation on iron.

Photochemical Surface Reactions

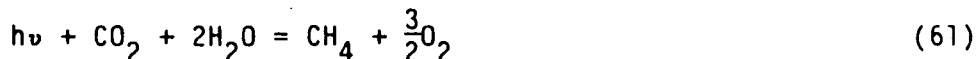
Photochemical surface reactions form their own class due to the fact that a thermodynamically uphill reaction ($\Delta G > 0$) may be carried out with the aid of an external source of energy, light. In fact, one of the most important chemical reactions of our planet, photosynthesis requires the input of 720 kcal/mol of energy to convert carbon dioxide and water to one mole of sugar:



It is useful to consider light as one of the reactants in photosynthesis. By adding the light energy to Eq. (59), the reaction becomes athermic or even exothermic if excess light energy is utilized, $h\nu + \text{H}_2\text{O} + \text{CO}_2 = \text{--- CH}_2\text{---} + \frac{3}{2}\text{O}_2$. We may consider photon-assisted or photochemical reactions of many types that lead to the formation of lower-molecular-weight hydrocarbons and of other products. One of the simplest of these important new classes of reactions leads to the dissociation of water:



Another leads to the formation of methane:



or to the fixation of nitrogen:



Light as a reactant may be employed in two ways. The adsorbed molecules can be excited directly by photons of suitable energy to a higher vibrational or electronic states. The excited species then may undergo chemical rearrangements or interactions that are different

from those in the ground vibrational or electronic states. Alternatively, the solid can be excited by light in the near-surface region. Photons of band-gap or greater energy may excite electron-hole pairs at the surface. As long as these charge carriers have a relatively long lifetime (i.e., they are trapped at the surface, so that their recombination is not an efficient process), there is a high probability of their capture by the adsorbed reactants. These, in turn, can undergo reduction or oxidation processes using the photogenerated electrons and holes, respectively. The photographic process is one example of this type of surface photochemical reaction. However, one would like the photogenerated electrons and holes to be captured by the adsorbed molecules in order to carry out photochemical surface reactions of the adsorbates instead of the photodecomposition of the solid at the surface. The cross sections for adsorption of band-gap or higher-than-band-gap energy photons are so large that the photogeneration of electron-hole pairs is a most efficient process. At present, this cannot be readily matched by the efficiency of direct photoexcitation of vibrational or electronic energy states of the adsorbed molecules.

Many solid surfaces efficiently convert light to long-lived electron-hole pairs that can induce the chemical changes leading to the reactions in Eqs. (60), (61), and (62). In fact, inorganic photo-reaction is one of the exciting new fields of surface science and heterogeneous catalysis.

It is important to distinguish between thermodynamically uphill photochemical reactions and thermodynamically allowed photon-assisted reactions. The latter reactions are thermodynamically feasible without any external energy input, but light is used to obtain certain product selectively. Excitation of selected vibrations, rotations, or electronic states of the incident or adsorbed molecules by light permits one to change the reaction path or increase the reaction rate. For example, the hydrogenation of acetylene or the oxidation of ammonia can be photon-assisted, leading to different reaction rates than in the absence of light.

As an example of a photocatalyzed surface reaction we will discuss the photoelectrochemical dissociation of water. It was shown in 1972 that upon illumination of reduced titanium oxide (TiO_2), which served as the anode in basic electrolyte solution, oxygen evolution was detectable at the anode, and hydrogen evolved at a metal (platinum) cathode. This reaction requires an energy of 1.23 V/electron (a two-electron process per dissociated water molecule). In the presence of light of energy equal to or greater than the band-gap energy of titanium oxide (3.1 eV), an external voltage as low as 0.2 V was sufficient to dissociate water. The process stopped as soon as the light was turned off, and started again upon re-illumination. Shortly after, several other systems showed the ability to carry out photon-assisted dissociation of water. When p-type gallium phosphide, GaP, was used as a cathode instead of platinum upon illumination of the TiO_2 anode, O_2 and H_2 could be generated at the semiconductor anode and cathode,

respectively, without the need of applying any external potential. When strontium titanate, SrTiO_3 , was substituted for TiO_2 as the anode, H_2O photodissociation was found to take place without external potential even when a platinum cathode was employed.

Figure 47 shows a schematic energy diagram to indicate the conditions necessary to carry out photoelectrochemical reactions efficiently. If the band-gap energy is greater than the free energies for the reduction and oxidation reactions, the photoelectron that is excited into the conduction band by light could reduce B^+ to B by electron transfer from the surface to the molecule. The photogenerated electron vacancies (holes) could also oxidize the A^- anions to A by capturing the electron. For the photodissociation of water, the conduction band must be above the H^+/H_2 potential and the valence band below the O_2/OH^- potential to be able to carry out the photoreaction without an external potential. The band gap has to be greater than 1.23 V and the "flat band" potential of the conduction and valence bands energetically well placed with respect to the (H^+/H_2) and O_2/OH^- couples. The flat-band potentials can be obtained by capacitance measurements as a function of external potential.

There is, of course, considerable band bending of the conduction and valence bands of any semiconductor at the surface. This is due to the presence of localized electronic surface states and to charge transfer between the adsorbates and semiconductor. Potential-energy diagrams that show the band positions schematically at an n-type or p-type semiconductor liquid interface are shown in Fig. 48. The band

bending provides an efficient means of separating electron-hole pairs, since the potential gradient as shown for the n-type semiconductor drives the electrons away from the semiconductor surface while it attracts the holes in the valence band toward the semiconductor electrolyte interface. As a result, the oxidation reaction takes place at the oxide anode while the reduction reaction takes place at the cathode to which the photoelectron migrates along the external circuit. The magnitude of the band bending at the surface depends primarily on the carrier concentration in the semiconductor and on the electron-donating or -accepting abilities of the adsorbates at the surface. Semiconductors that are not likely to carry out the photodissociation of water, according to the location of their flat-band potential, may become photochemically active as a result of strong band bending at the surface.

Often the oxidation or reduction photoreactions lead to the decomposition of the semiconductor electrode material. Instead of the photoreactions of adsorbate ions or molecules, a solid-state photoreaction occurs. This is particularly noticeable at the surfaces of illuminated CdS, Si, and GaP. Much of the research is therefore directed toward stabilizing these photoelectrode materials by suitable adsorbates that could prevent the occurrence of photodecomposition by providing an alternative chemical route for the photoreduction or photooxidation.

Bibliography

- Adamson, A.W., Physical Chemistry of Surfaces, 4th Ed., Wiley, New York, 1982.
- Anderson, J.R., and Boudart, M., Catalysis Science and Technology, Vols. 1-7, Springer-Verlag, Berlin 1981-85.
- Ertl, G., and Gomer, R., (Eds.), Springer Series in Surface Sciences, Vols. 1-4, Springer-Verlag, Berlin, 1983-85.
- Ertl, G., and Koppers, J., Low Energy Electrons and Surface Chemistry, Verlag Chemie, Weinheim, 1979.
- Feuerbacher, B., Fitton, B., and Willis, R.F., Photoemission and the Electronic Properties of Surfaces, Wiley, London, 1979.
- King, D.A., and Woodruff, W.P., (Eds.), The Chemical Physics of Solid Surfaces and Heterogeneous Catalysis, Vols. 1-4, Elsevier, New York, 1983-85.
- Morrison, S.R., The Chemical Physics of Surfaces, Plenum, New York, 1977.
- Roberts, M.W., and McKee, C.S., Chemistry of the Metal-Gas Interface, Oxford University Press, New York, 1978.
- Somorjai, G.A., Chemistry in Two Dimensions: Surfaces, Cornell University Press, Ithaca, New York, 1981.
- Tompkins, F.C., Chemisorption of Gases on Metals, Academic, London, 1978.
- Vanselow, R., and Howe, R., (Eds.), Chemistry and Physics of Solid Surfaces, Vols. 1-6, Springer-Verlag, Berlin 1979-85.

Table 1
 Ordered structures induced by CO on Rh(111)

Type of molecule	LEED pattern	System
Alkylidynes	$c(4 \times 2)$	$CCH_3 + CO$
	$(2\sqrt{3} \times 2\sqrt{3})R30^\circ$	$3CCH_2CH_3 + CO$
Acetylene	$c(4 \times 2)$	$C_2H_2 + CO$
Aromatics	(3×3)	$C_6H_5F + 2CO$
	(3×3)	$C_6H_6 + 2CO$
	$c(2\sqrt{3} \times 4)Rect$	$C_6H_5F + CO$
	$c(2\sqrt{3} \times 4)Rect$	$C_6H_6 + CO$
Alkalis	$(\sqrt{3} \times 7)Rect$	$Na + 7CO$
	$c(4 \times 2)$	$Na + CO$

Table 2. Selected values of surface tension of solids and liquids.

Material	γ ergs cm^{-2}	T °C
He (l)	0.308	-270.5
N ₂ (l)	9.71	-195
Ethanol (l)	22.75	20
Water	72.75	20
Benzene	28.88	20
n-Octane	21.80	20
Carbon tetrachloride	26.95	20
Bromine	41.5	20
W (s)	2900	1727
Nb (s)	2100	2250
Au (s)	1410	1027
Ag (s)	1140	907
Ag (l)	879	1100
Fe (s)	2150	1400
Fe (l)	1880	1535
Pt (s)	2340	1311
Cu (s)	1670	1047
Ni (s)	1850	1250
Hg (l)	487	16.5
NaCl (s)	227	25
KCl (s)	110	25
CaF ₂ (s)	450	-195
MgO (s)	1200	25
SiO ₂ (s)	307	1300
Al ₂ O ₃ (s)	690	2323
Polytetrafluoroethylene	18.5	20
Polyethylene	31	20
Polystyrene	33	20
Poly (vinyl chloride)	39	20

Table 3. Surface composition of alloys: experimental results and predictions of the regular solution model.

Alloy System	Segregating constituent	
	Predicted regular solution	Experimental
Ag-Pd	Ag	Ag
Ag-Au	Ag	Ag
Au-Pd	Au	Au
Ni-Pd	Pd	Pd
Fe-Cr	Cr	Cr
Au-Cu	Cu	Au, none, or Cu depending upon composition
Cu-Ni	Cu	Cu
Au-Ni	Au	Au
Au-Pt	Au	Au
Pb-In	Pb	Pb
Au-In	In	In
Al-Cu	Al	Al
Pt-Sn	Sn	Sn
Fe-Sn	Sn	Sn
An-Sn	Sn	Sn

TABLE 4

Work functions measured from different crystal faces of tungsten and molybdenum

Crystal face	Work function (eV)	
	Tungsten	Molybdenum
(110)	4.68	5.00
(112)	4.69	4.55
(111)	4.39	4.10
(001)	4.56	4.40
(116)	4.39	--

Table 5. Chemical Processes Based on Heterogeneous Catalysis

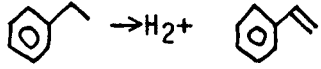
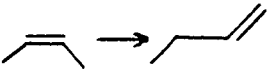
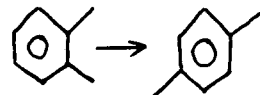
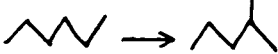
Processes	Typical Reactions	Catalysis	Reaction Conditions
Ammonia Synthesis	$N_2+3H_2 \rightarrow 2NH_3$	Triply promoted iron (Fe-K ₂ O-Al ₂ O ₃ -CaO);	720-800 K 40-100 atm
Dehydrogenation		Fe ₂ O ₃ -Cr ₂ O ₃ -K ₂ O mixed metal oxides	800-900 K 10-50 atm.
Epoxidation	$C_2H_4 + 1/2O_2 \rightarrow C_2H_4O$	AgCl-K ₂ O/Al ₂ O ₃	520-600K
Fischer-Tropsch synthesis of hydrocarbons	$CO+H_2 \rightarrow$ alkanes olefins aromatics	Fe ₃ O ₄ -K ₂ O/Al ₂ O ₃ supported Co, Ru, Ni, Rh	500-700 K 10-50 atm.
Fischer-Tropsch synthesis of oxygenates	$CO+H_2 \rightarrow$ aldehydes acids alcohols	Rh ₂ O ₃ .H ₂ O-K ₂ O LaRhO ₄ supported Pd, Pt	500-700 K 10-50 atm.
Hydrotreating (desulfurization and denitrification)	$R-S-R+H_2 \rightarrow 2RH+H_2S$	Co-Mo, Ni-Mo,	570-770 K
	$R=N-R+3/2H_2 \rightarrow 2RHH+NH_3$	Ni-Co-Mo/Al ₂ O ₃ Ni-W/Al ₂ O ₃ , MoS ₂ , WS ₂	30-200 atm.
Isomerization: olefins		solid acids, zeolites Group VIII metals	270-470 K 1-5 atm.
xylene		ZSM-5-zeolites	480-580 K 2-5 atm.
alkanes		zeolites, Pt/Al ₂ O ₃	570-770 K 5-50 atm.
Methanol synthesis	$CO+2H_2 \rightarrow CH_3OH$	ZnCrO ₃ ZnO-Cu ₂ O-Cr ₂ O ₃ ZnO-Cu ₂ O-Al ₂ O ₃	570-670 K 100-600 atm.
Methanol to gasoline	$CH_3OH \rightarrow$ aromatics olefins, H ₂ O	ZSM-5 zeolites	480-540 K 2-15 atm.

Table 5. (continued)

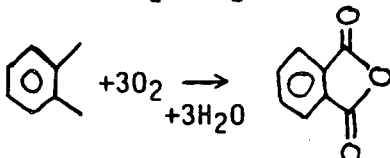
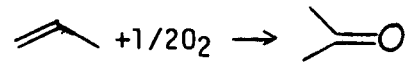
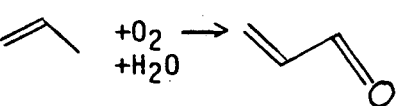
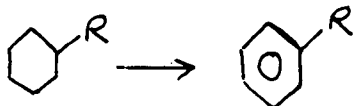
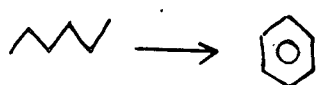
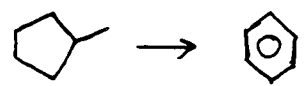

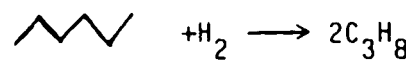
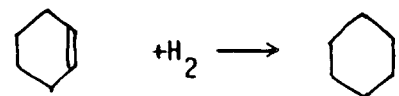
Processes	Typical Reactions	Catalysis	Reaction Conditions
NO _x Reduction	$\text{NO} + 5/2\text{H}_2 \rightarrow \text{NH}_3 + \text{H}_2\text{O}$ $2\text{NO} + 2\text{H}_2 \rightarrow \text{N}_2 + 2\text{H}_2\text{O}$ $2\text{CO} + 2\text{NO} \rightarrow 2\text{CO}_2 + \text{N}_2$	Ru, Rh, Pd, Pt/SiO ₂ Ru, Rh, metal oxides	370–520 K 1–10 atm. 450–650 K 1–10 atm.
Oxidation	olefins) alkanes) + O ₂ → CO ₂ + H ₂ O $2\text{NH}_3 + 5/2\text{O}_2 \rightarrow \text{NO} + 3\text{H}_2\text{O}$ $\text{CO} + 1/2\text{O}_2 \rightarrow \text{CO}_2$	Group VIII metals	370–670 K
Partial oxidations: alcohols	$\text{CH}_3\text{OH} + 1/2\text{O}_2 \rightarrow \text{H}_2\text{CO} + \text{H}_2\text{O}$	Ag, Fe ₂ (MoO ₄) ₃	550–570 K
o-xylene		V ₂ O ₅	1–10 atm.
olefins	$\text{C}_2\text{H}_4 + 1/2\text{O}_2 \rightarrow \text{CH}_3\text{CHO}$	V ₂ O ₅	
		SnO ₂ .MoO ₃	
		Bi ₂ O ₃ .MoO ₃	
Reforming:			
Dehydro- generation		Pt, Pt-Re, Pt-Ge +3H ₂	700–800 K
Dehydro- cyclization		Pt-Au, Pt-Re-Cu +3H ₂	5–50 atm.
Dehydro- isomerization		Ir-Au/Al ₂ O ₃ +3H ₂	
Isomerization			
Hydrogenolysis			
Hydrogenation			

Table 5. (continued)

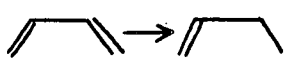
Processes	Typical Reactions	Catalysis	Reaction Conditions
Selective Hydrogenation olefins	$H_2 + $ 	NiS	420-500 K 1-10 atm.
alkynes	$R-C \equiv CH + H_2 \rightarrow RHC=CH_2$	Pt/Al ₂ O ₃	220-250 K 1-10 atm.
Steam Reforming	$CH_4 + H_2O \rightarrow CO + 3H_2$	Ni-K ₂ O/Al ₂ O ₃	850-1100K 30-100 atm.
Water Gas	$CO + H_2O \rightarrow CO_2 + H_2$	Fe ₂ O ₃ .Cr ₂ O ₃ ZnO-Cu ₂ O	650-800 J 20-50 atm.

Table 6. Structure-sensitive and Structure-insensitive
Catalytic Reactions

Structure sensitive	Structure insensitive
Hydrogenolysis Ethane: Ni Methylcyclopentane: Pt	Ring opening Cyclopropane: Pt
Hydrogenation Benzene: Ni	Hydrogenation Benzene: Pt
Isomerization Isobutane: Pt Hexane: Pt	Dehydrogenation Cyclohexane: Pt
Cyclization Hexane: Pt Heptane: Pt	

Figure Captions

- Figure 1: Field ion micrograph of a tungsten tip. Various crystal planes are labelled.
- Figure 2: Scheme of the low-energy electron diffraction experiment.
- Figure 3: Scheme of the low-energy electron diffraction apparatus employing the post-acceleration technique.
- Figure 4: LEED pattern from a Pt(111) crystal surface at 51 eV (upper left), 63.5 eV (upper right), 160 eV (lower left) and 181 eV (lower right) incident electron energy.
- Figure 5: Helium diffraction traces for Au(110)-(1x2) at a surface temperature of 100 K with incident angle $\theta_i = 48^\circ$. The wavelength λ_{He} is a) 1.09 Å and b) 0.57 Å.
- Figure 6: Scanning tunneling microscope picture of a clean (1x5) reconstructed Au(100) surface with monatomic steps. Divisions on the crystal axes are 5 Å, with approximately 1.5 Å from scan to scan. The inset shows the LEED pattern of the predominant (1x5) corrugation.
- Figure 7: Schematic showing the interactions at the surface of an aligned single crystal and the formation of the shadow cone. The energy spectra for the aligned and non-aligned case is shown below.

Figure 8: Schematic of the dependence of the intensity of the surface peak (SP) on different crystal surface structures. (a) The ideal crystal SP from "bulk-like" surface; (b) enhanced SP observed in normal incidence for a reconstructed surface; (c) enhanced SP observed in non-normal incidence for a relaxed surface; (d) reduced SP observed in normal incidence for a registered overlayer.

Figure 9: Model of a heterogeneous solid surface, depicting different surface sites. These sites are distinguishable by their number of nearest neighbors.

Figure 10: LEED patterns (left) and surface structures (right) of (a) flat (b) stepped and (c) kinked platinum surfaces.

Figure 11: Monolayer and multilayer phases of the n -paraffins C_3 to C_8 on Pt(111) and the temperatures at which they are observed at 10^{-7} Torr.

Figure 12: Top and side views (in top and bottom sketches of each panel) of adsorption geometries on various metal surfaces. Adsorbates are drawn shaded. Dotted lines represent clean surface atomic positions; arrows show atomic displacements due to adsorption.

Figure 13: Structure of the p(2x2) and c(2x2) sulphur overlayers on Ni(100).

Figure 14: Schematic representation of the CO on Pd(111) system. Structure models and observed LEED structures for the various CO coverages, θ , are shown.

Figure 15: Observed surface unit cells for n-paraffins on Pt(111).

Figure 16: Schematic diagram of an EELS spectrometer of the single-pass 127° cylindrical electrostatic deflector type.

Figure 17: Electron energy loss spectrum of CO adsorbed on Rh(111).

The loss peak at 468 cm^{-1} is due to the Rh-CO symmetric stretch, and that at 2036 cm^{-1} is due to the C-O symmetric stretch. The spectrum was recorded at a resolution of 30 cm^{-1} .

Figure 18: EELS spectra of the adsorption and decomposition of ethylene (C_2H_4) on Rh(111).

Figure 19: Surface phase diagram of Au-Ag alloy.

Figure 20: Definition of the contact angle between a liquid and solid and the balance of surface forces at the contact point among the three phases (solid, vapor and liquid).

Figure 21: Free energy of homogeneous nucleation as a function of particle size.

Figure 22: One-dimensional potential energy of an adatom in a physisorbed state on a planar surface as a function of its distance z from the surface.

Figure 23: One-dimensional potential energy curves for dissociative adsorption through a precursor or physisorbed state (a) represents adsorption into the stable state with no activation energy; (b) represents adsorption into the chemisorption well with activation energy ΔE .*

Figure 24: Adsorption isotherms for CO on Pt(111) single-crystal surfaces.

- Figure 25: Typical thermal desorption spectra of CO from a Pt(553) stepped crystal face as a function of coverage. The two peaks are indicative of CO bonding at step and terrace sites. The higher temperature peak corresponds to CO bound at step sites.
- Figure 26: Isoteric heat of adsorption for CO on Pd(111) crystal face as a function of coverage.
- Figure 27: Heats of adsorption of CO on single-crystal surfaces of transition metals.
- Figure 28: Heats of adsorption of CO on polycrystalline transition-metal surfaces.
- Figure 29: Energy-level diagram as a function of distance x from the surface ($x = 0$).
- Figure 30: Charge density oscillation and redistribution at a metal-vacuum interface.
- Figure 31: Energy-level diagram (a) in the absence of any space charge and (b) with a surface space charge due to depletion of electrons in the surface region.
- Figure 32: Potential energy diagram illustrating the work function. E_F is the Fermi energy, ϕ is the work function and W is the potential well bonding the conduction band electrons into the solid.
- Figure 33: Field emission pattern of a tungsten tip. The (011) plane is in the center.

Figure 34: Energy-level diagrams for an intrinsic semiconductor in the presence of (a) electron-donor or (b) electron-acceptor surface states.

Figure 35: "Universal curve" for the electron mean free path as a function of electron kinetic energy. Dots indicate individual measurements.

Figure 36: Experimental number of scattered electrons $N(E)$ of energy E versus electron energy, E , curve.

Figure 37: Scheme of the Auger electron emission process.

Figure 38: Typical Auger spectra from a clean Mo(100) single-crystal and a Mo(100) surface contaminated with sulfur.

Figure 39: 1s Electronic binding energy shifts in nitrogen, indicating the different photoelectron energies observed in various chemical environments.

Figure 40: One dimensional potential energy diagram parallel to the surface plane.

Figure 41: Diffusion of rhenium atoms on W(211) at 327 K. Field ion images are taken after 60s diffusion intervals.

Figure 42: Rectilinear plot displaying the (a) specular scattering and (b) cosine angular distribution of scattered beams. The arrow indicates the angle of incidence.

Figure 43: HD production as a function of angle of incidence, θ , of the molecular beam, normalized to the incident D_2 intensity. (a) Pt(332) surface with the step edges perpendicular to the incident beam ($\theta = 90^\circ$); (b) Pt(332) where the projection of the beam on the surface is parallel to the step edges ($\theta = 0^\circ$); (c) Pt(111).

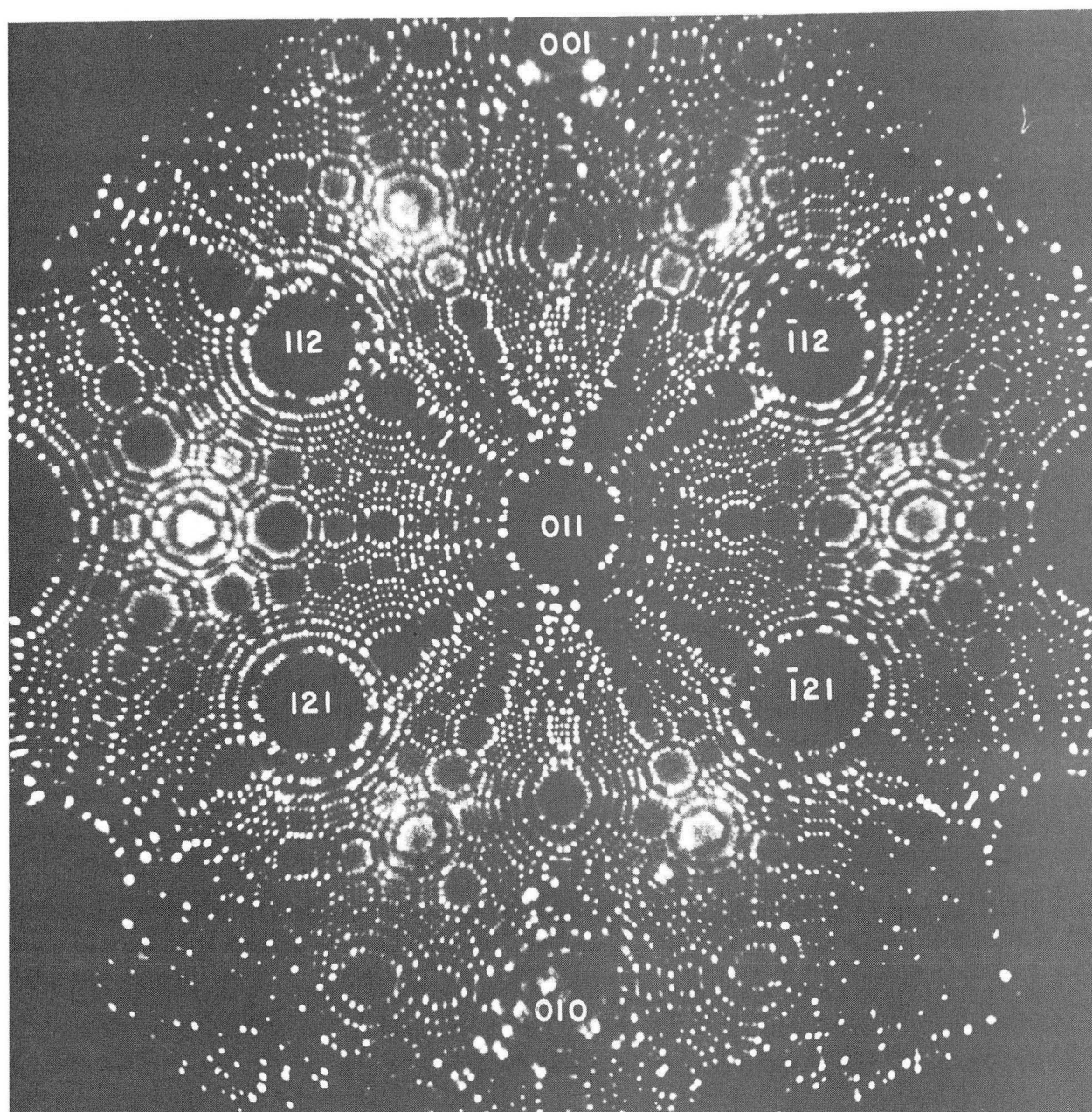
Figure 44: Line drawing of the structure of the zeolite faujasite.

Figure 45: Catalyst particle viewed as a crystallite, composed of well-defined atomic planes.

Figure 46: Schematic representation of the experimental apparatus to carry out catalytic-reaction-rate studies on single-crystal surfaces of low surface area at low and high pressures in the range 10^{-7} to 10^4 Torr.

Figure 47: Energy conditions needed to reduce B^+ to B and oxidize A^- to A at a semiconductor surface. Electrons that are excited by photons into the conduction band E_{CB} must be able to reduce B^+ , and electron vacancies (holes) in the valence band E_{VB} must be able to oxidize A^- .

Figure 48: Band bending at the n-type and p-type semiconductor interfaces.



XBB 861-545

Fig. 1

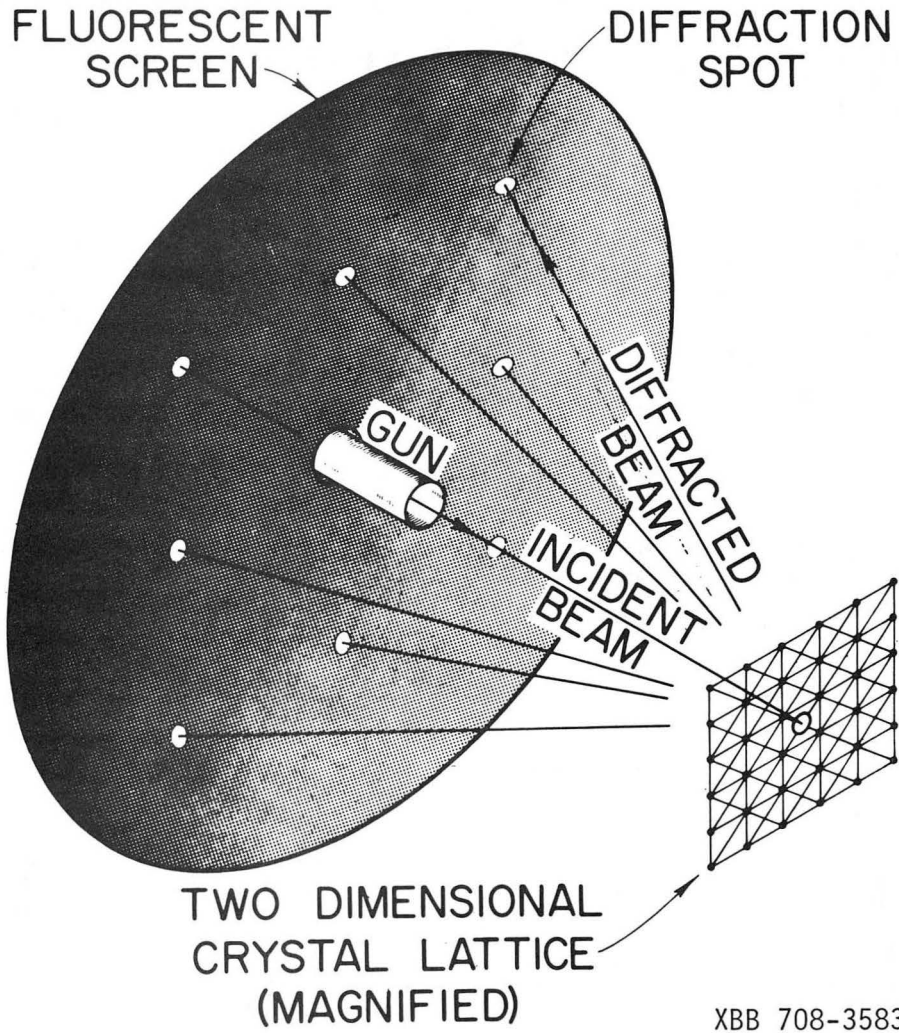


Fig. 2

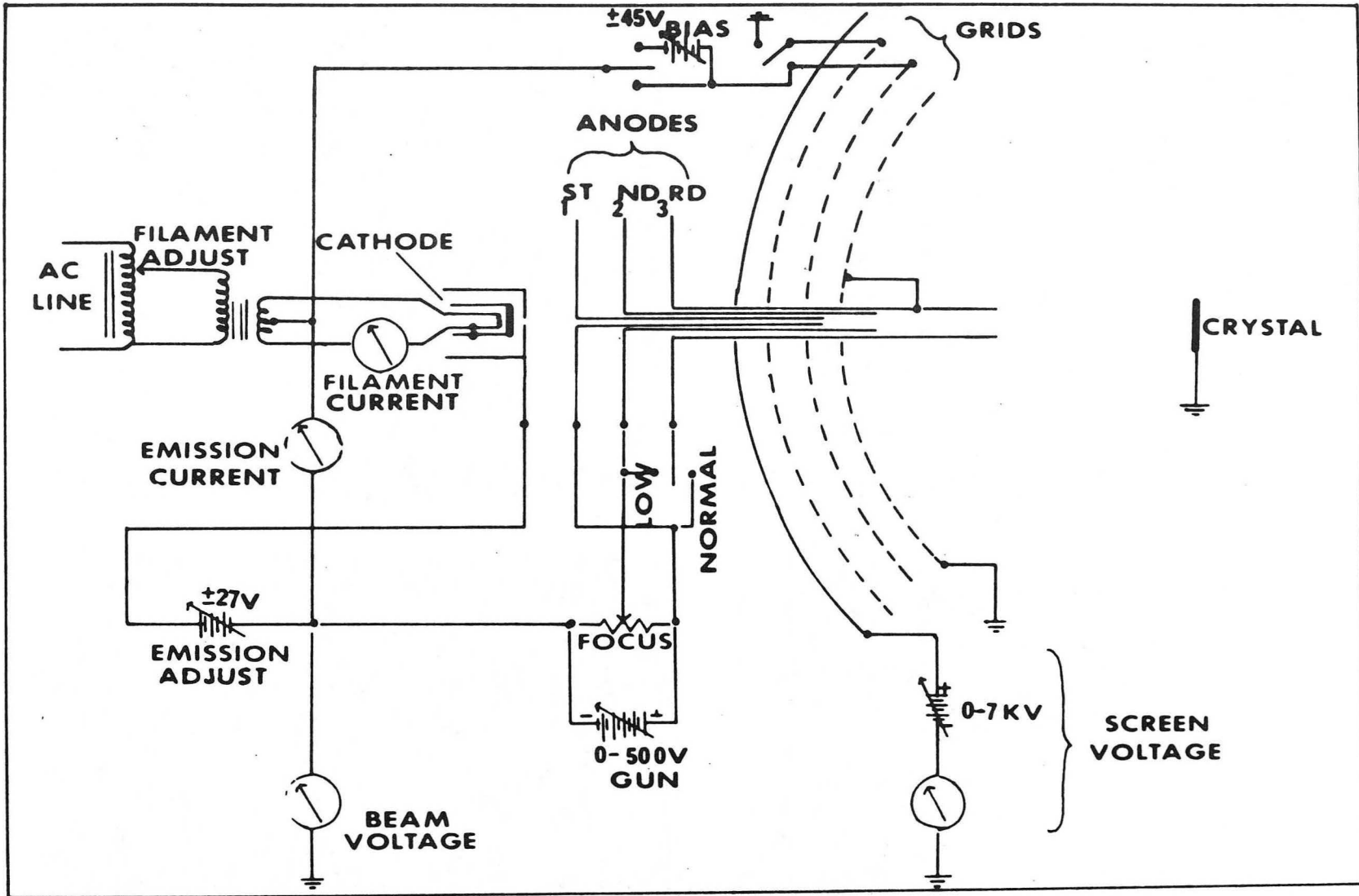
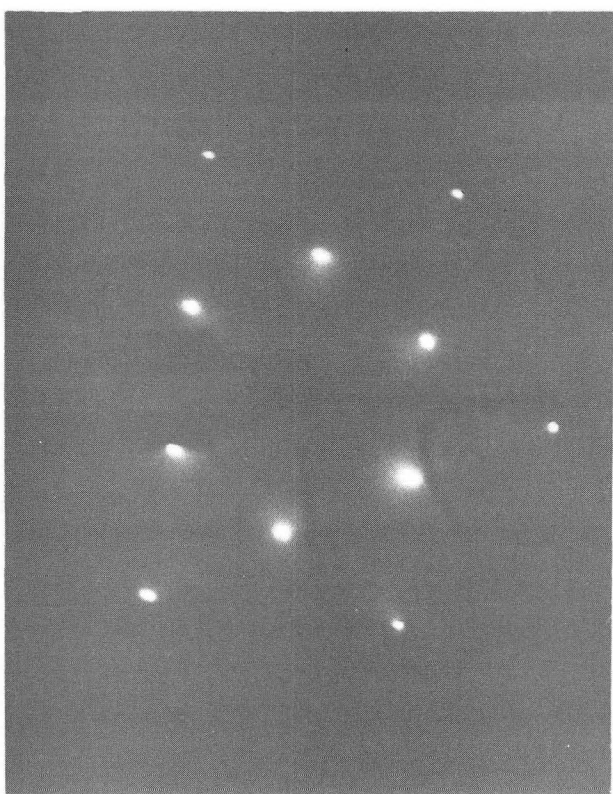
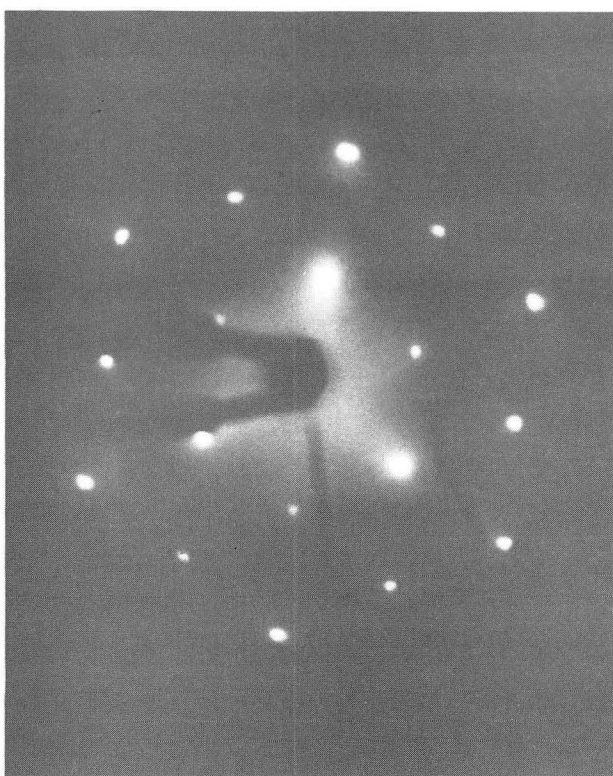
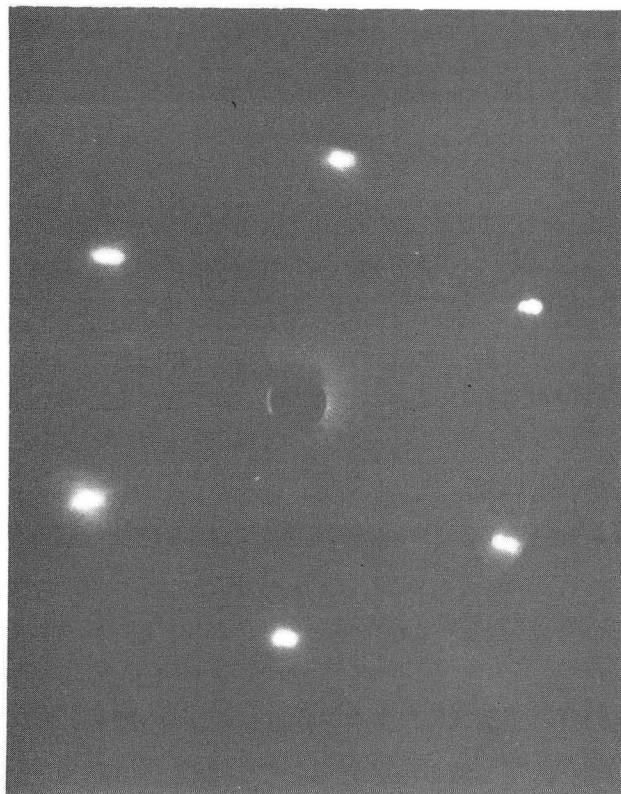
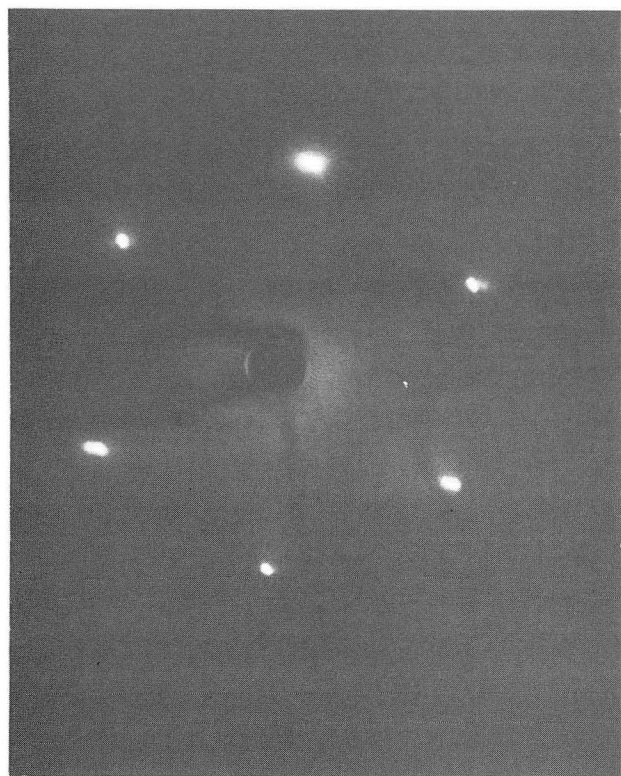


Fig. 3

XBL 861-120



XBB 700-5685

Fig. 4

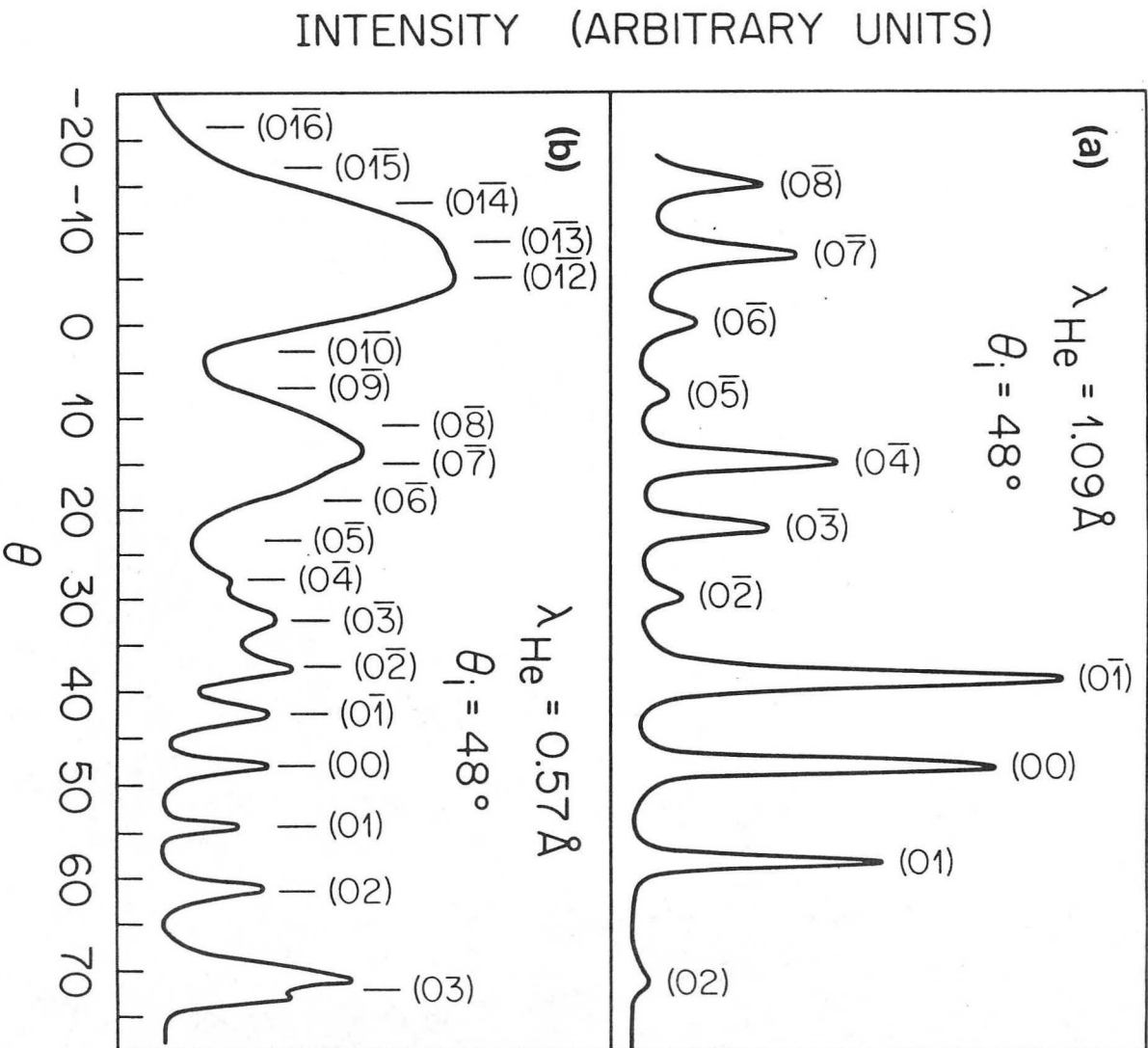
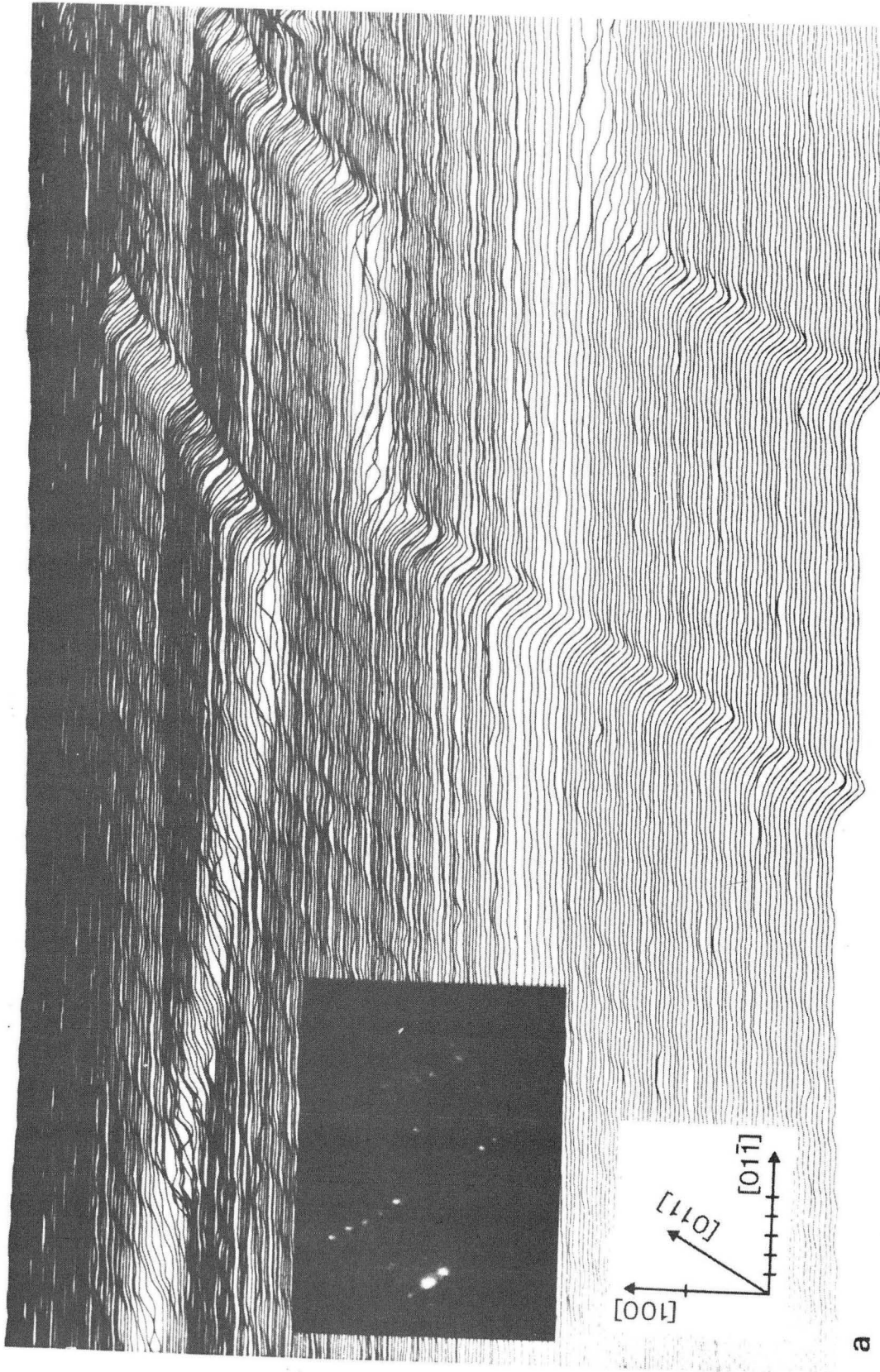


Fig. 5

XBL 861-157



XBB 861-236

Fig. 6

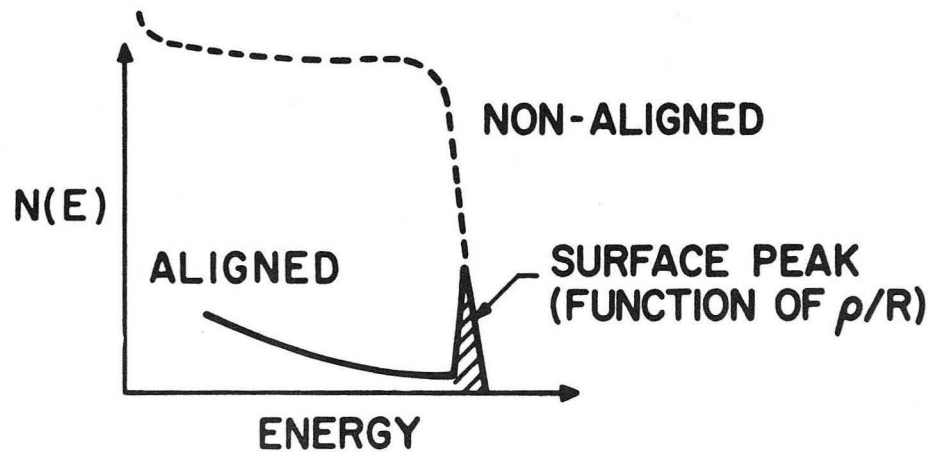
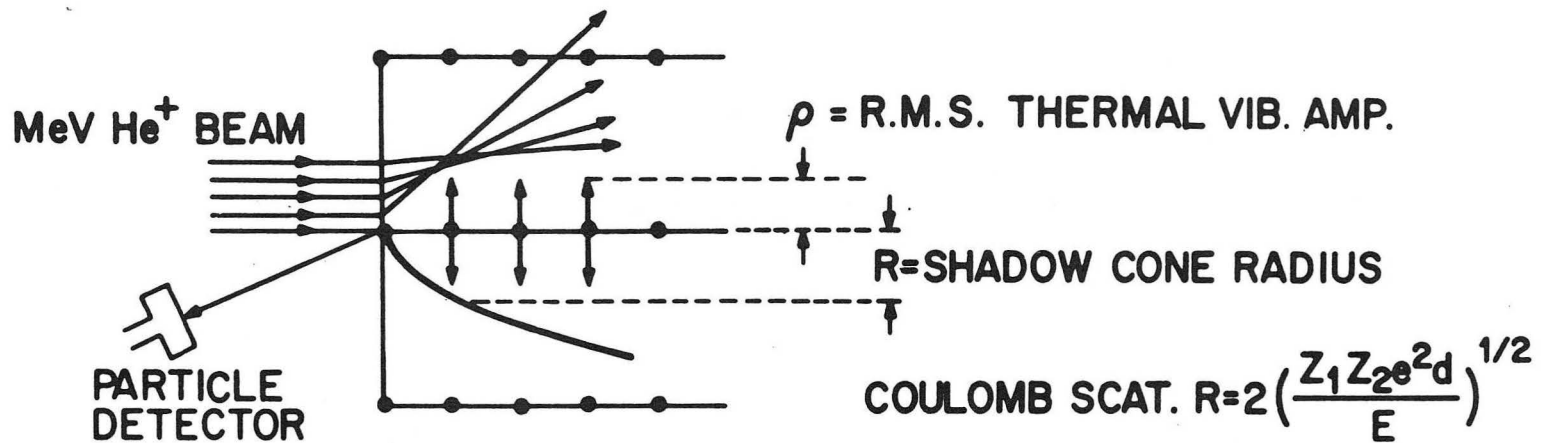
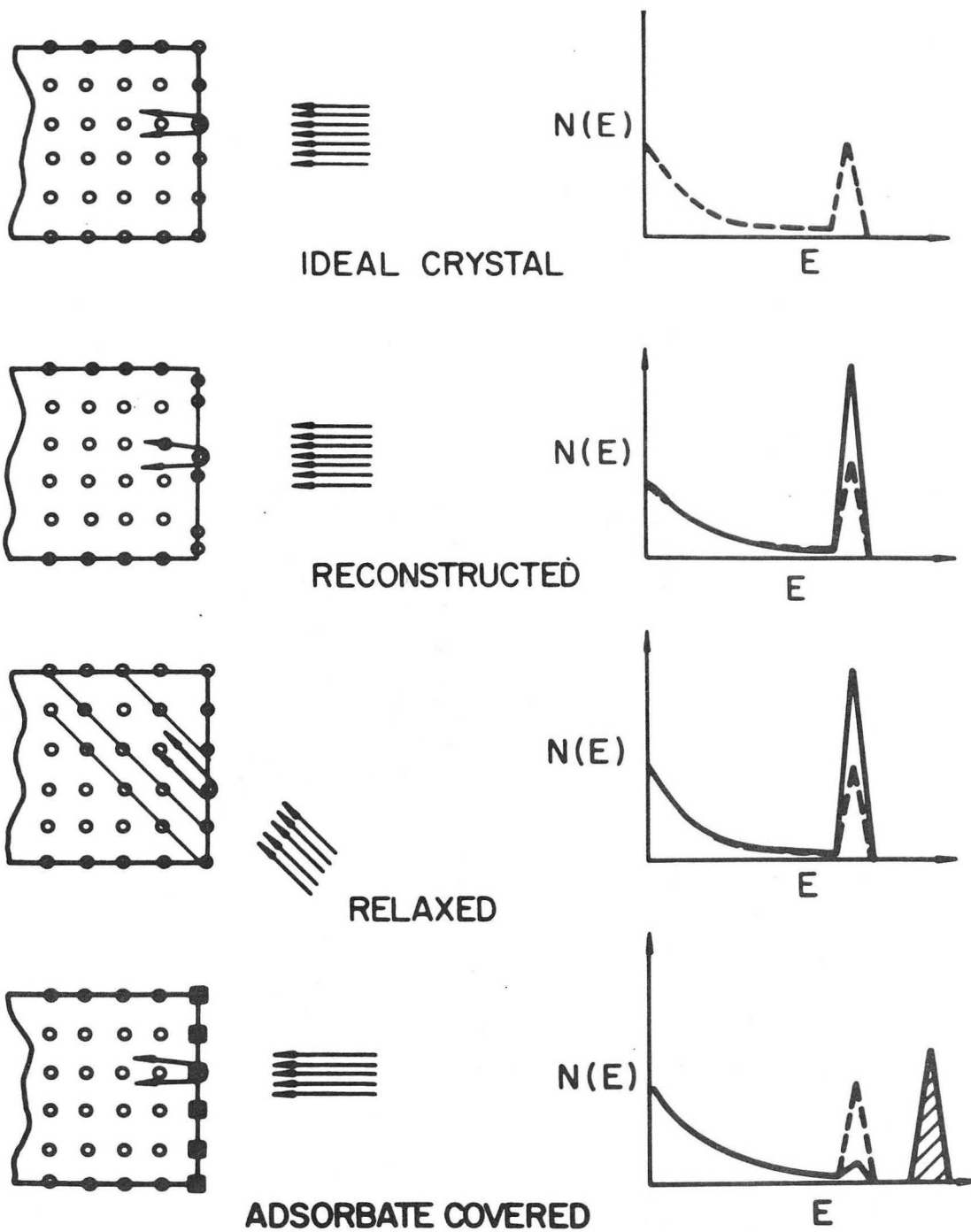


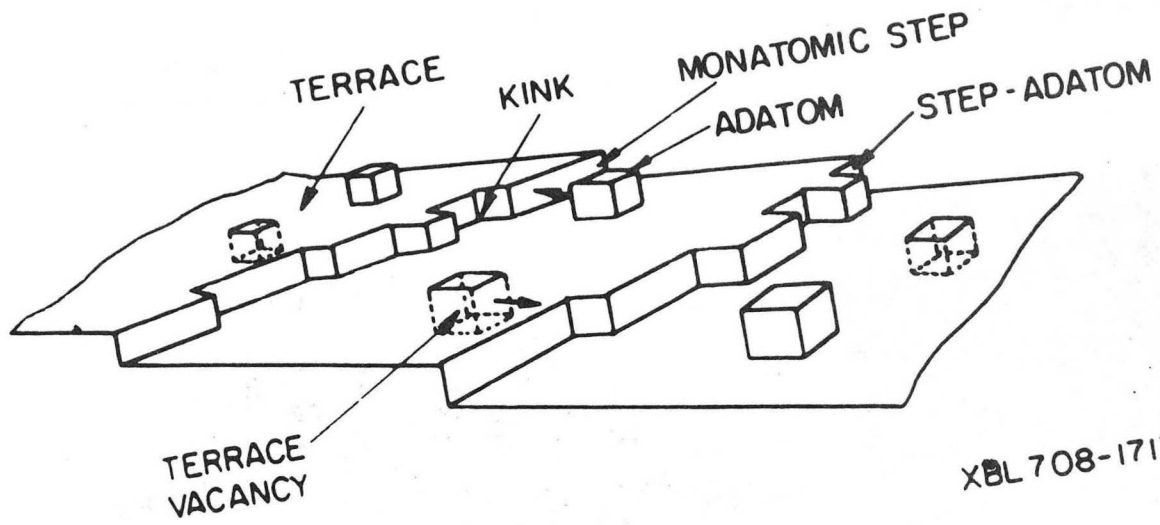
Fig. 7

XBL 861-110



XBL 861-111

Fig. 8



XBL 708-1717 A

Fig. 9

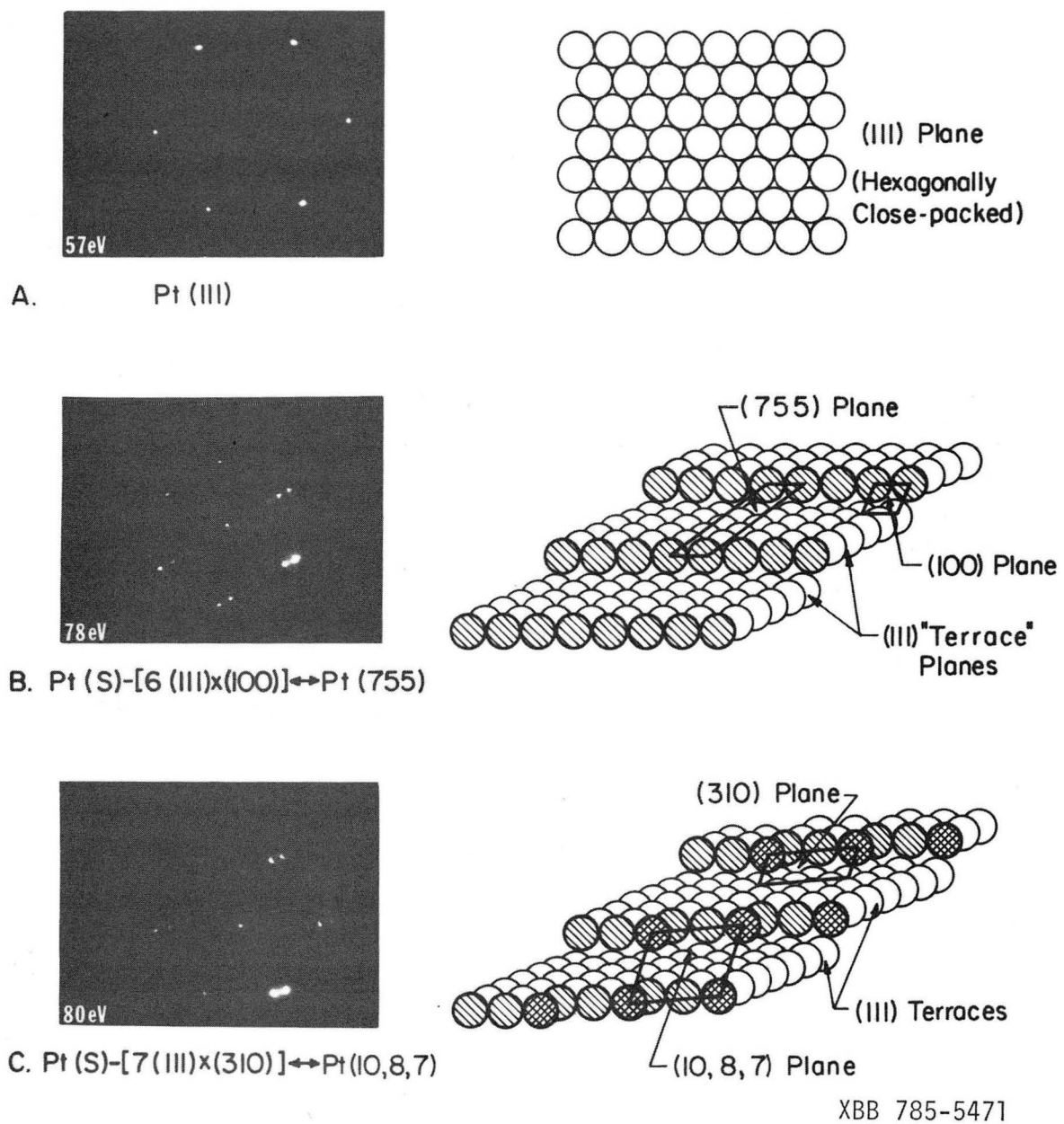
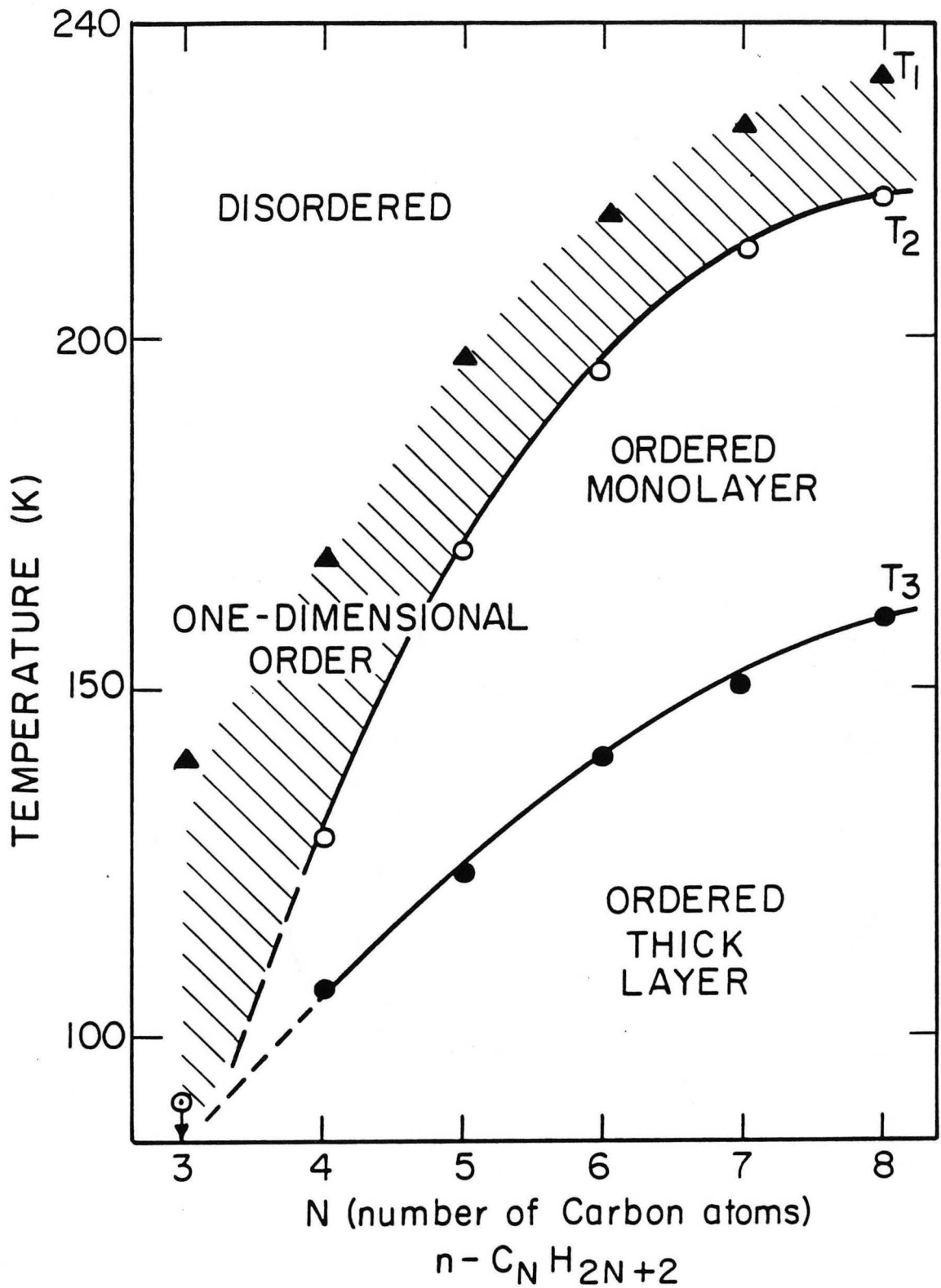
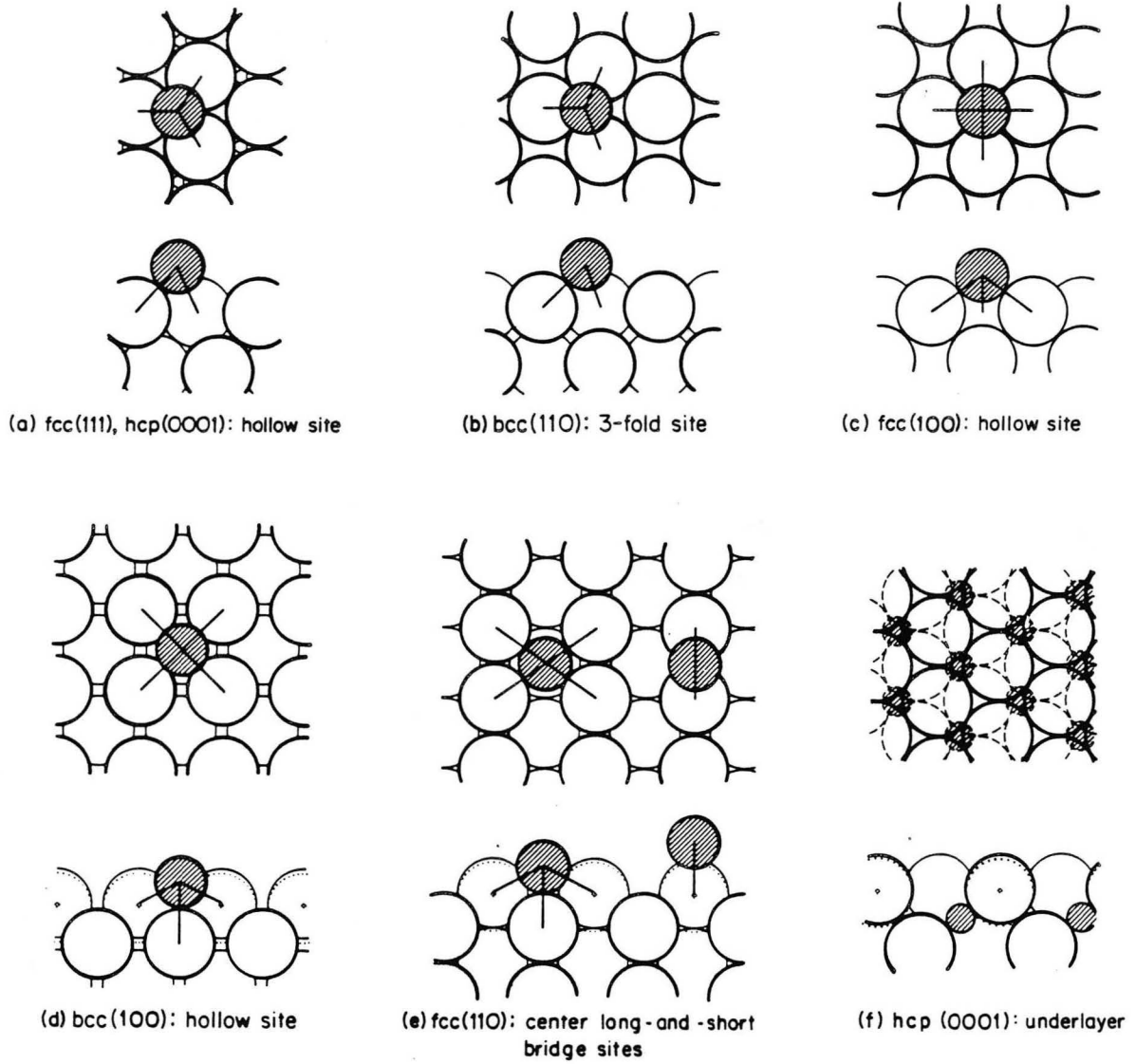


Fig. 10



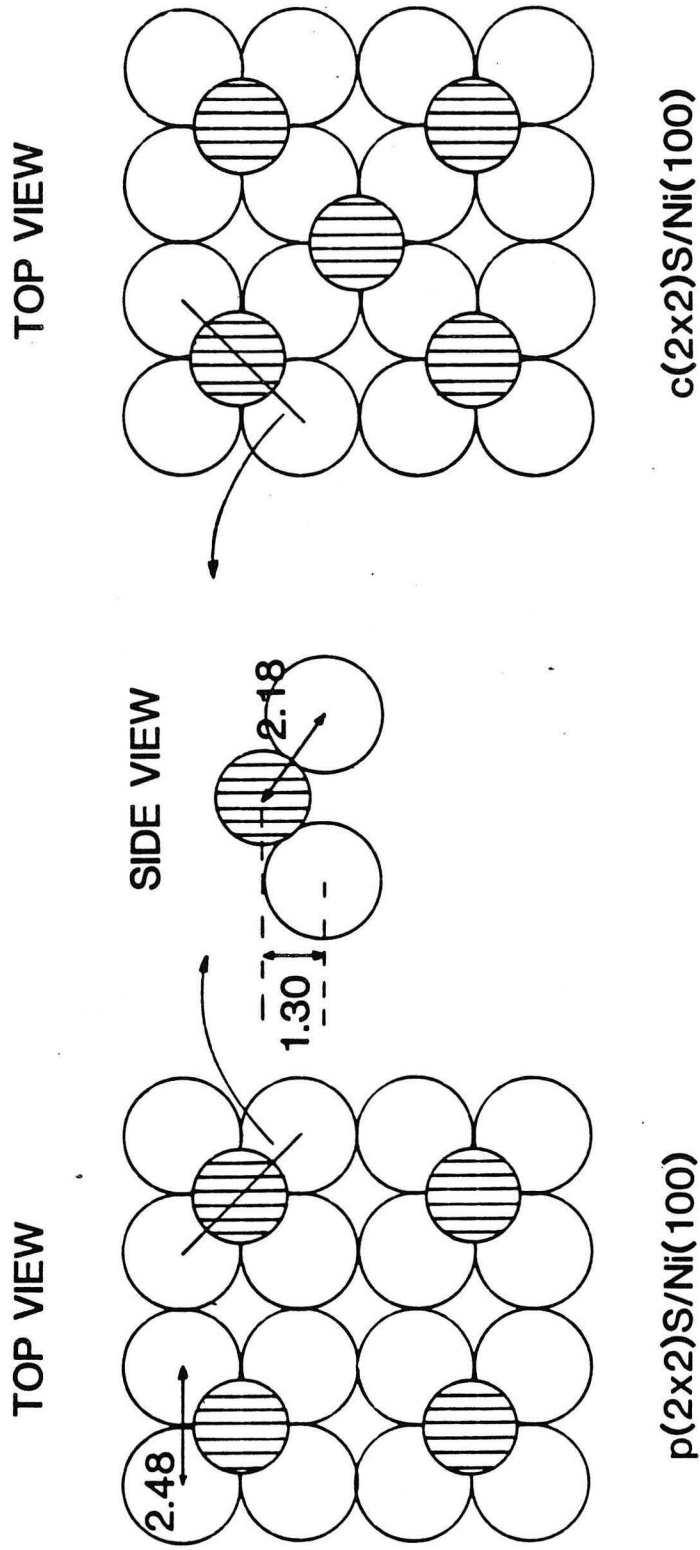
XBL 765-6794

Fig. 11



XBL 7812-6293

Fig. 12



XBL 861-163

Fig. 13

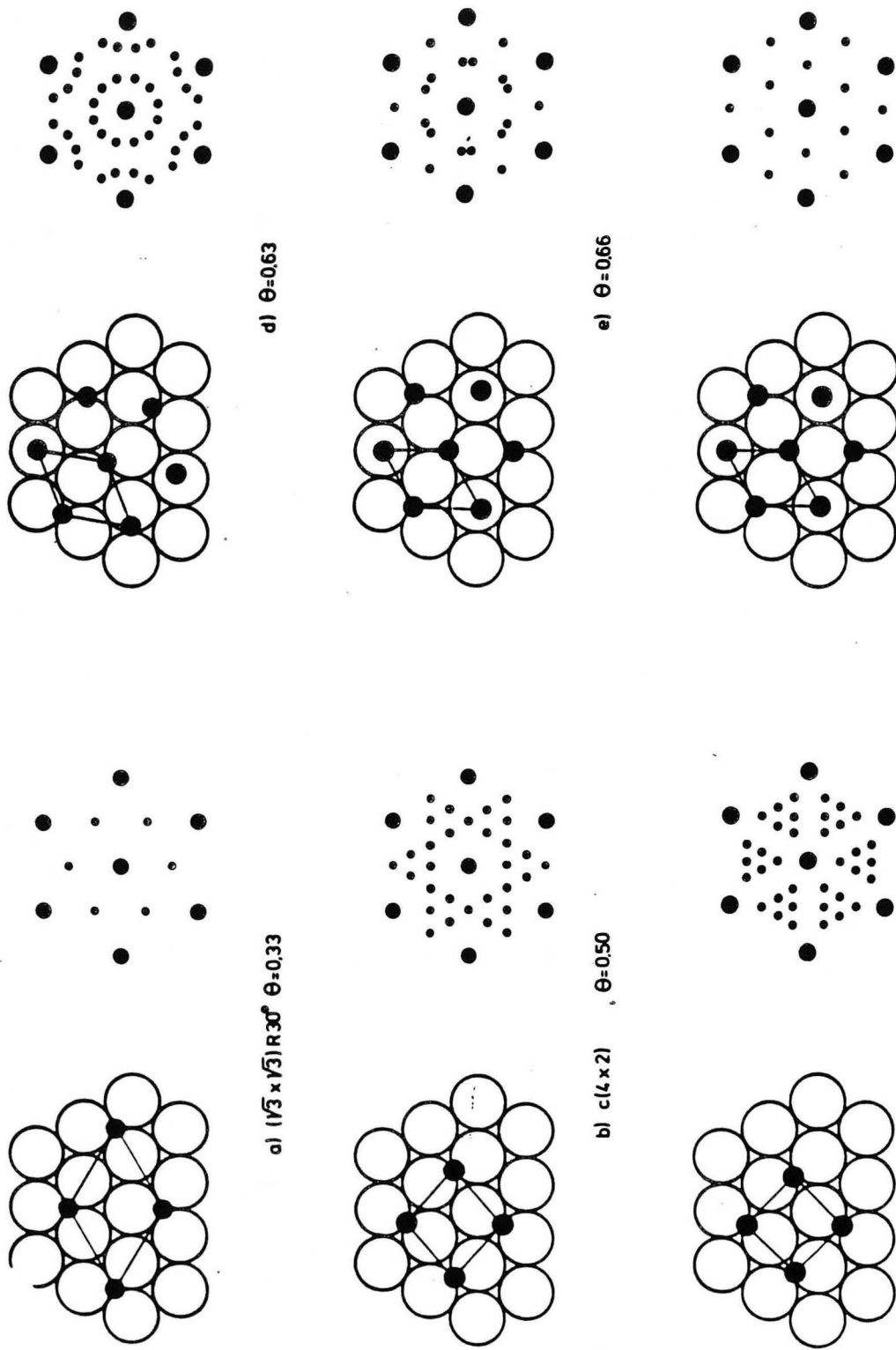
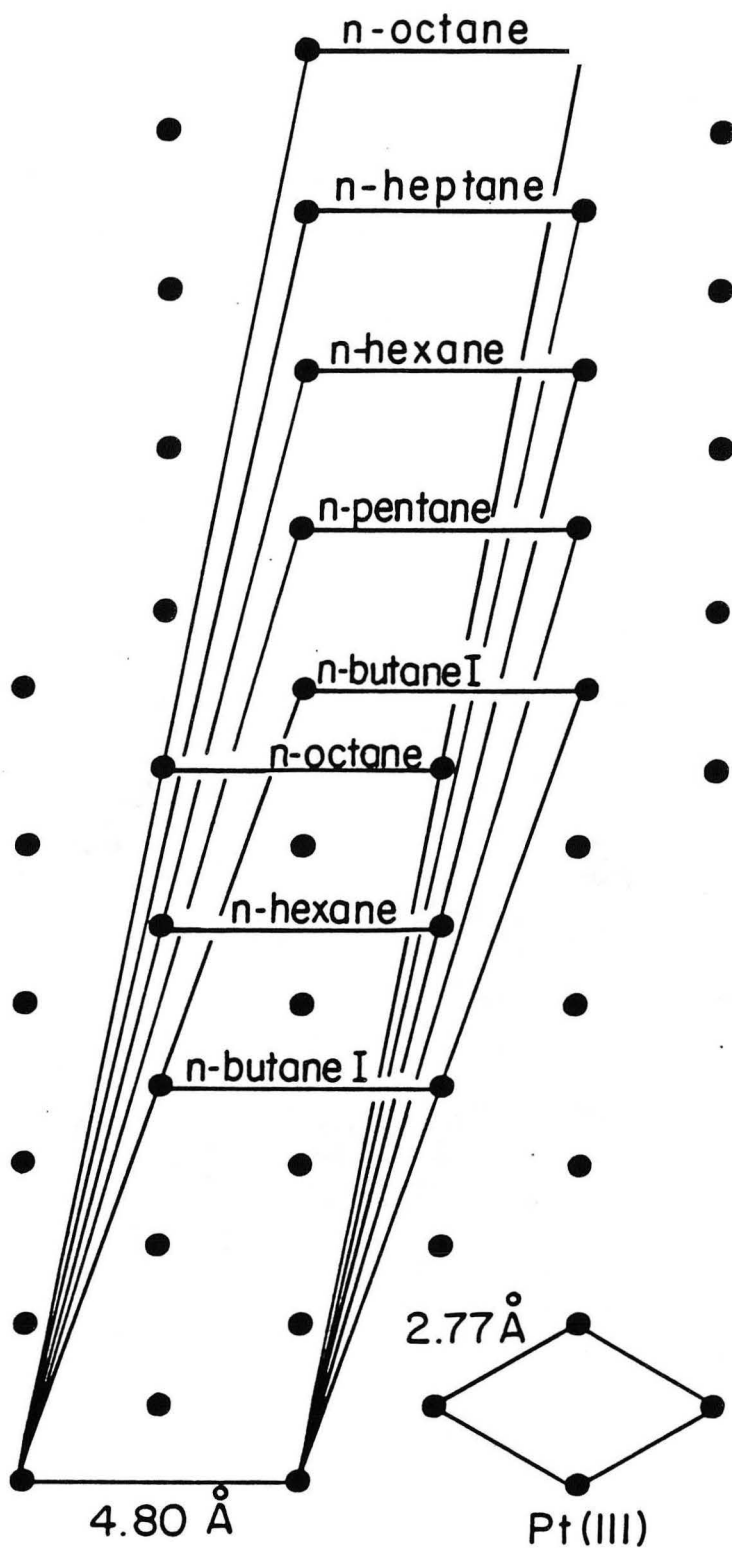


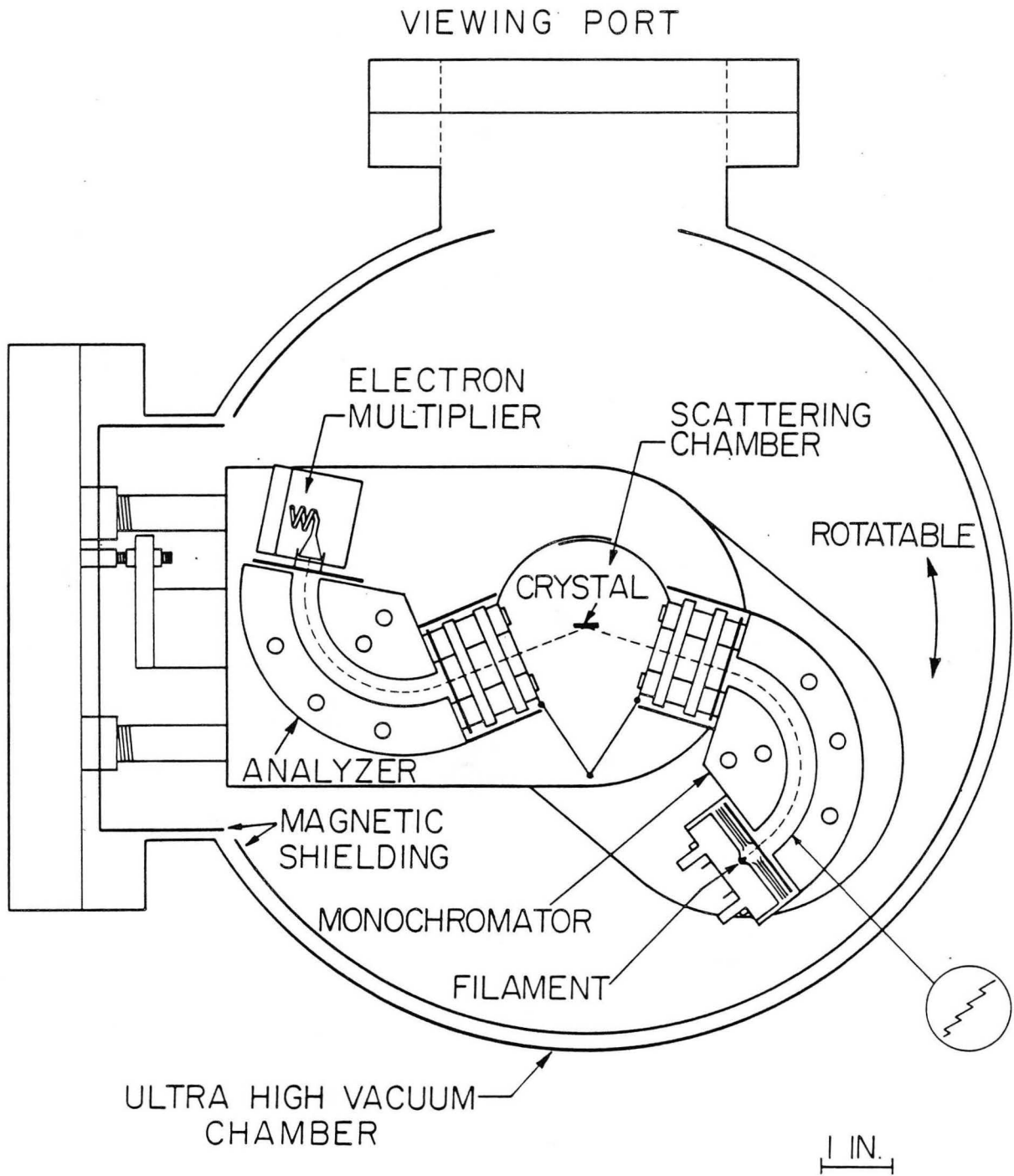
Fig. 14

XBL 861-109



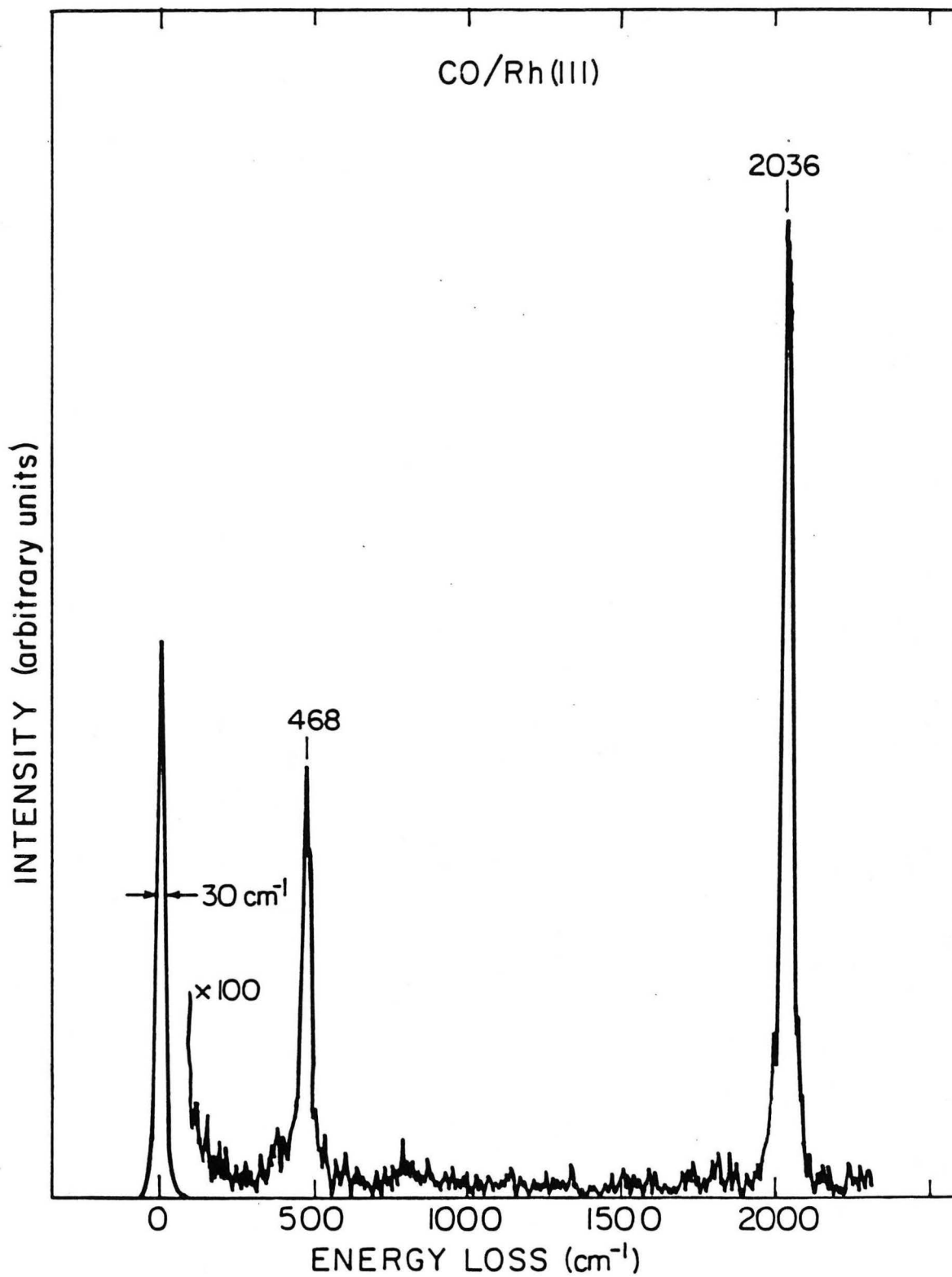
XBL766-7126

Fig. 15



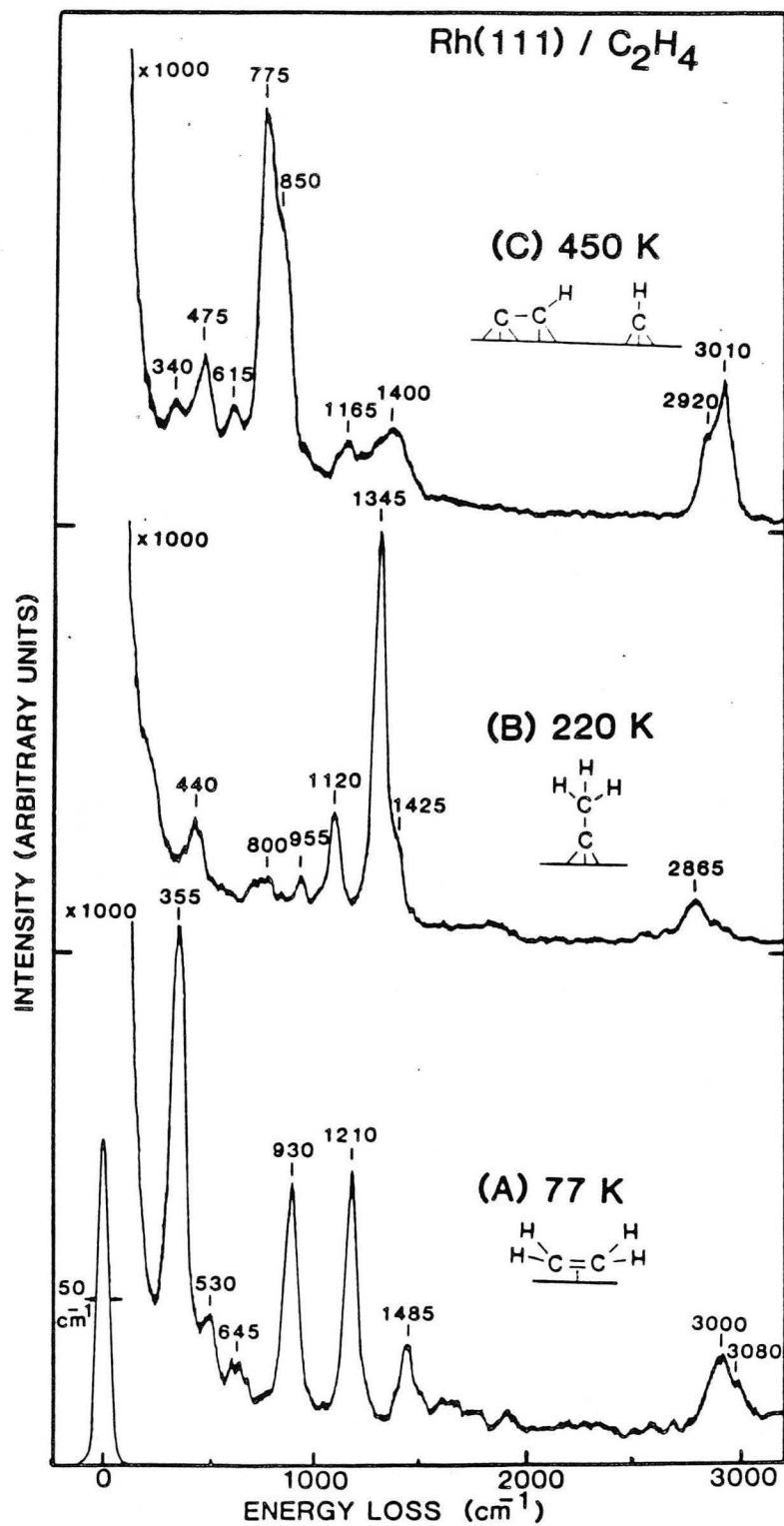
XBL 7712-6527

Fig. 16



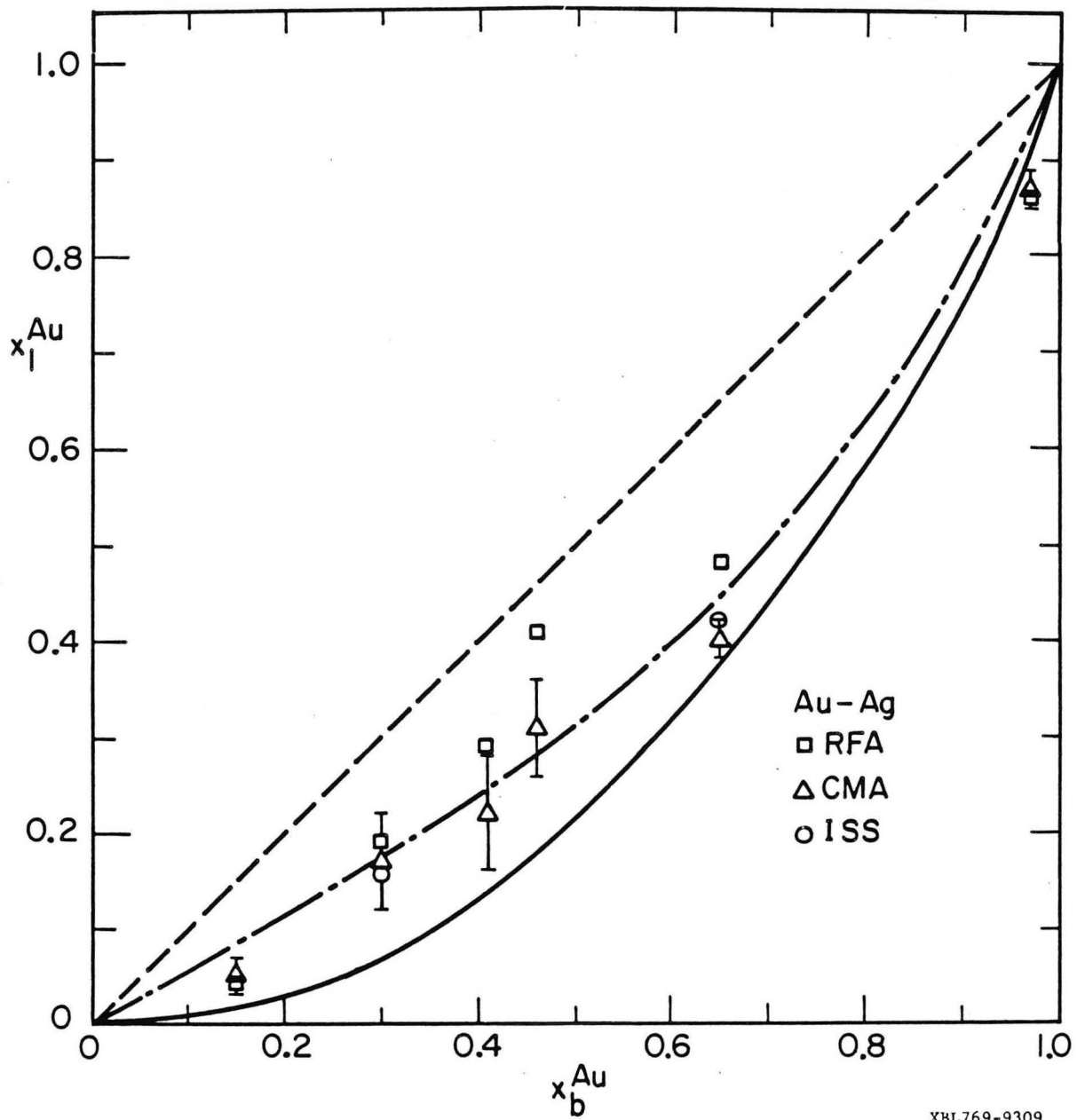
XBL 8312-6684

Fig. 17



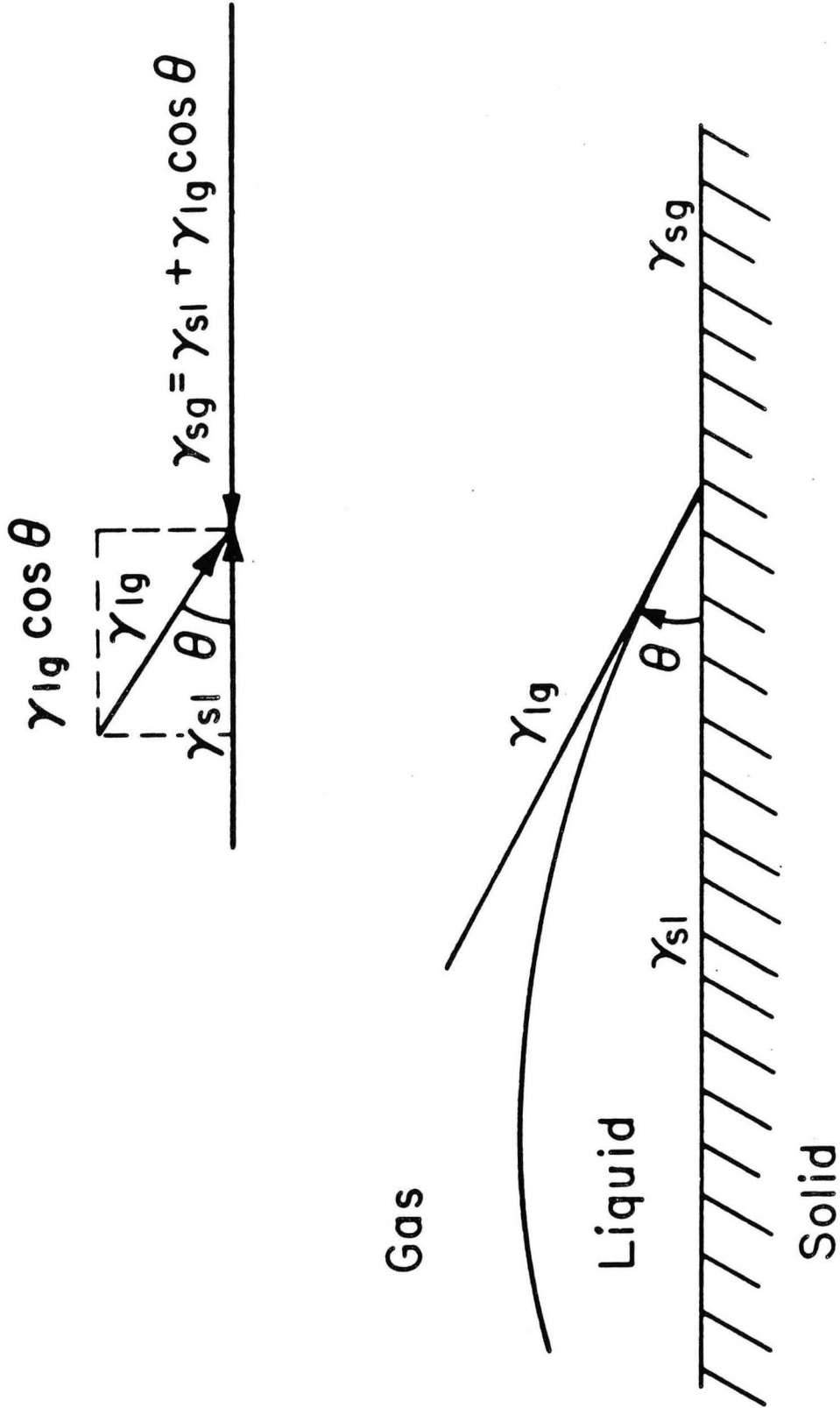
XBL 8512-4941

Fig. 18



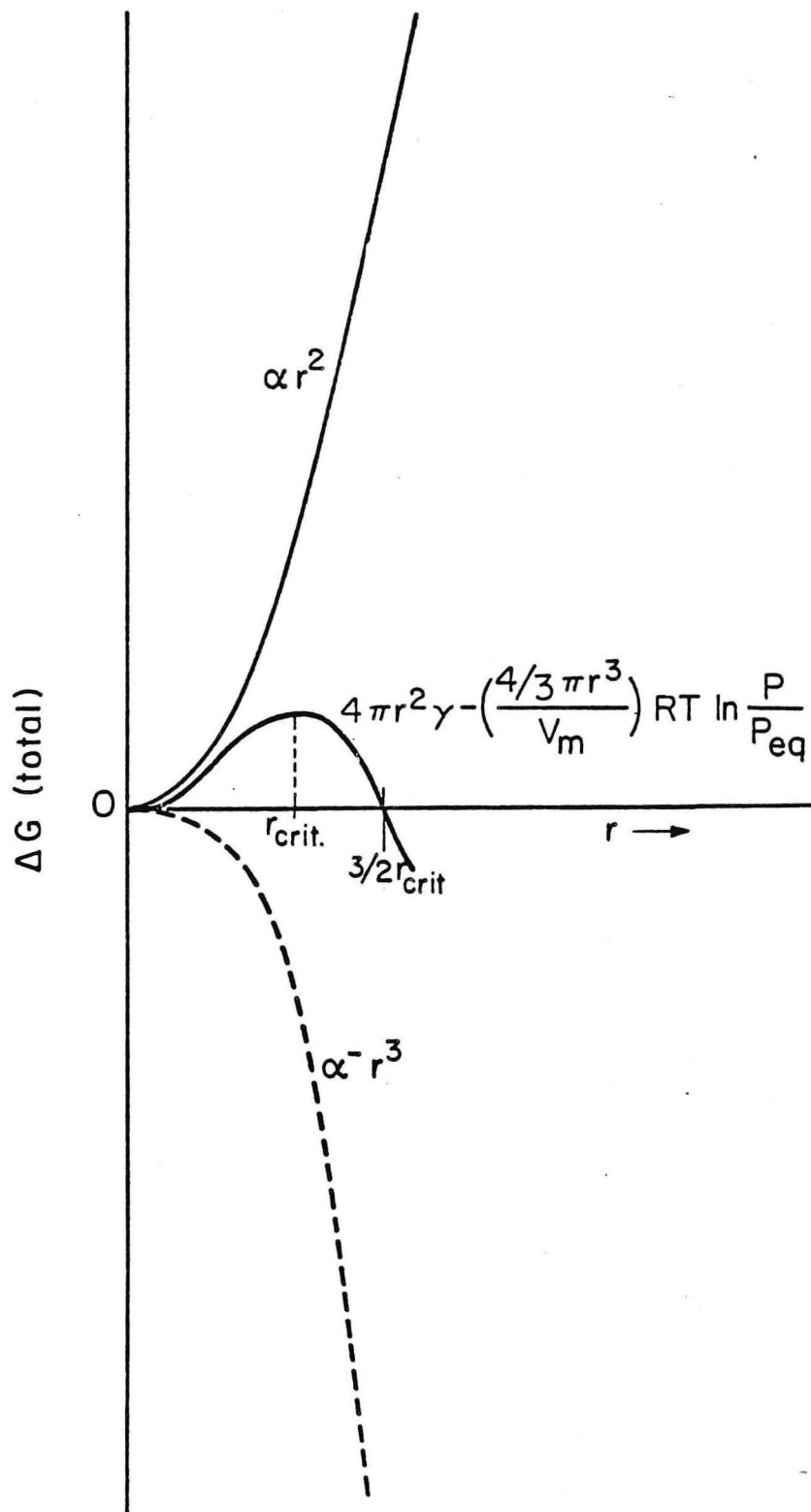
XBL769-9309

Fig. 19



XBL 861-121

Fig. 20



XBL 798-6896

Fig. 21

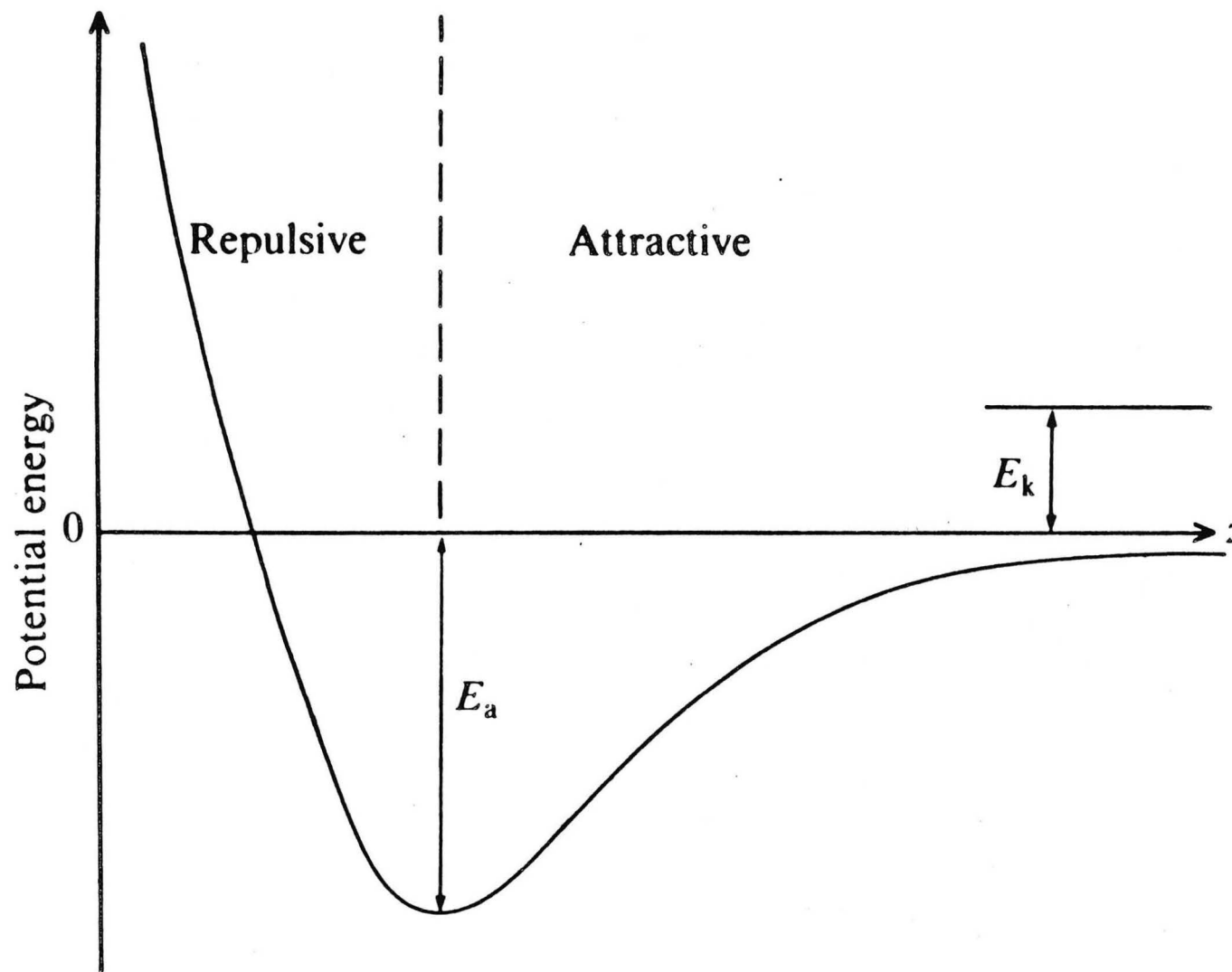
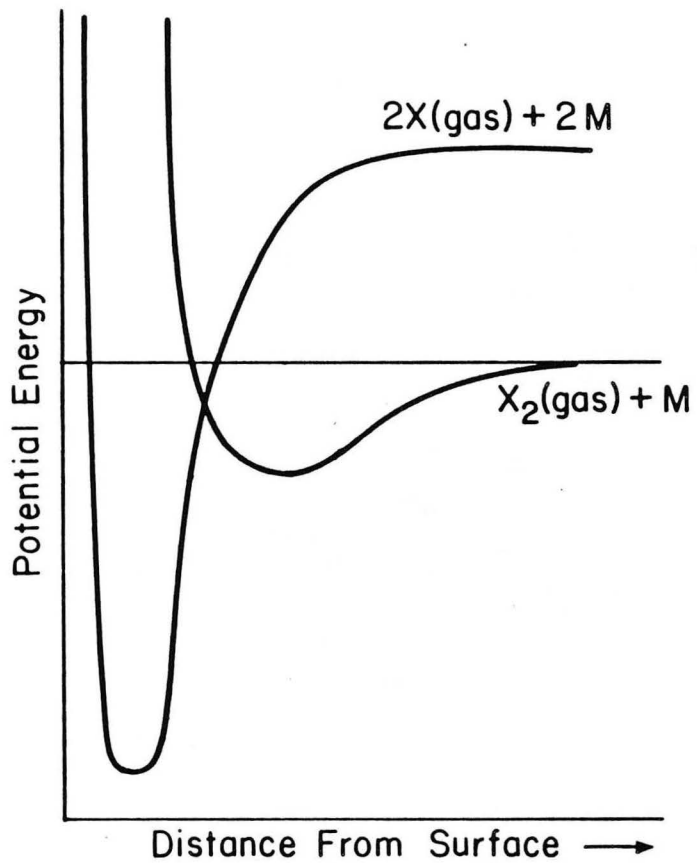
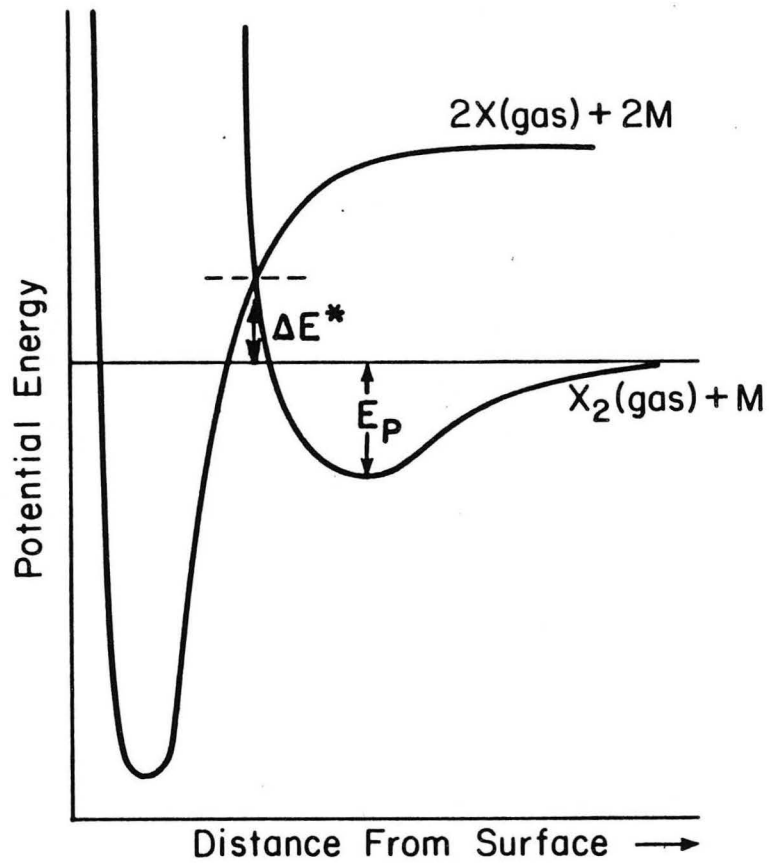


Fig. 22



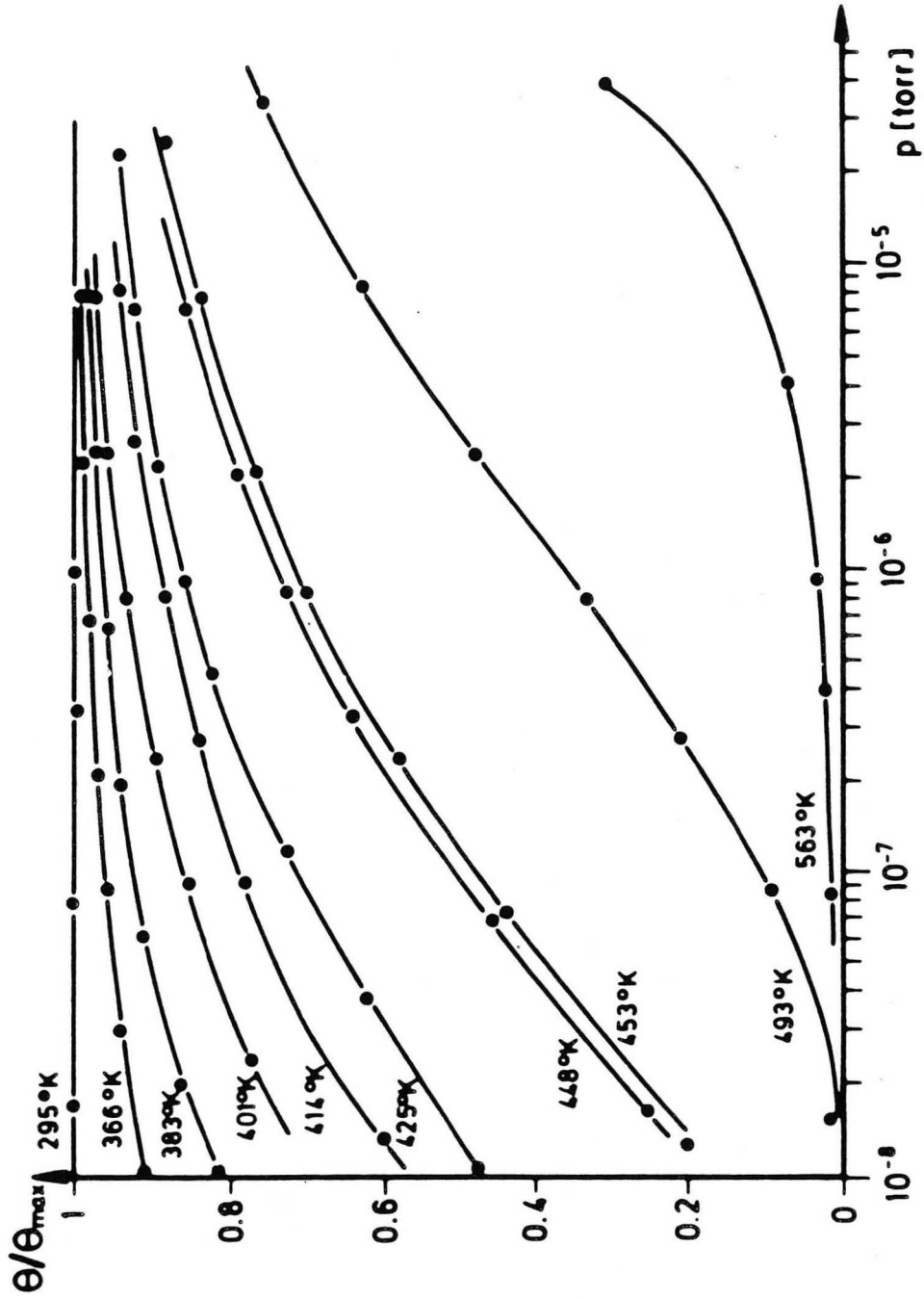
a.



b.

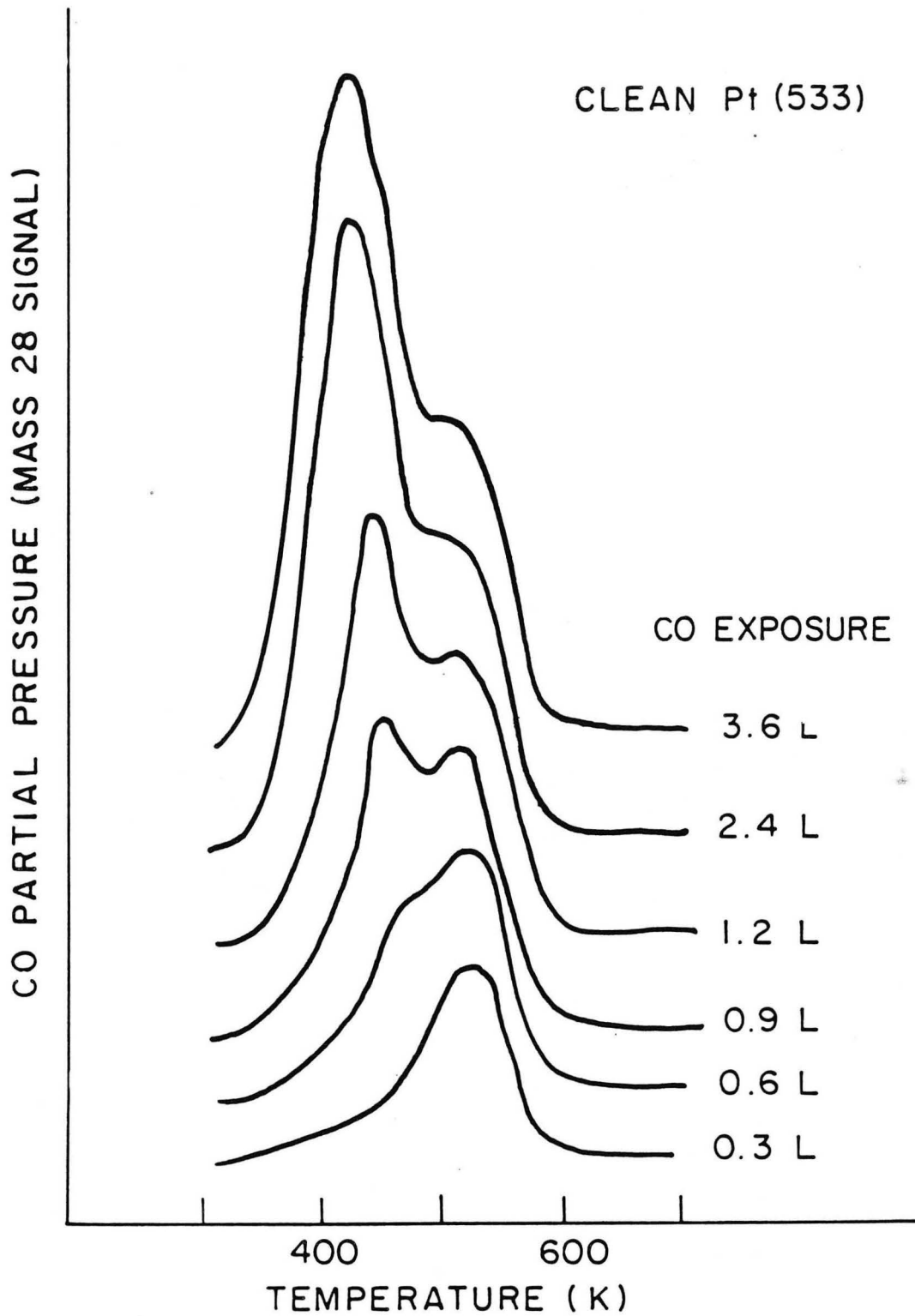
XBL 7912-13719 A

Fig. 23



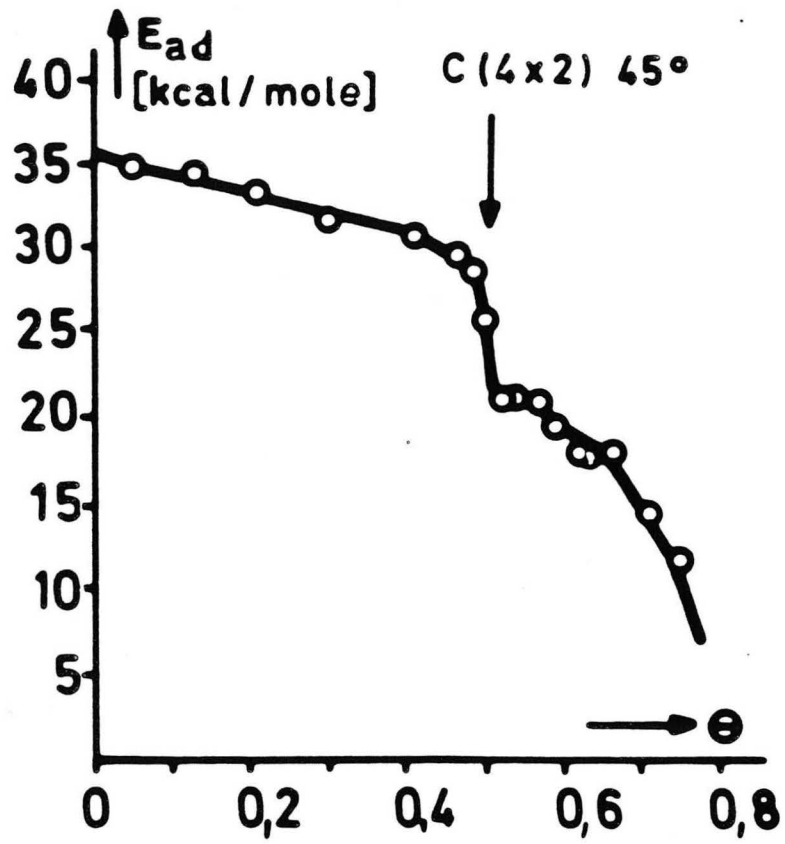
XBL 7911-12821

Fig. 24



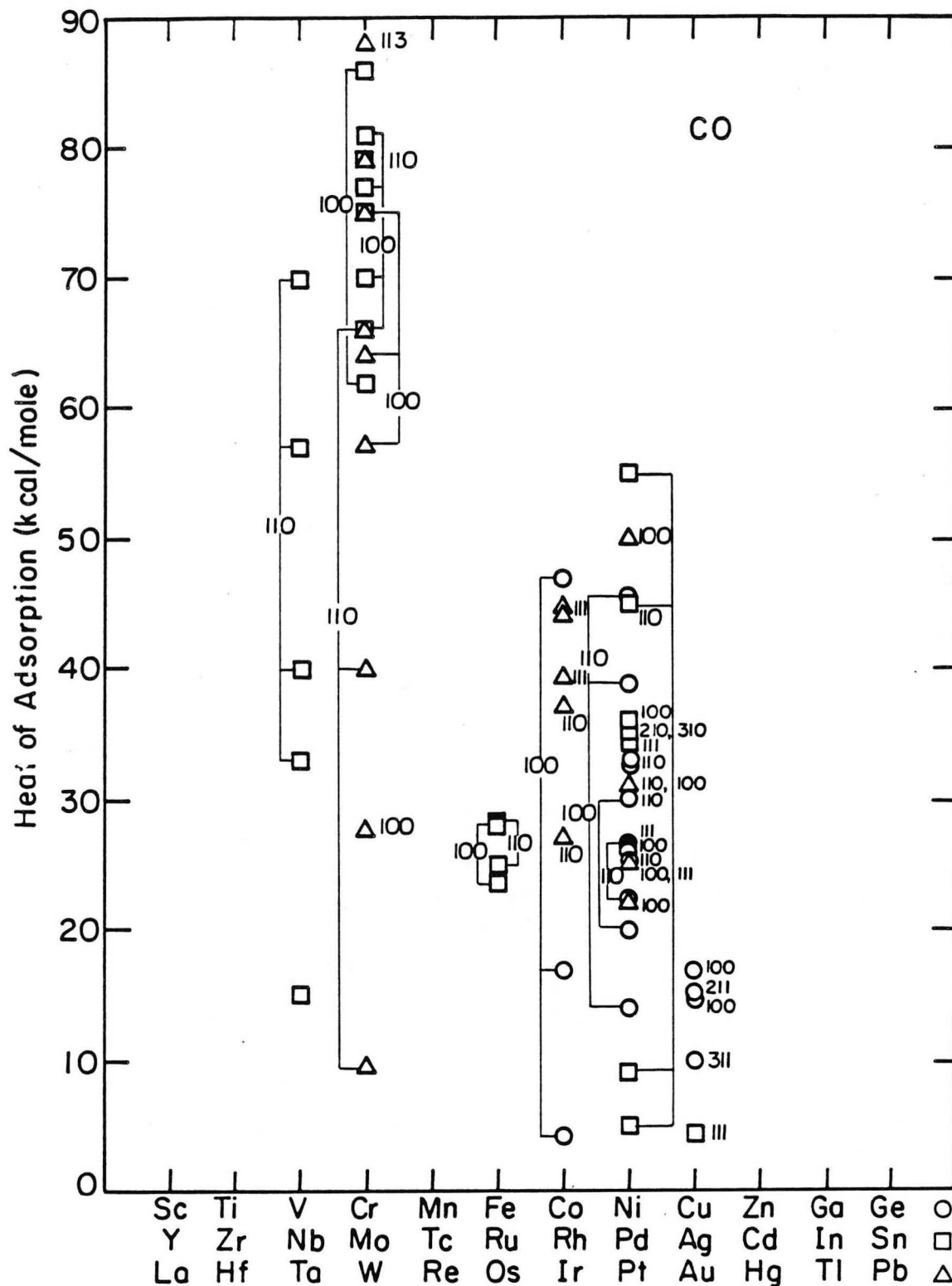
XBL814-5540

Fig. 25



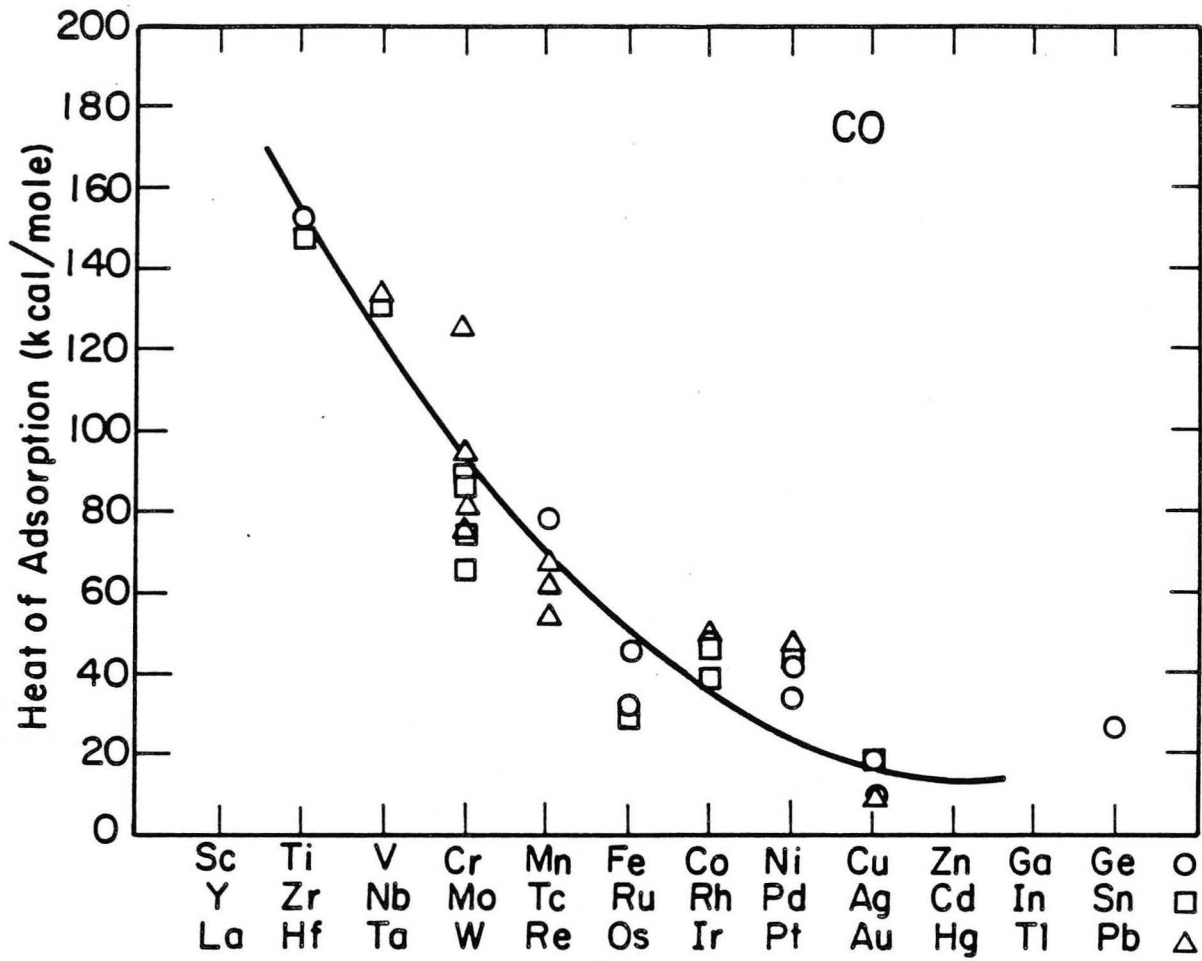
XBL 7911-12823

Fig. 26



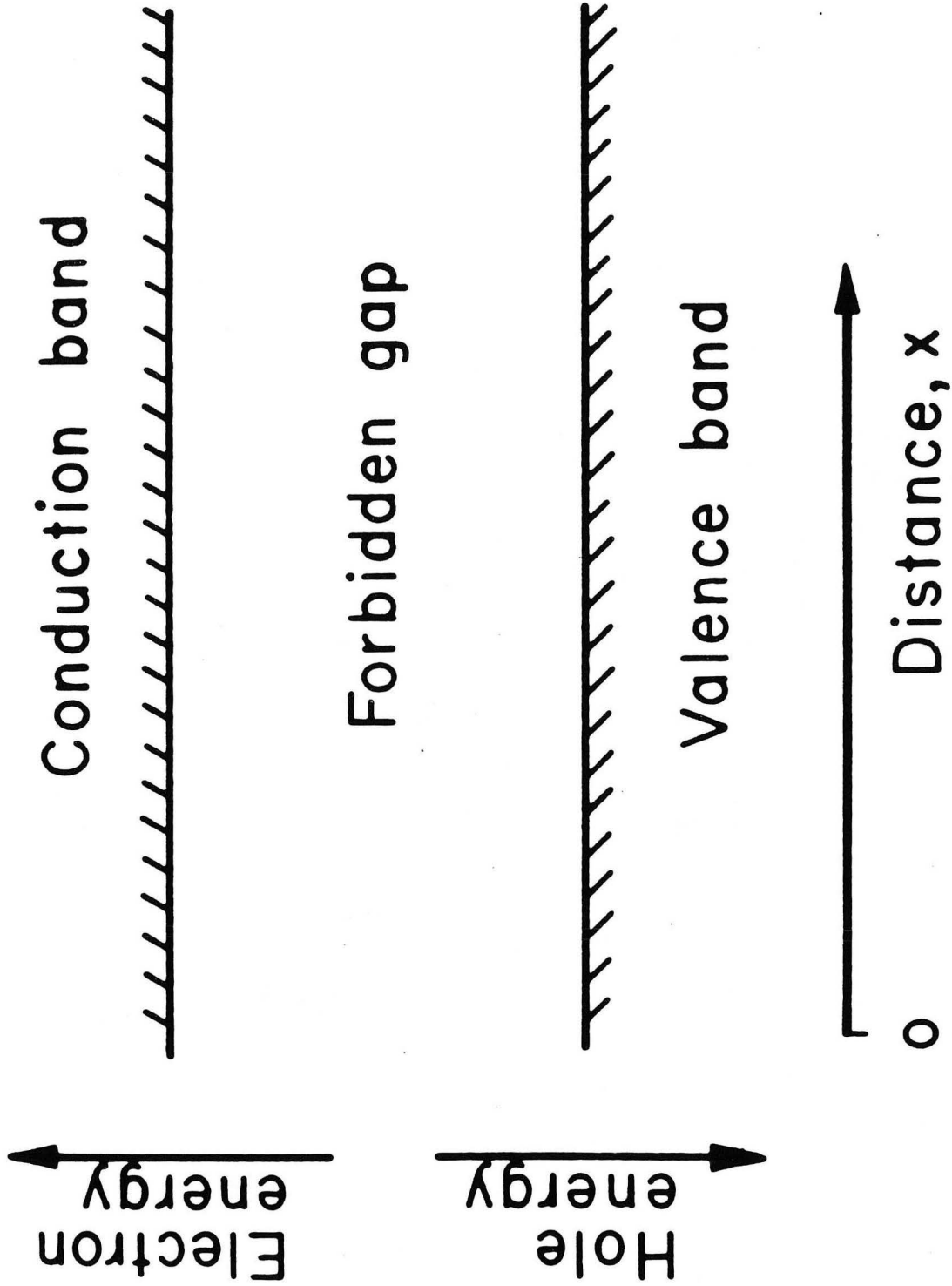
XBL777-5699

Fig. 27



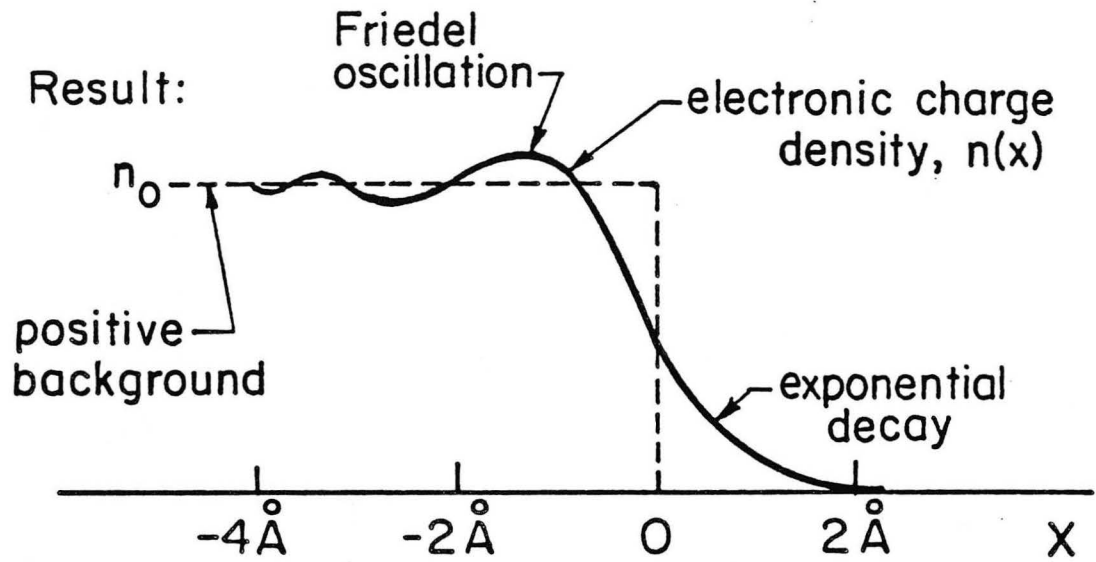
XBL 773-5236

Fig. 28



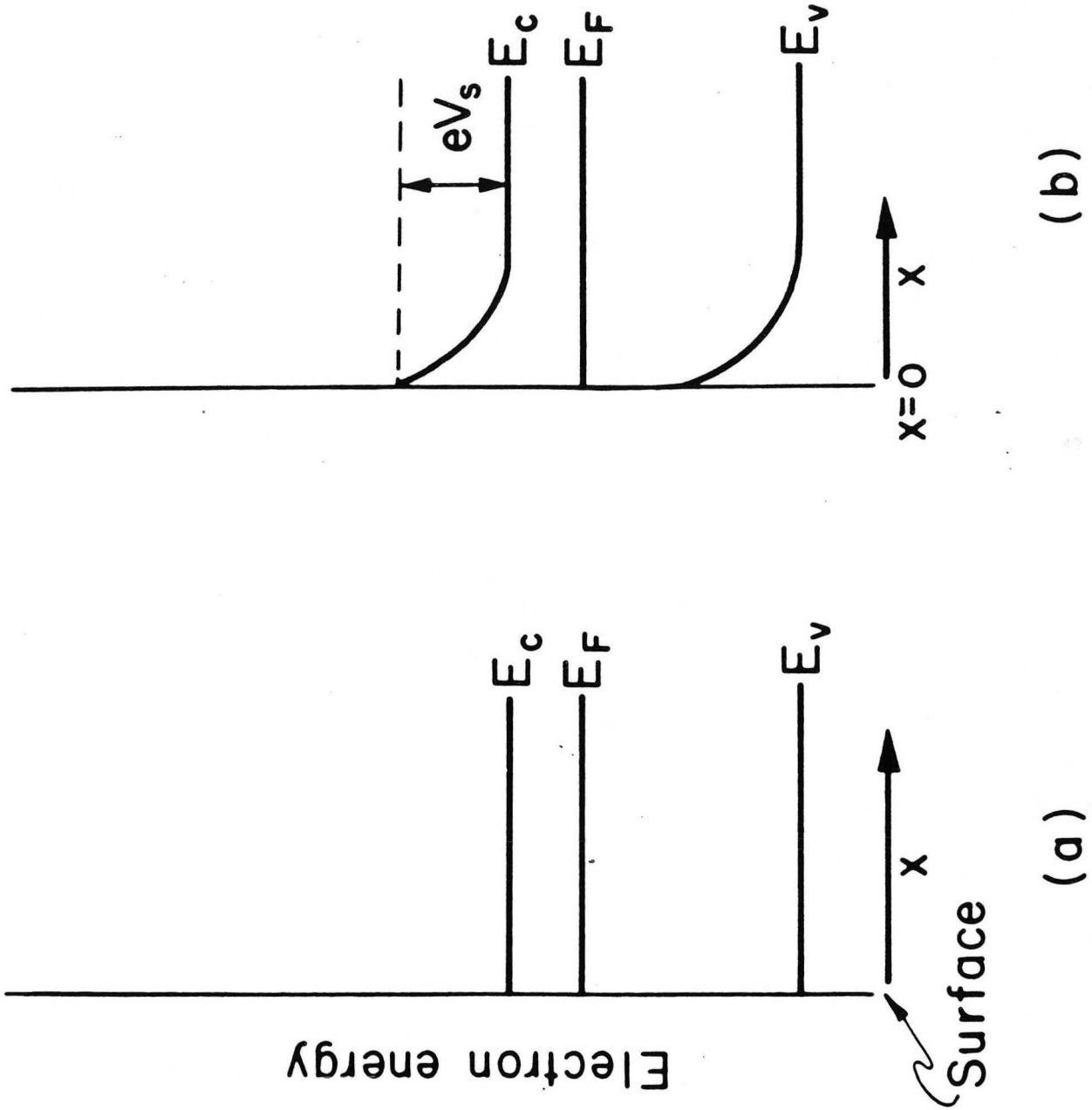
XBL 861-122

Fig. 29



XBL 798-6897

Fig. 30



XBL 861-115

Fig. 31

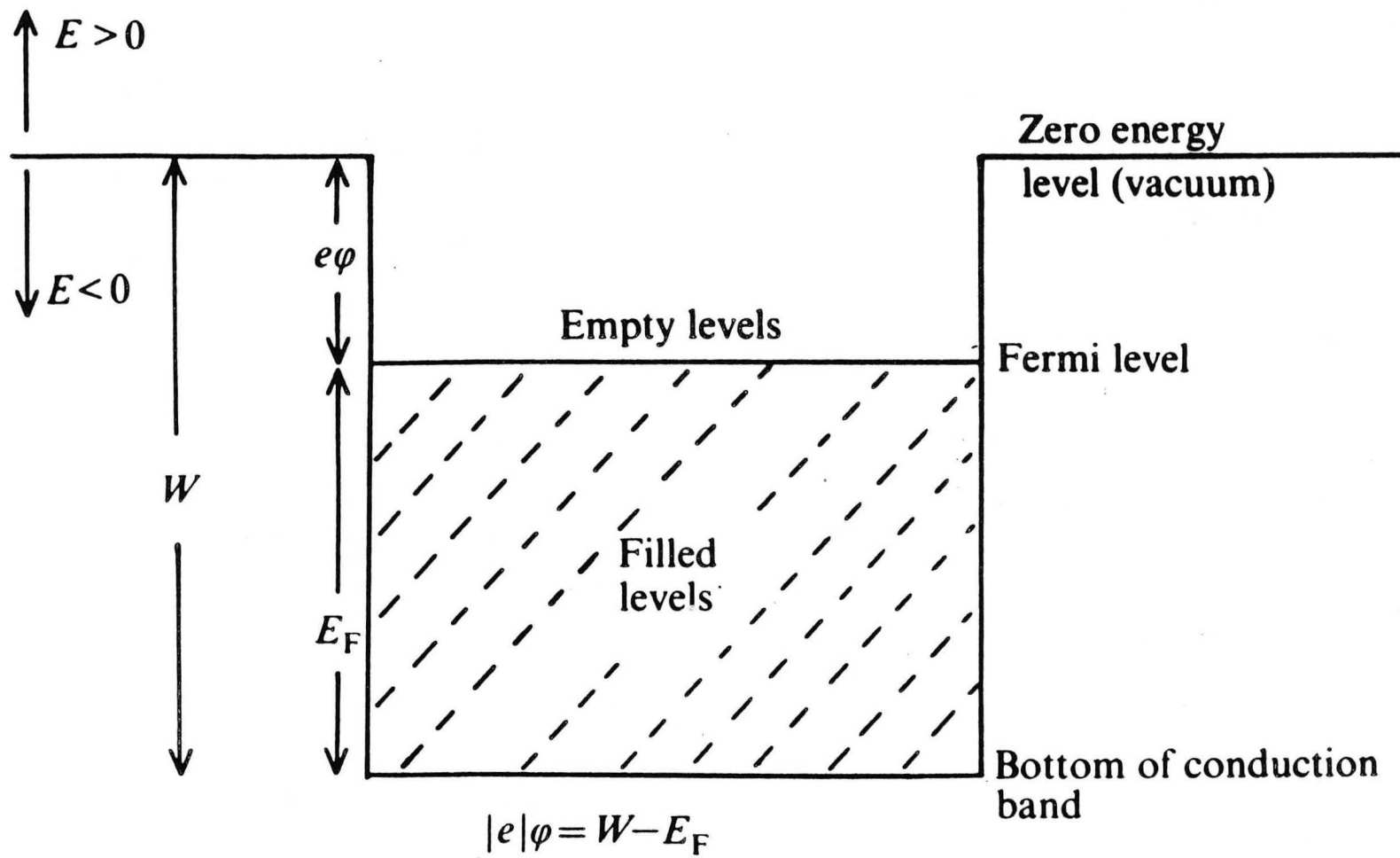
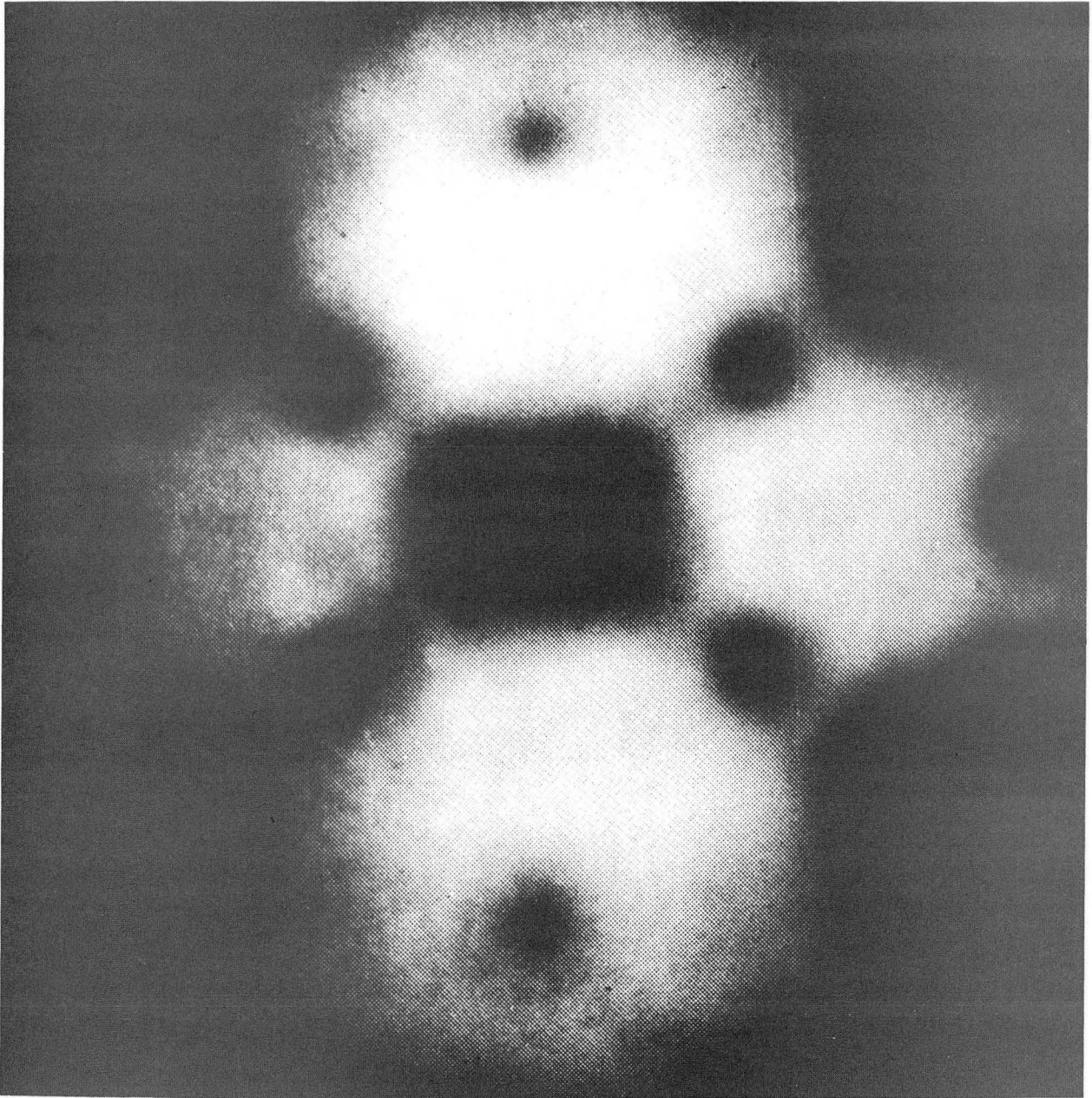
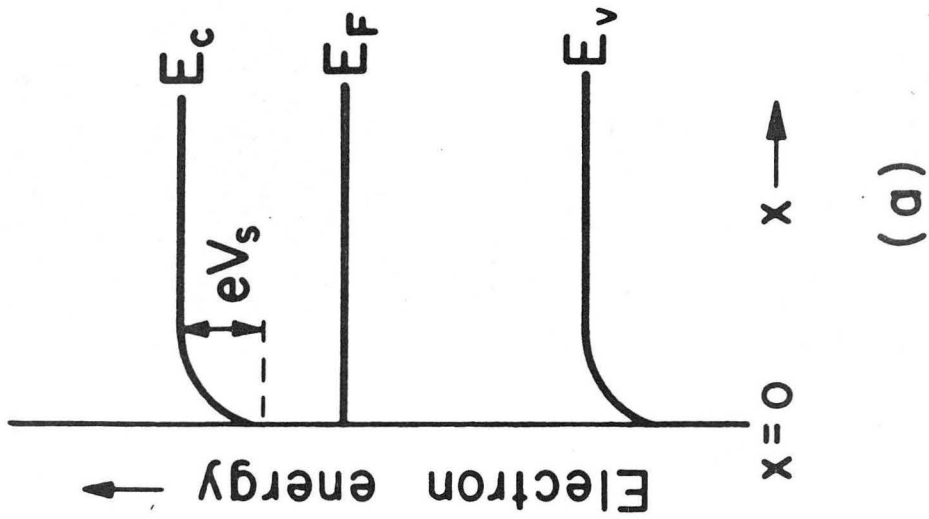
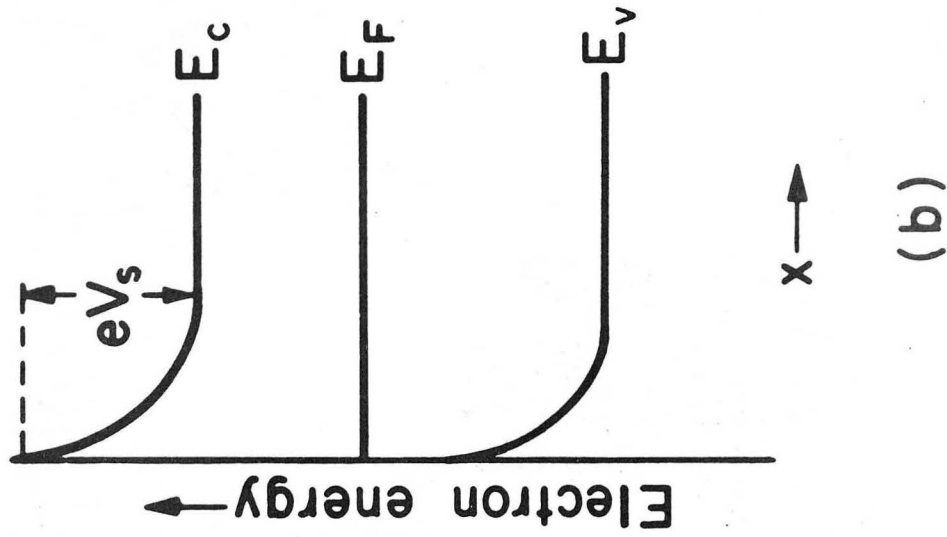


Fig. 32



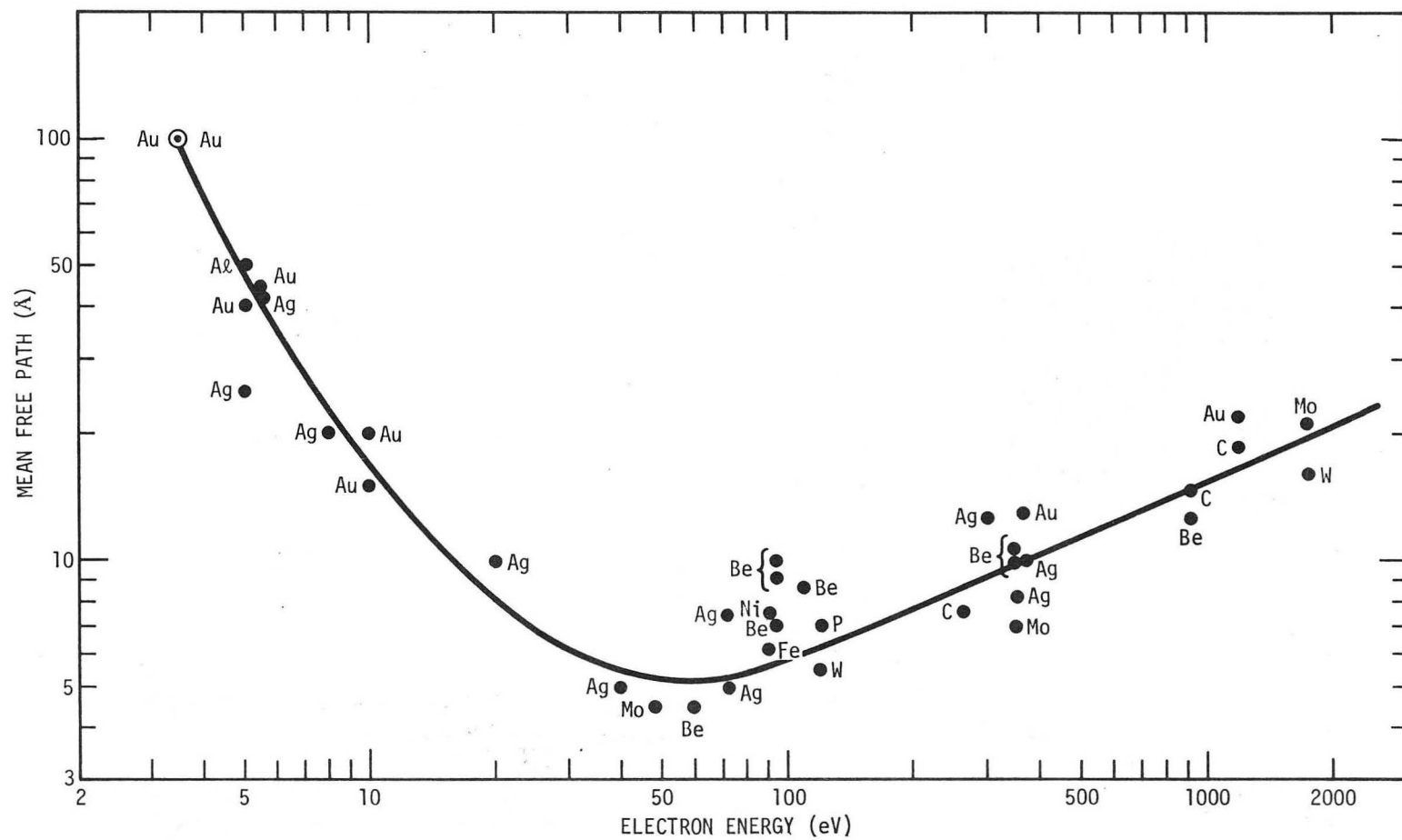
XBB 861-544

Fig. 33



XBL 861-116

Fig. 34



XBL 733-5917

Fig. 35

ENERGY DISTRIBUTION OF SCATTERED ELECTRONS FROM
A $c(4 \times 2)$ MONOLAYER OF C_2H_3 ON Rh(III) AT 300K

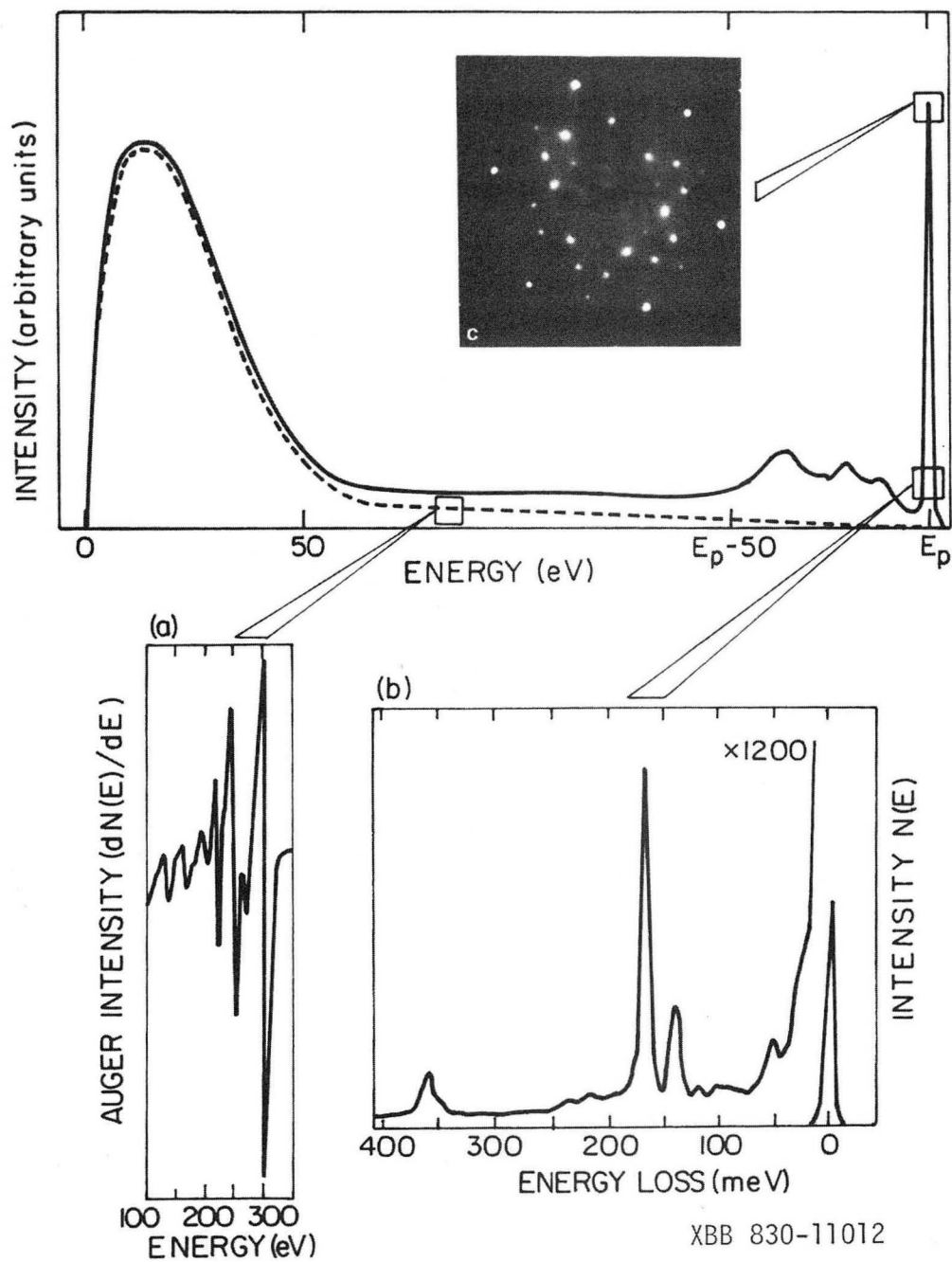
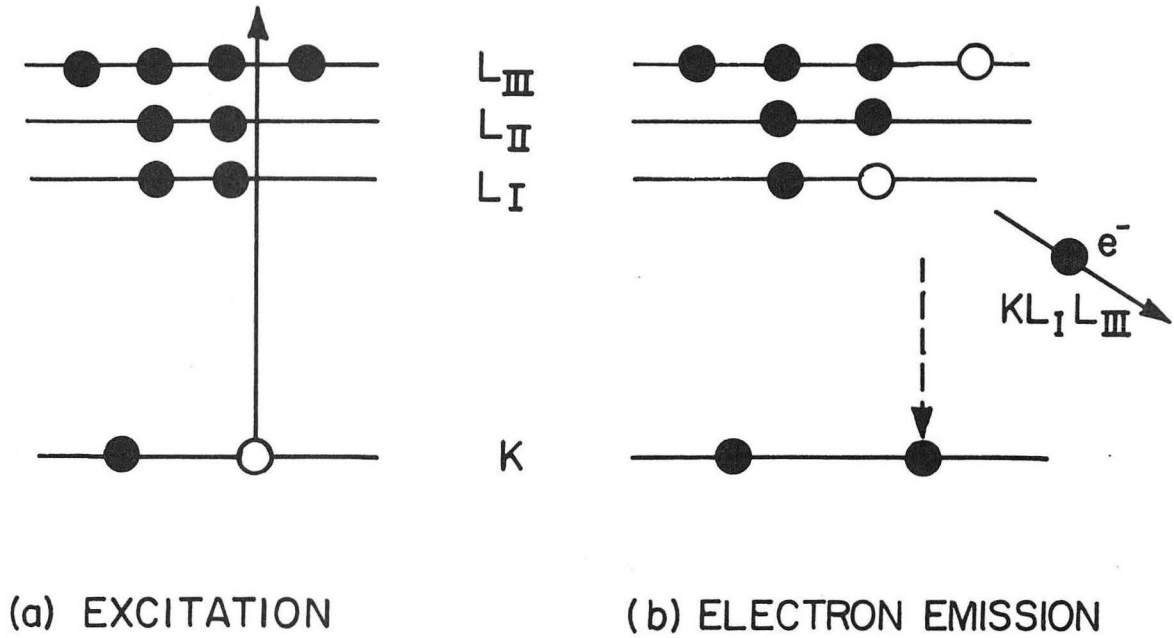


Fig. 36

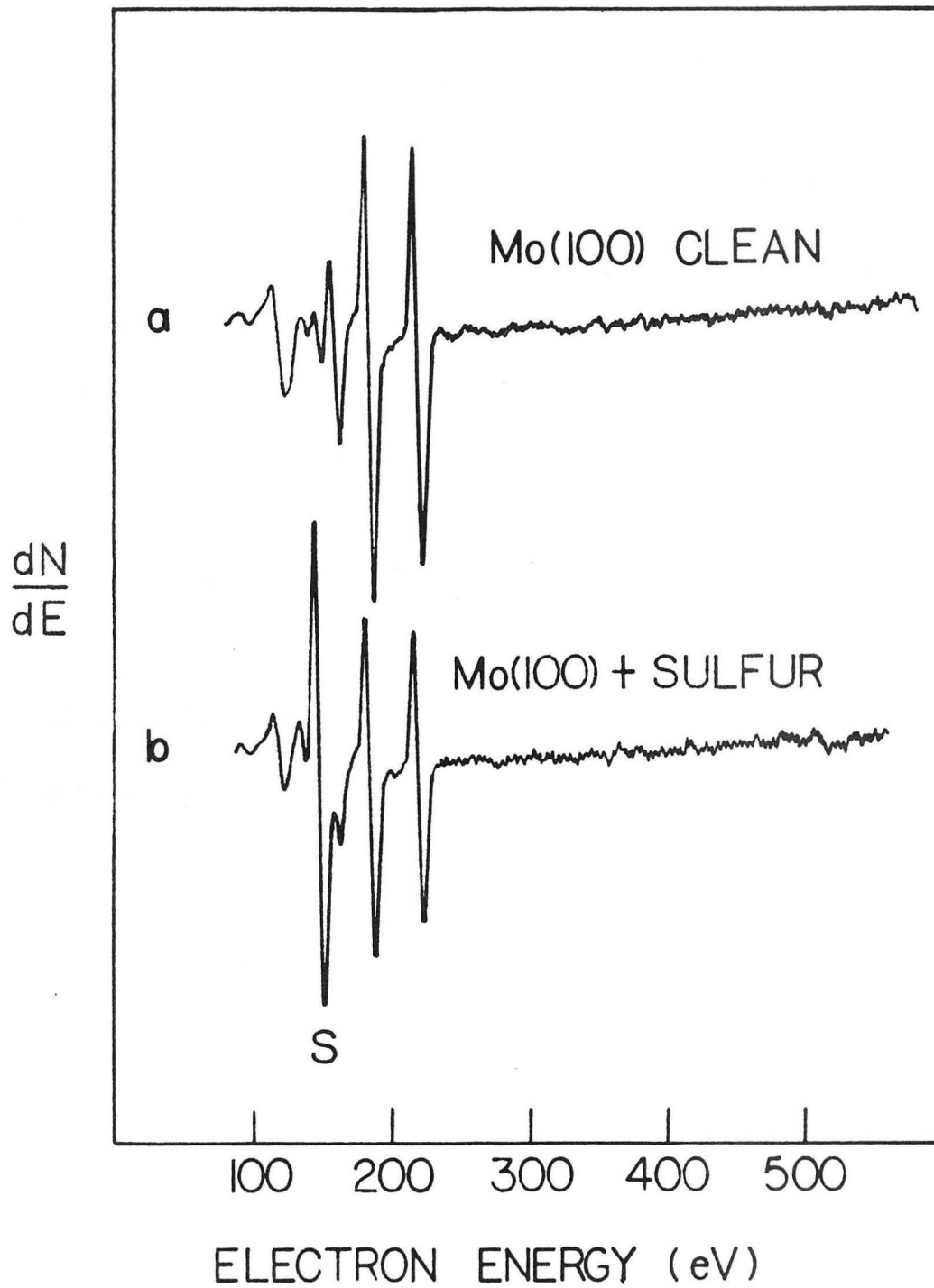
AUGER ELECTRON EMISSION



XBL 7611-7873

Fig. 37

AUGER ELECTRON SPECTRA



XBL 831-7989

Fig. 38

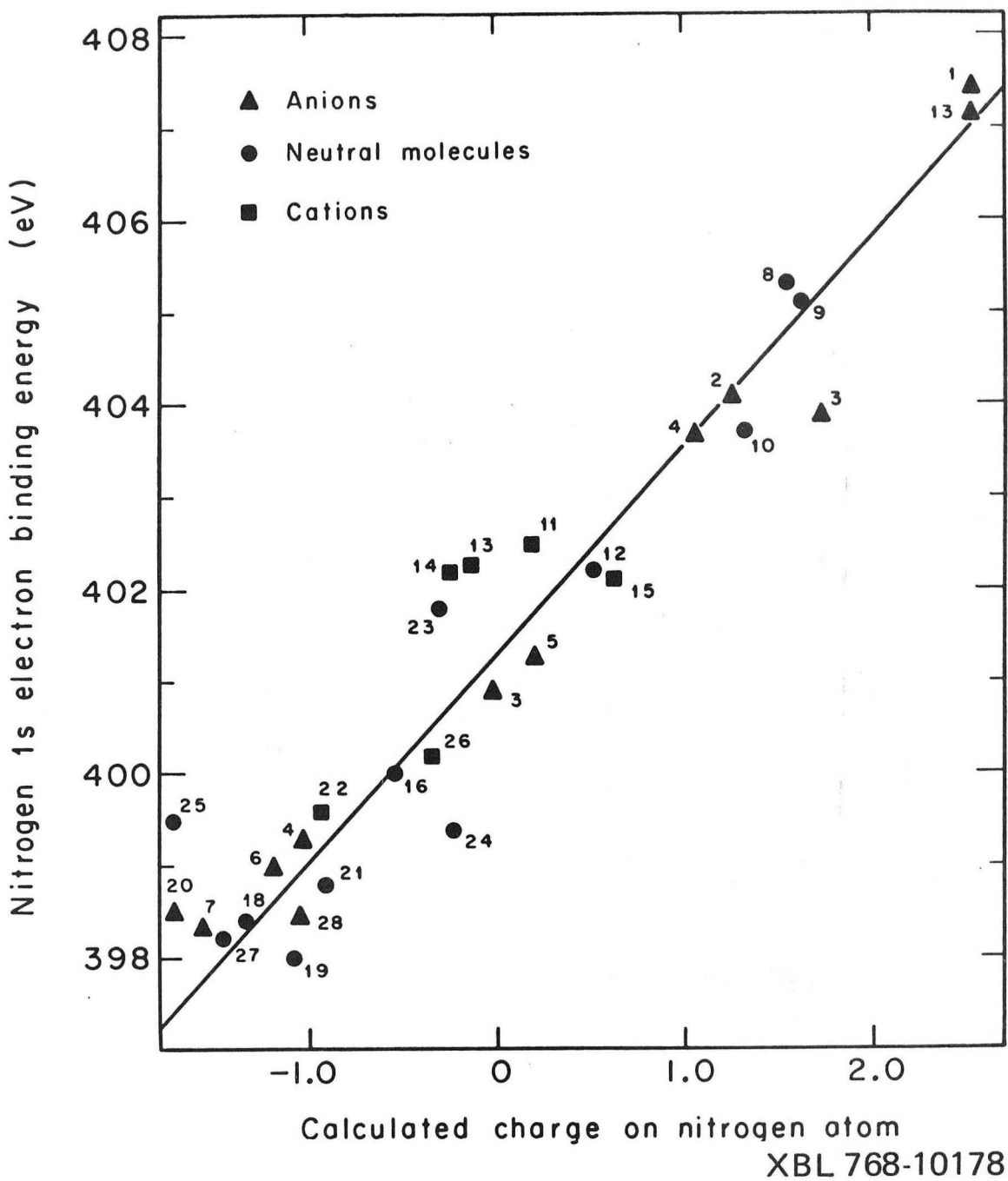
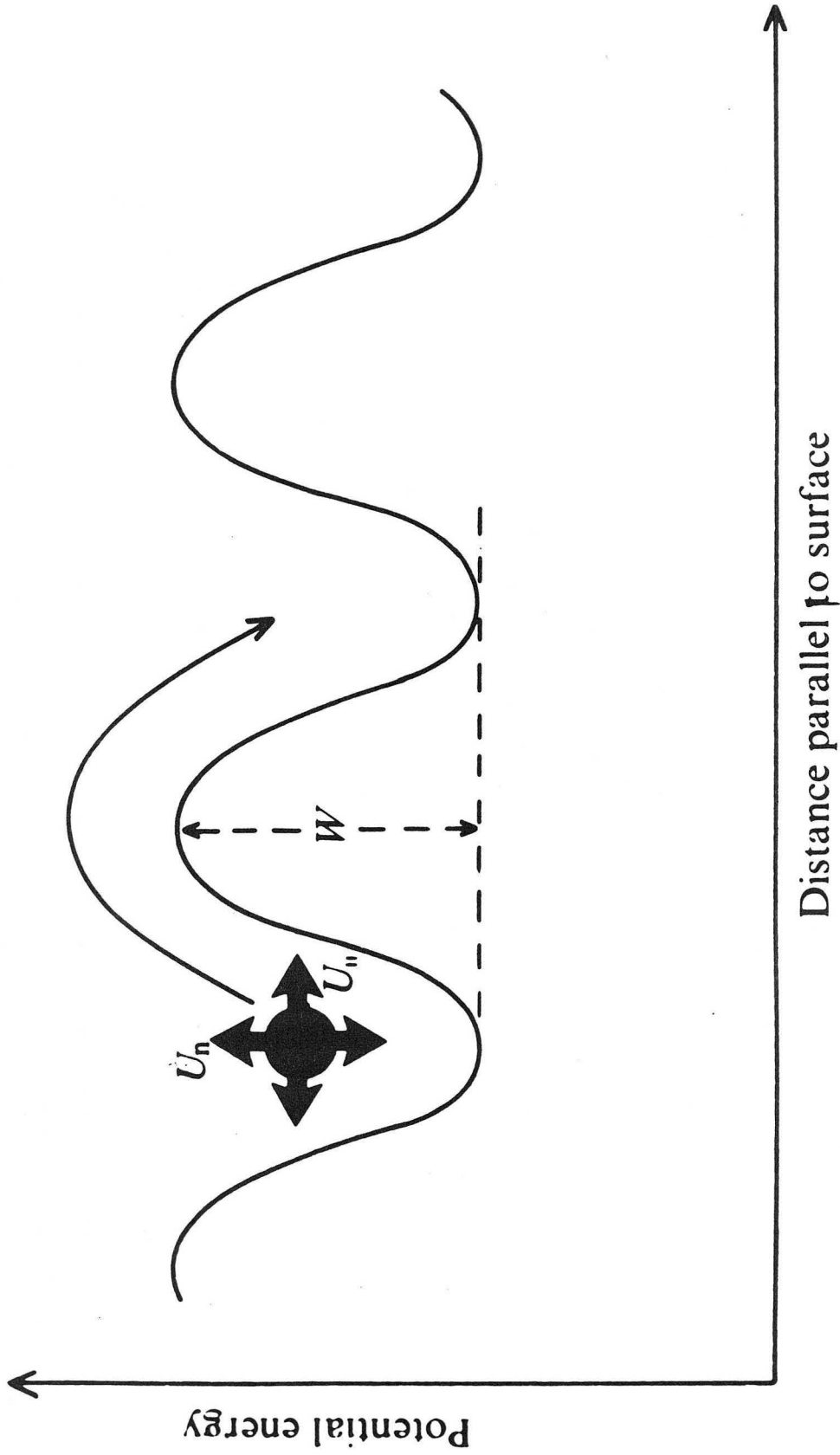
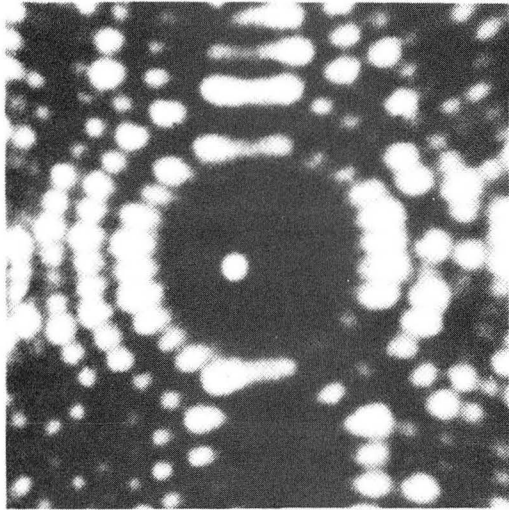


Fig. 39

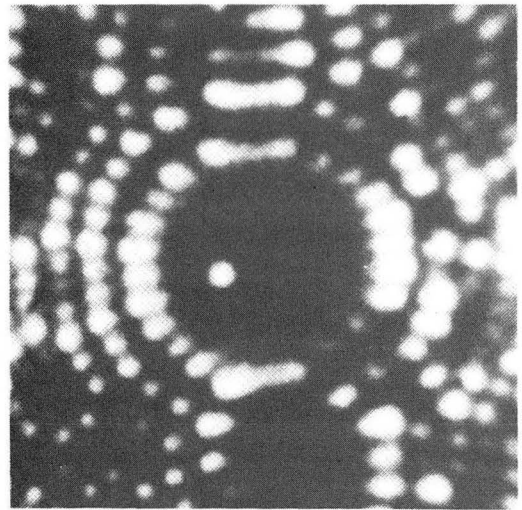


XBL 861-113

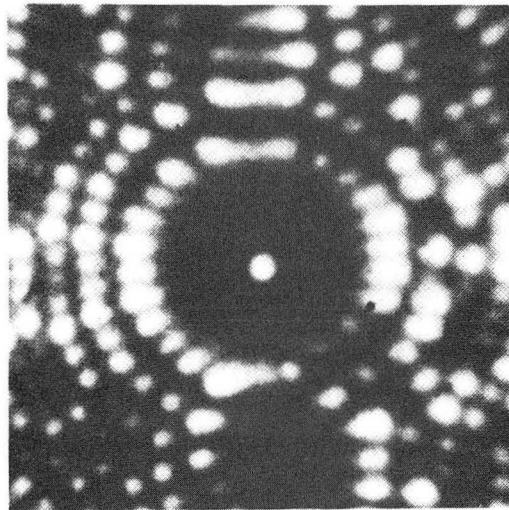
Fig. 40



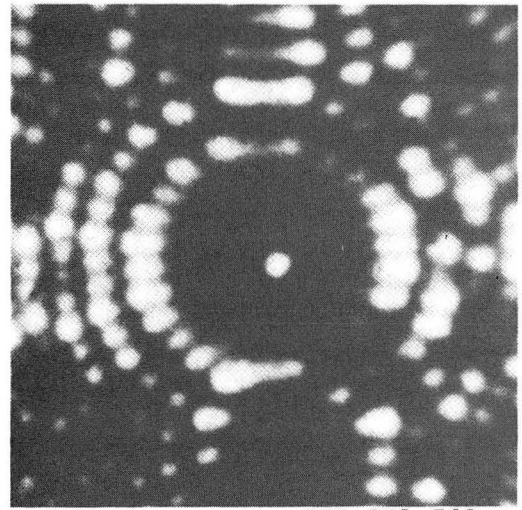
(a)



(b)



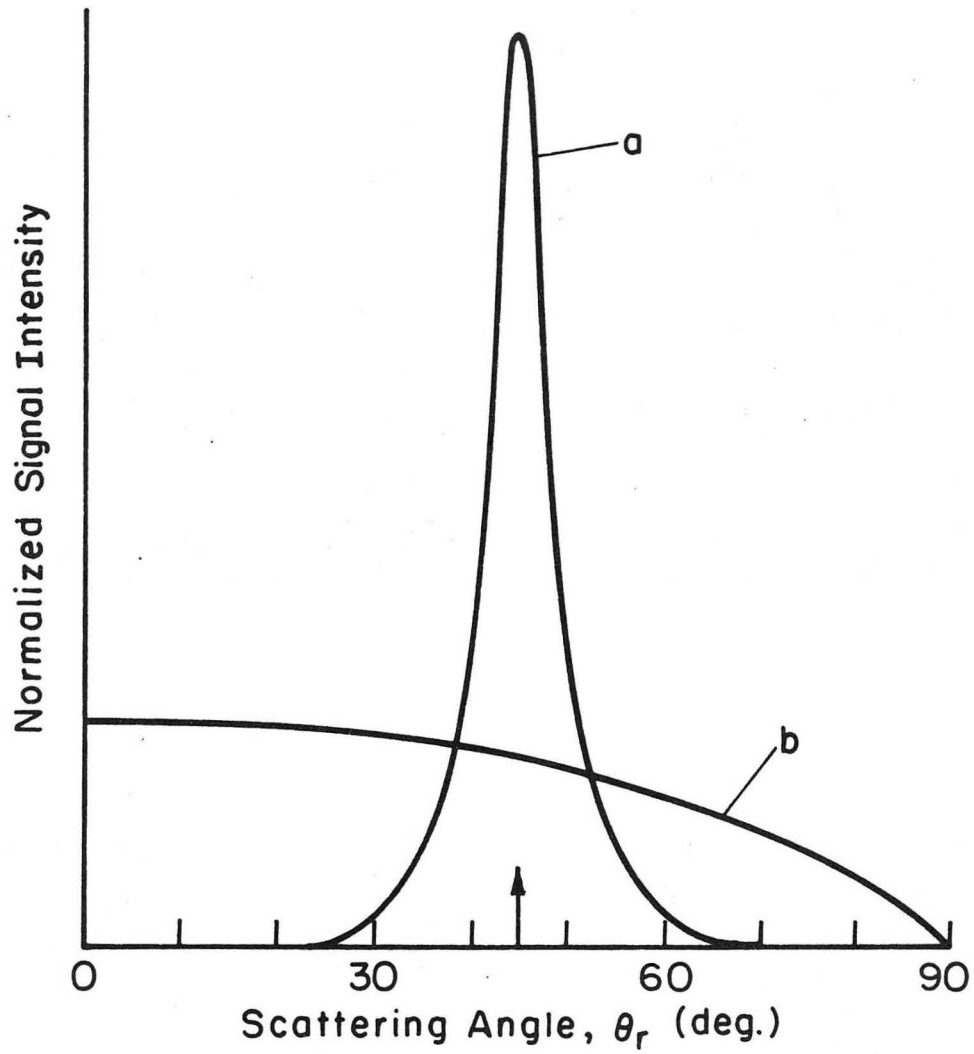
(c)



XBB 861-543

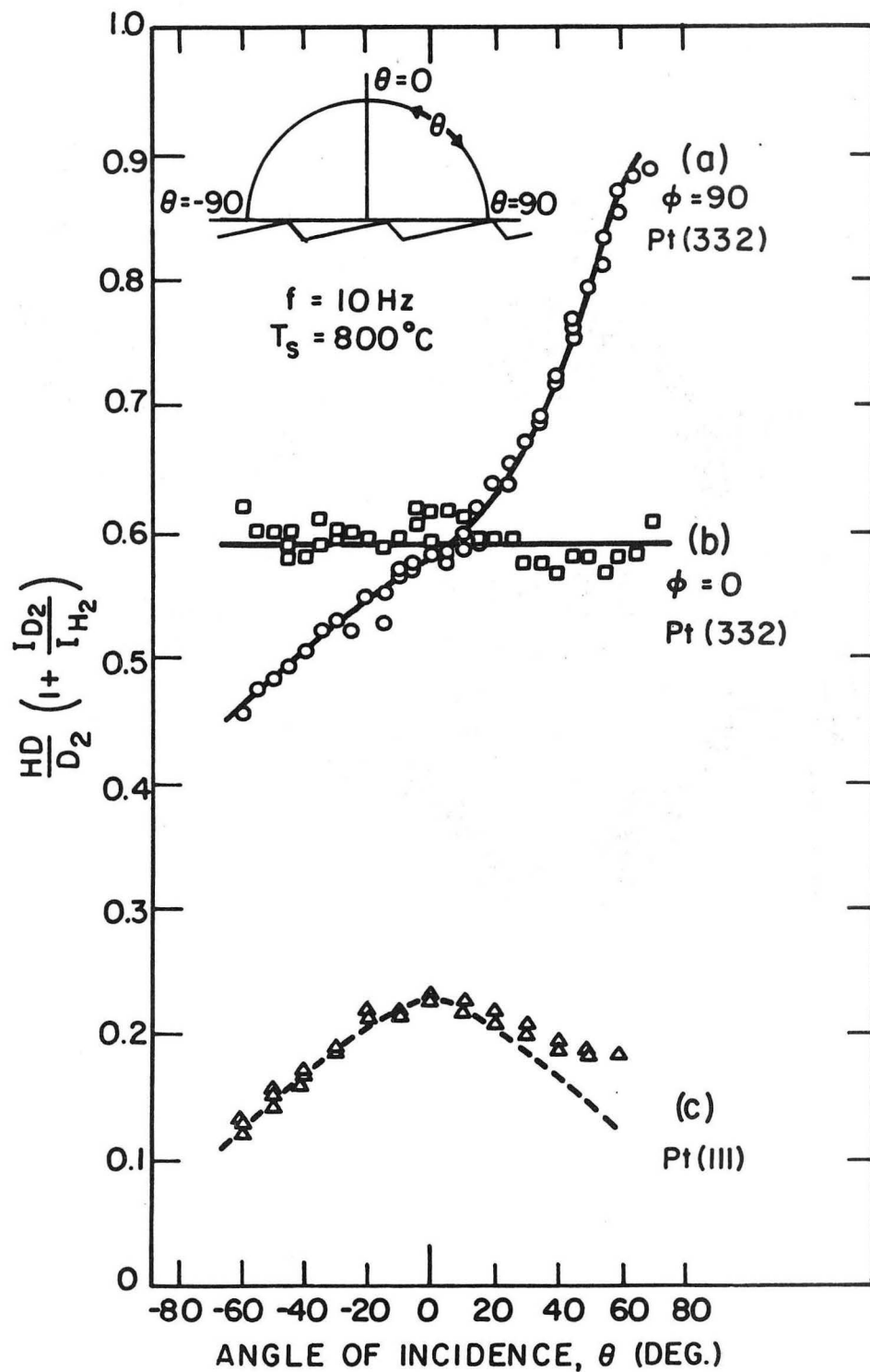
(d)

Fig. 41



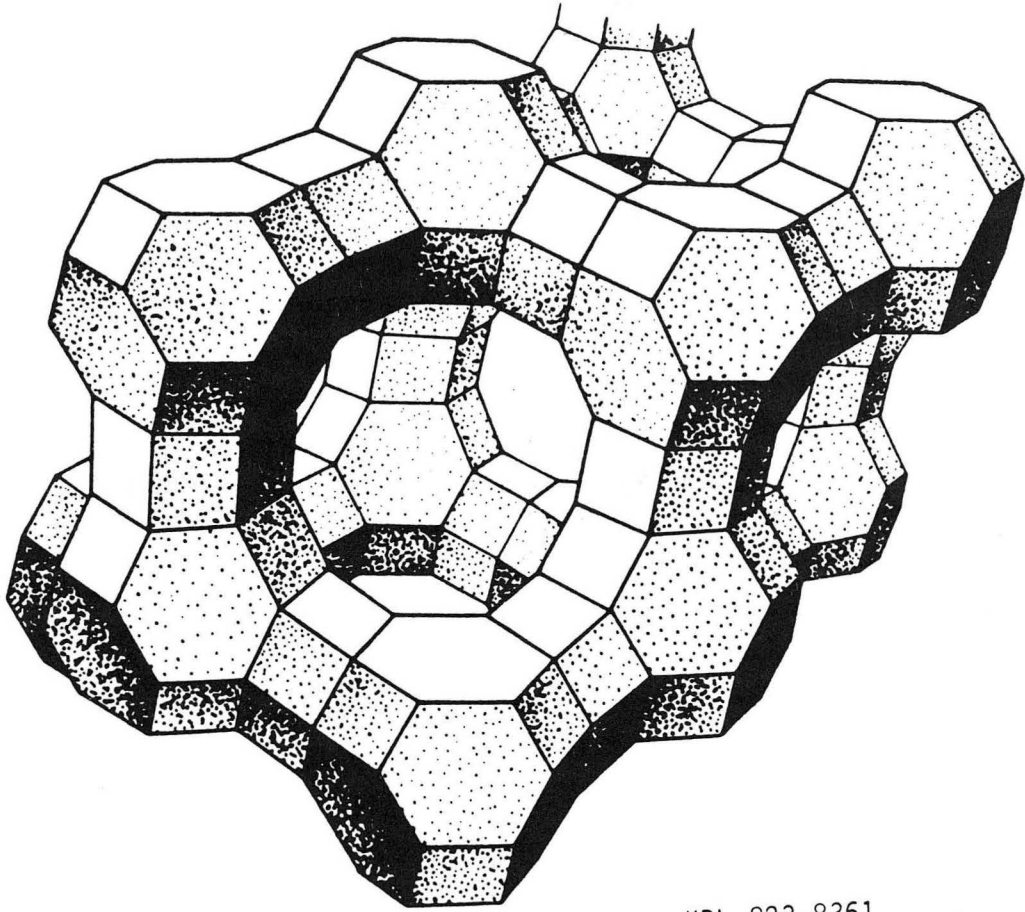
XBL 738-1710

Fig. 42



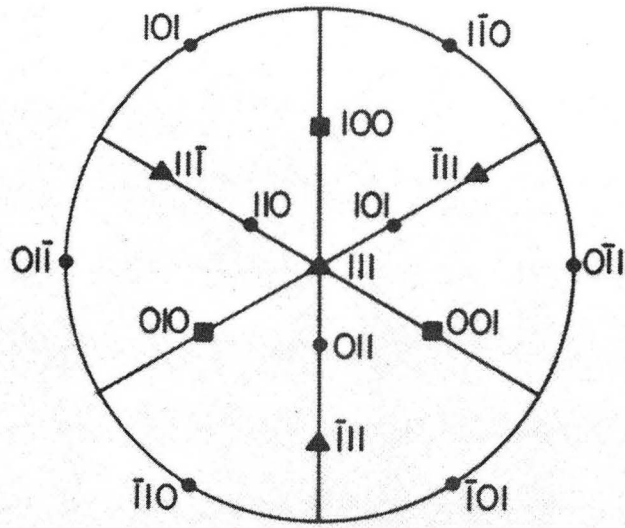
XBL772-5084A

Fig. 43

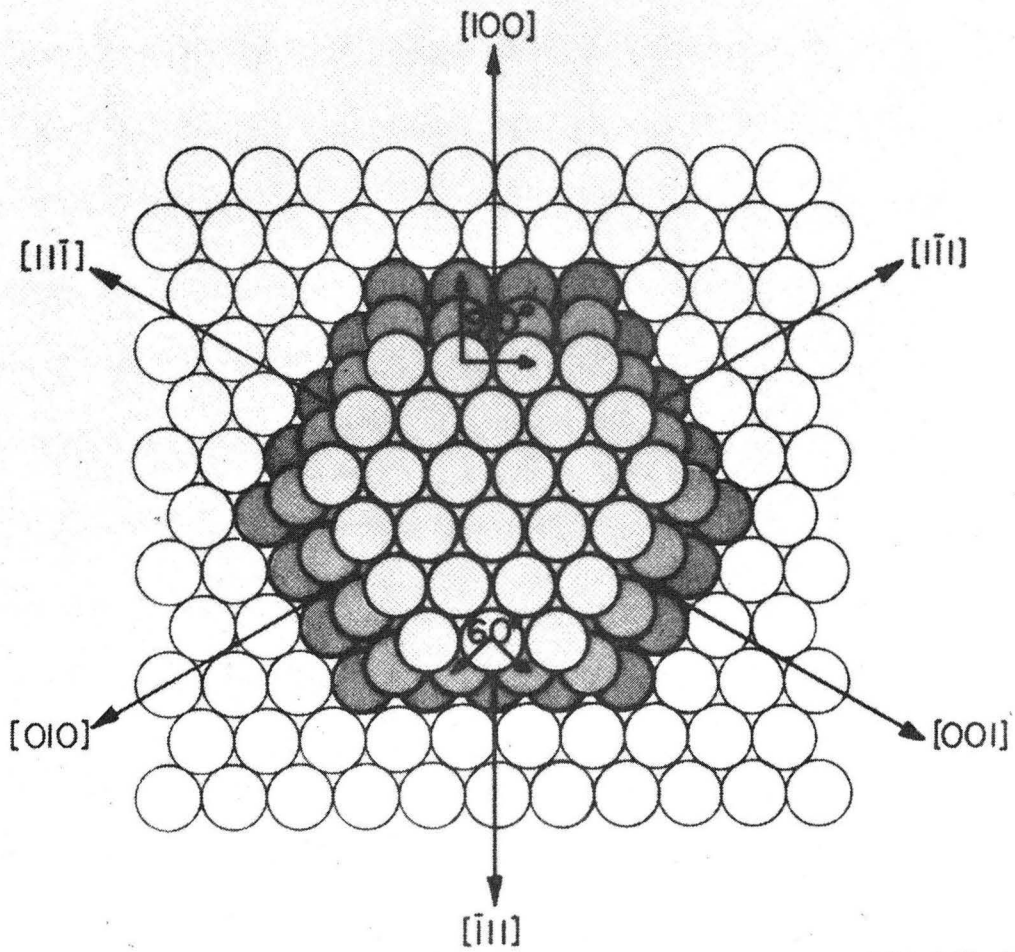


XBL 823-8361

Fig. 44



Standard Cubic (111) Projection



XBB 861-655

Fig. 45

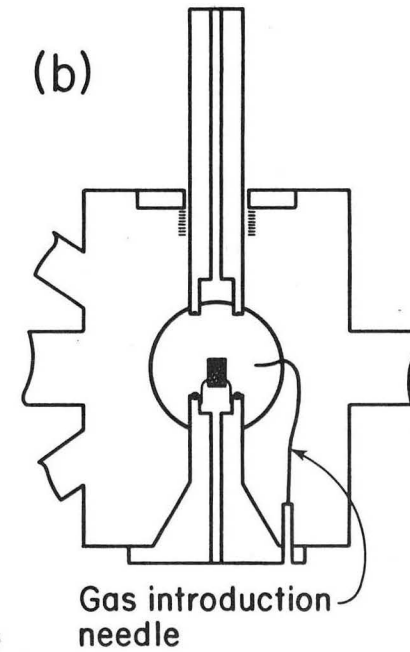
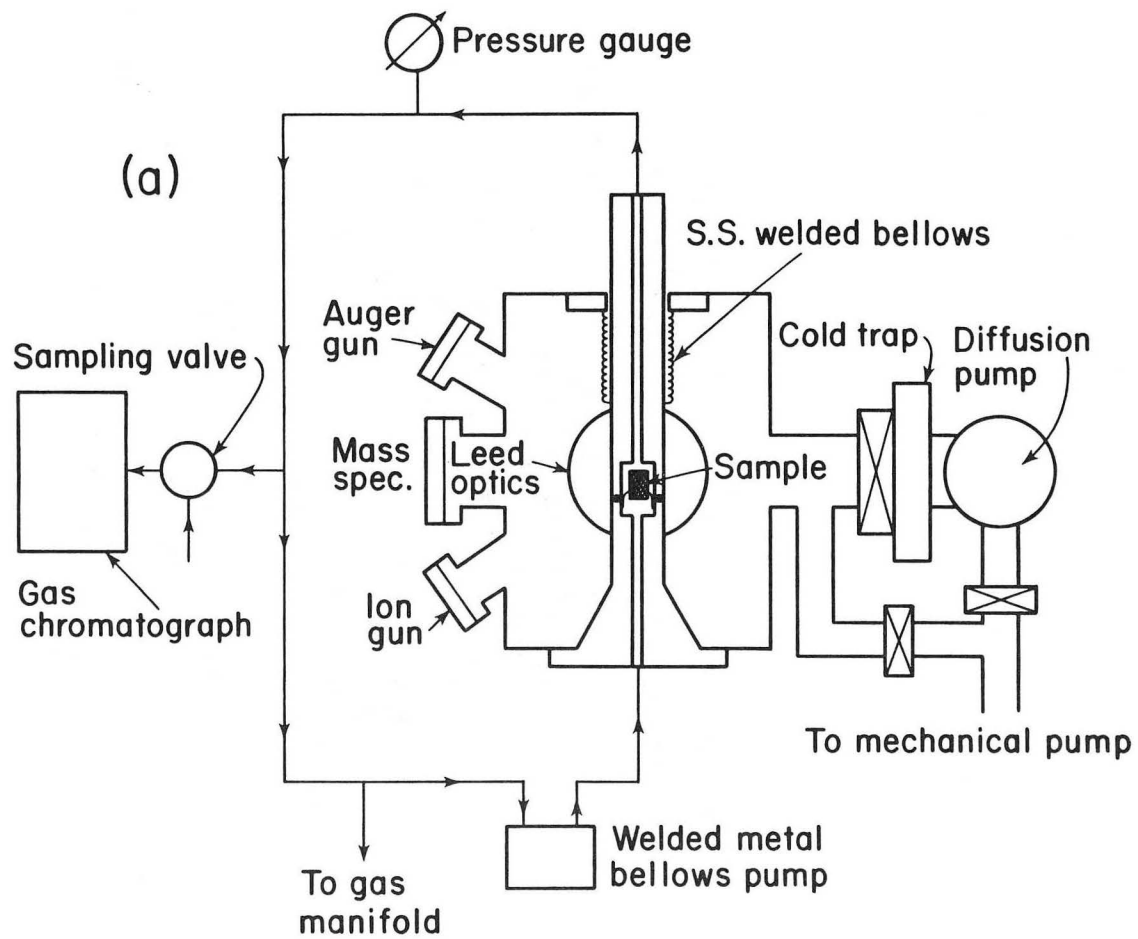
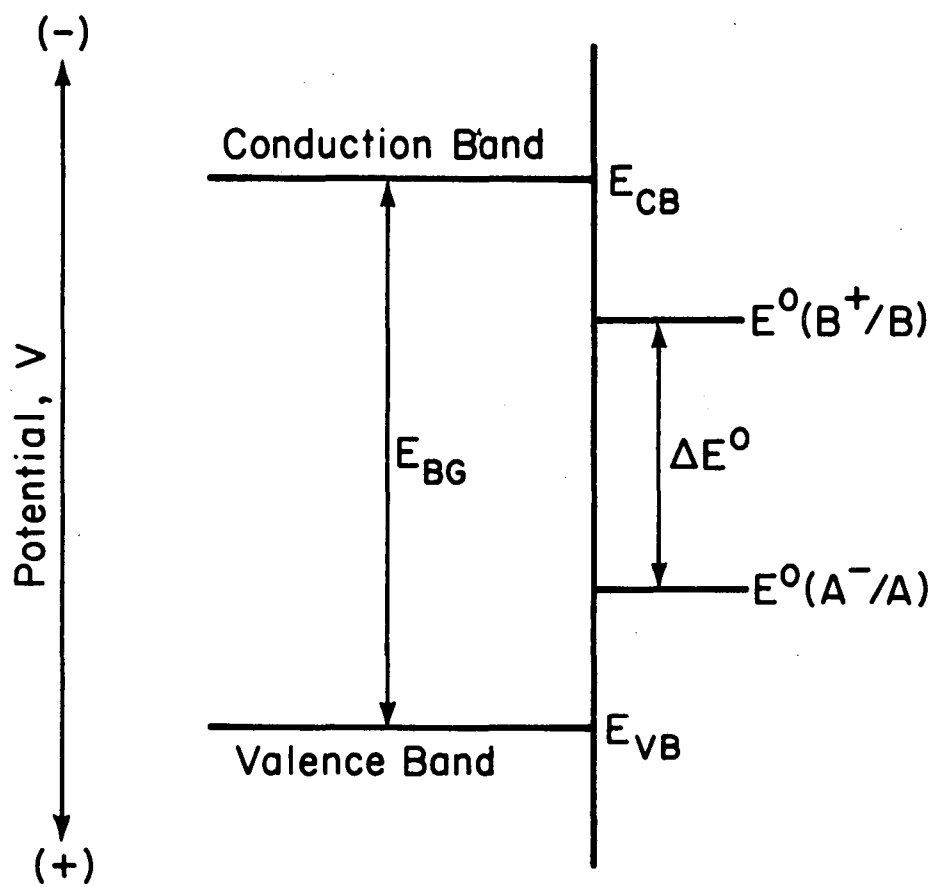


Fig. 46

XBL 756-3160



XBL 7910-12609

Fig. 47

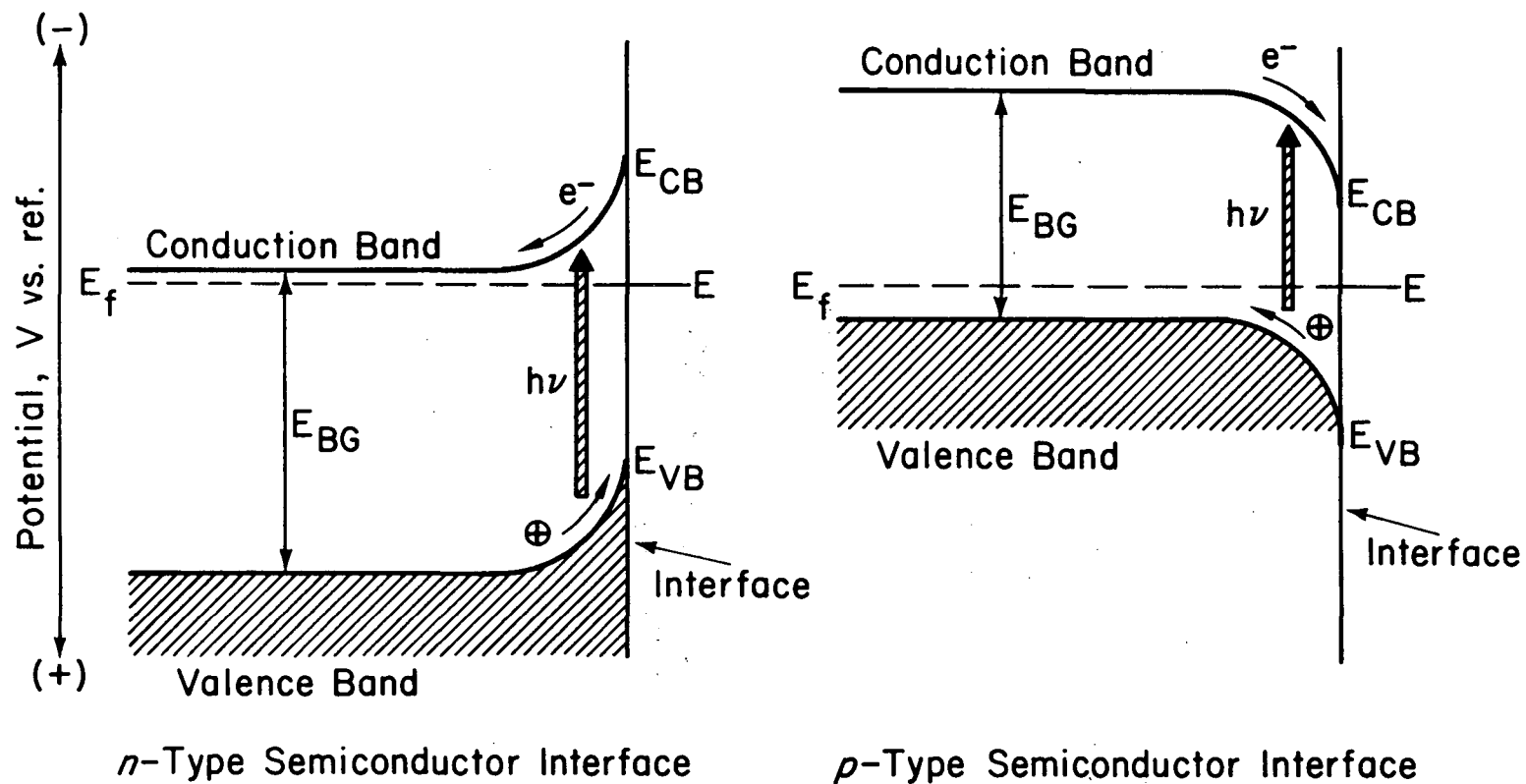


Fig. 48

XBL 7910-12608

This report was done with support from the Department of Energy. Any conclusions or opinions expressed in this report represent solely those of the author(s) and not necessarily those of The Regents of the University of California, the Lawrence Berkeley Laboratory or the Department of Energy.

Reference to a company or product name does not imply approval or recommendation of the product by the University of California or the U.S. Department of Energy to the exclusion of others that may be suitable.

*LAWRENCE BERKELEY LABORATORY
TECHNICAL INFORMATION DEPARTMENT
UNIVERSITY OF CALIFORNIA
BERKELEY, CALIFORNIA 94720*